SRNL-STI-2011-00547
Revision 0

Keywords: *DWPF, SB7b, SRAT, qualification*

Retention: *Permanent*

DWPF Simulant CPC Studies for SB7b

D. C. Koopman

November 2011

Savannah River National Laboratory
Savannah River Nuclear Solutions, LLC
Aiken, SC 29808

Prepared for the U.S. Department of Energy under contract number DE-AC09-08SR22470.

SRNL
SAVANNAH RIVER NATIONAL LABORATORY

DISCLAIMER

Printed in the United States of America

Prepared for
U.S. Department of Energy

REVIEWS AND APPROVALS

AUTHOR:

D. C. Koopman, Process Technology Programs Date

TECHNICAL REVIEW:

M. E. Stone, Process Technology Programs Date

APPROVAL:

C. C. Herman, Manager Date
Process Technology Programs

S. L. Marra, Manager Date
Environmental & Chemical Process Technology Research Programs

J. E. Occhipinti, Manager Date
Waste Solidification Engineering

EXECUTIVE SUMMARY

Lab-scale DWPF simulations of Sludge Batch 7b (SB7b) processing were performed. Testing was performed at the Savannah River National Laboratory – Aiken County Technology Laboratory (SRNL-ACTL). The primary goal of the simulations was to define a likely operating window for acid stoichiometry for the DWPF Sludge Receipt and Adjustment Tank (SRAT). In addition, the testing established conditions for the SRNL Shielded Cells qualification simulation of SB7b-Tank 40 blend, supported validation of the current glass redox model, and validated the coupled process flowsheet at the nominal acid stoichiometry.

An acid window of 105-140% by the Koopman minimum acid (KMA) equation (107-142% DWPF Hsu equation) worked for the sludge-only flowsheet. Nitrite was present in the SRAT product for the 105% KMA run at 366 mg/kg, while SME cycle hydrogen reached 94% of the DWPF Slurry Mix Evaporator (SME) cycle limit in the 140% KMA run. The window was determined for sludge with added caustic (0.28M additional base, or roughly 12,000 gallons 50% NaOH to 820,000 gallons waste slurry). A suitable processing window appears to be 107-130% DWPF acid equation for sludge-only processing allowing some conservatism for the mapping of lab-scale simulant data to full-scale real waste processing including potentially non-conservative noble metal and mercury concentrations. This window should be usable with or without the addition of up to 7,000 gallons of caustic to the batch. The window could potentially be wider if caustic is not added to SB7b. It is recommended that DWPF begin processing SB7b at 115% stoichiometry using the current DWPF equation. The factor could be increased if necessary, but changes should be made with caution and in small increments. DWPF should not concentrate past 48 wt.% total solids in the SME cycle if moderate hydrogen generation is occurring simultaneously.

The coupled flowsheet simulation made more hydrogen in the SRAT and SME cycles than the sludge-only run with the same acid stoichiometric factor. The slow acid addition in MCU seemed to alter the reactions that consumed the small excess acid present such that hydrogen generation was promoted relative to sludge-only processing. The coupled test reached higher wt.% total solids, and this likely contributed to the SME cycle hydrogen limit being exceeded at 110% KMA. It is clear from the trends in the SME processing GC data, however, that the frit slurry formic acid contributed to driving the hydrogen generation rate above the SME cycle limit. Hydrogen generation rates after the second frit addition generally exceeded those after the first frit addition.

SRAT formate loss increased with increasing acid stoichiometry (15% to 35%). A substantial nitrate gain which was observed to have occurred after acid addition (and nitrite destruction) was reversed to a net nitrate loss in runs with higher acid stoichiometry (nitrate in SRAT product less than sum of sludge nitrate and added nitric acid). Increased ammonium ion formation was also indicated in the runs with nitrate loss. Oxalate loss on the order 20% was indicated in three of the four acid stoichiometry runs and in the coupled flowsheet run. The minimum acid stoichiometry run had no indicated loss. The losses were of the same order as the official analytical uncertainty of the oxalate concentration measurement, but were not randomly distributed about zero loss, so some actual loss was likely occurring.

Based on the entire set of SB7b test data, it is recommended that DWPF avoid concentrating additional sludge solids in single SRAT batches to limit the concentrations of noble metals to SB7a processing levels (on a grams noble metal per SRAT batch basis). It is also recommended that DWPF drop the formic acid addition that accompanies the process frit 418 additions, since

SME cycle data showed considerable catalytic activity for hydrogen generation from this additional acid (about 5% increase in stoichiometry occurred from the frit formic acid). Frit 418 also does not appear to need formic acid addition to prevent gel formation in the frit slurry.

Simulant processing was successful using 100 ppm of 747 antifoam added prior to nitric acid instead of 200 ppm. This is a potential area for DWPF to cut antifoam usage in any future test program. An additional 100 ppm was added before formic acid addition. Foaming during formic acid addition was not observed. No build-up of oily or waxy material was observed in the off-gas equipment. Lab-scale mercury stripping behavior was similar to SB6 and SB7a. More mercury was unaccounted for as the acid stoichiometry increased.

TABLE OF CONTENTS

LIST OF TABLES

LIST OF FIGURES

LIST OF ABBREVIATIONS

ACTL	Aiken County Technology Laboratory
AD	Analytical Development
CPC	Chemical Process Cell
CS	Calcined Solids
CSTR	Continuous-Stirred Tank Reactor
DWPF	Defense Waste Processing Facility
FAVC	Formic Acid Vent Condenser
GC	Gas Chromatography
IC	Ion Chromatography
ICP-AES	Ion Chromatography-Atomic Energy Spectroscopy
IS	Insoluble Solids
KMA	Koopman minimum acid equation
MST	Monosodium Titanate
MWWT	Mercury Water Wash Tank
PSAL	Process Science Analytical Laboratory
REDOX	Reduction/Oxidation Potential
SBx	Sludge Batch number x
SME	Slurry Mix Evaporator
SRAT	Sludge Receipt and Adjustment Tank
SRNL	Savannah River National Laboratory
SS	Soluble Solids
SVOA	Semi-Volatile Organic Analysis
TIC	Total Inorganic Carbon
TOC	Total Organic Carbon
TS	Total Solids
TT&QAP	Technical Task and Quality Assurance Plan
TTR	Technical Task Request
VOA	Volatile Organic Analysis
WAPS	Waste Acceptance Product Specification

1.0 Introduction

Lab-scale DWPF simulations of Sludge Batch 7b (SB7b) processing were performed. Testing was performed at the SRNL-ACTL. The primary goal of the simulations was to define a likely operating window for acid stoichiometry for the DWPF SRAT. In addition, the testing established conditions for the SRNL Shielded Cells qualification simulation of SB7b-Tank 40 blend, supported validation of the current glass redox model, and validated the coupled process flowsheet at the nominal (recommended) acid stoichiometry. Work was performed under the Task Technical and Quality Assurance Plan for SB7b simulant flowsheet studies written in response to HLW-DWPF-TTR-2011-0003.[1]

SB7b is comprised of material from Tanks 4, 7, and 12 that did not get incorporated into the original SB7, hereafter referred to as SB7a. The fresh SB7b slurry appears to be primarily made up of Tank 4 slurry with some Tank 12 and an even smaller quantity of Tank 7. Tank 7 contents were primarily the byproducts of chemically cleaning Tanks 5 and 6 with oxalic acid. The result of the blending was to produce a batch that was high in noble metals (from Tank 4) and fairly low in mercury (low HM sludge fraction). Composition projections changed frequently as preliminary tank-to-tank transfers were made, as sample results became available, and as projected needs for caustic additions were solidified. SB7b-Tank 51 simulant was prepared in March 2011 and tested in April 2011. The Tank 51 simulant was intended to be used in Phase I of the SB7b simulant program to support qualification of SB7b-Tank 51 slurry prepared in the SRNL Shielded Cells from a SB7b-Tank 7 sample (FTF-07-11-3), the SB7a Confirmation Sample (HTF-51-11-28), an H canyon Pu solution, and a supernate adjustment.

Subsequently, a decision was made to qualify SB7b-Tank 40 slurry in the Shielded Cells simulation. Available Tank 4, 7, 12, and SB7a simulants were blended to synthesize a SB7b-Tank 40 (blend) simulant which was characterized for use in lab-scale SRAT simulations. This testing was originally planned as Phase II of the SB7b simulant work where an acid window would be developed for use in DWPF processing. At about this time, revised composition projections, driven largely by the SB7a Waste Acceptance Product Specification (WAPS) sample results (HTF-40-11-66), indicated that the composition of SB7b was moving into a region that would not support waste loadings of up to 40% waste oxides in glass (a nominal 36% waste loading with up to a ±4% window for uncertainties). The most obvious driver was that washing to reduce sulfur to an acceptable level was reducing sodium to an unacceptable level. Several alternate washing scenarios were derived, and the addition of some sodium hydroxide was also considered as a way to maintain sodium concentration while reducing sulfur concentration. Glass assessments were finding that a maximum waste loading of about 39% was possible only in a 1-2% band of wt.% Na_2O in the waste oxides.

In the Shielded Cells, some of the SB7b-Tank 51 simulant was combined with some of the SB7a WAPS sample to produce a SB7b-Tank 40 slurry for the Shielded Cells qualification work. The blend was 29% Tank 51 on an insoluble solids basis. Analytical data for this sample indicated that no extra sodium was needed, since it was near the target addition needed to find an acceptable glass window. Tank 40 and Tank 51 data combined with projected transfer masses indicated, at varying times, that from 2-6% additional Na_2O in the sludge oxides would be needed for waste loading considerations. Simulant lab-scale work to support the Shielded Cells qualification was needed by mid-June. Two lab-scale DWPF scoping simulations were performed at a reasonable acid stoichiometry with a well characterized simulant already on hand to which was added a mixture of sodium hydroxide and sodium oxalate to align it with what was

being considered for SB7b in terms of acid consumers, while mercury and noble metals were trimmed in at the best estimates for SB7b as well. These two runs were followed by four lab-scale simulations using the SB7b-blend simulant with added caustic covering four different acid stoichiometries. Results from these simulations were used to set processing conditions for the SB7b Shielded Cells qualification simulation, SC-12.

Following completion of the Shielded Cells qualification, a fifth SB7b simulant run was made using the remaining SB7b blend simulant. This test demonstrated the coupled DWPF flowsheet incorporating streams from the Actinide Removal Process (ARP) and Modular Caustic Side Solvent Extraction Unit (MCU, C = CSSX). ARP slurry was added at 7,000 gallons relative to 6,000 gallons of receipt slurry from Tank 40, while MCU solution was added at 8,000 gallons on the same basis. Noble metal and mercury targets were adjusted slightly based on the latest sample results (SB7a WAPS and first SB7b Tank 51 confirmation samples). The run was performed in early August 2011.

The main body of this report documents the four acid stoichiometry runs and the coupled flowsheet run that started with SB7b blend (Tank 40) simulant, since these are of primary interest. SRAT and Slurry Mix Evaporator (SME) processing data are presented. Appendix A includes the data for the initial SB7b-batch (Tank 51) simulant tests which were at three different acid stoichiometries (Phase I). Appendix B includes the data from the two SRAT/SME runs with two bounding levels of added caustic (bounding in that both had more caustic added than the SB7b blend simulant tests).

Several sidebar studies occurred during these ten process simulations to continue to add to the understanding of CPC chemistry. These included the following:

- Slurry mercury concentration versus time data.
- Data on mercury solubility in the SRAT supernate.
- Mercury material balance data, but only for streams where process knowledge indicated significant mercury could be expected.
- The frequency of suspect, or off trend, mercury concentration data during slurry sampling.

These items all tied into the on-going investigation of mercury chemistry during the SRAT process.

In addition, a new SRAT vessel design was undergoing testing during SB7b. It was used for the two caustic addition scoping runs discussed in Appendix B. It differs from the old lab-scale SRAT design in using heating rods immersed in the slurry to deliver the process heat instead of using an external heating mantle. The new SRAT design allows visual observation of part of the bottom of the SRAT vessel during processing. The new SRAT design was not considered fully vetted in time for the SB7b blend simulant work.

Finally, the three SB7b-batch simulant tests were used to evaluate the efficiency of using hexane rinses and hexane extractions to perform an accounting of the 747 antifoam in the system. The principal idea was to extract the organic antifoam from the inorganic solids and aqueous supernate, then to quantitatively identify the antifoam (or its decomposition products) in the various samples. This was very preliminary work, and it is discussed in the context of the SB7b-batch simulations in Appendix A.

2.0 Summary of Experimental and Analytical Methods

2.1 Process and Sample Analytical Methods

The automated data acquisition system developed for the 4-L SRAT rigs was used to collect electronic data on a computer. Collected data included SRAT slurry temperature, bath temperatures for the cooling water to the SRAT condenser and Formic Acid Vent Condenser (FAVC), slurry pH, SRAT mixer speed and torque, air and helium purge flows (helium is used as an internal standard and is set to 0.5% of the nominal SRAT air purge flow). Cumulative acid addition volume data were collected from the automated dispensers using an algorithm that matches the indicated total on the dispenser. Raw GC chromatographic data were acquired on a separate computer interfaced to the data acquisition computer.

Agilent 3000A micro GC's were used for all runs. The GC's were baked out before and between runs. Column-A can collect data related to He, H_2, O_2, N_2, NO, and CO, while column-B can collect data related to CO_2, N_2O, and water. GC's were calibrated with a standard calibration gas containing 0.510 vol% He, 1.000 vol% H_2, 20.10 vol% O_2, 50.77 vol% N_2, 25.1 vol% CO_2 and 2.52 vol% N_2O. The calibration was verified prior to starting the SRAT cycle and after completing the SME cycle. Room air was used to give a two point calibration for N_2. No evidence for CO generation was obtained while examining the region of the chromatogram where it would elute. The chilled off-gas leaving the FAVC was passed through a Nafion dryer in counter-current flow with a dried air stream to reduce the moisture content at the GC inlet. The dried, chilled off-gas stream was sampled by a GC from the beginning of heat-up to temperature to start the SRAT cycle through most of the cool down following the SME cycle.

Process samples were analyzed by various methods. Slurry and supernate elemental compositions were determined by inductively coupled plasma-atomic emission spectroscopy (ICP-AES) after lithium metaborate and sodium peroxide fusions at the Process Science Analytical Laboratory (PSAL). Slurry samples were calcined at 1100°C. The main advantage of this approach is to permit easier comparisons between SRAT product elements and sludge elements. Noble metals and mercury are trimmed uniquely to each SRAT, and their concentrations are known more accurately from material balance considerations than they could be from ICP-AES analyses.

Water soluble slurry anions were determined by ion chromatography (IC) on 100-fold weighted dilutions of slurry with water followed by filtration to remove the remaining insoluble solids. SRAT cycle, SRAT product, and SME product slurry samples were submitted to PSAL for mercury analysis by ICP-AES. A SB7b-batch and an SB7b-blend simulant sample were submitted to AD for total inorganic carbon analysis of both the starting slurry and the supernate. These two slurries were analyzed by PSAL for slurry and supernate density using the Anton-Parr instrument. Starting sludges were titrated to pH 7 using the PSAL auto-titrator to determine the base equivalents for input into the stoichiometric acid equation. Samples from the ammonia scrubber reservoir vessel were analyzed by AD using cation chromatography for ammonium ion.

SRAT and SME product slurries were submitted to AD for a special acid strike preparation used to draw insoluble oxalate into solution.[2] Analysis of the prepared samples was by IC. The five SB7b-Tank 40 SRAT products and five SME products were submitted for this analysis.

As part of the scoping SB7b-Tank 51 (batch) simulant testing, some special samples were taken for analysis by volatile organic analysis (VOA) and semi-volatile organic analysis (SVOA).

Samples of various condensates, as well as the SME product slurry, were extracted into hexane in an attempt to draw 747 antifoam (or its decomposition products) out of the aqueous phase. A high level summary of the findings is included in Appendix A where the SB7b batch testing is summarized.

As a second part of the SB7b-Tank 51 testing, a sample of SRAT product slurry was diluted with de-ionized water and centrifuged to concentrate the insoluble solids in a reduced formate concentration supernate. The solids (in diluted supernate following decanting) were submitted to AD for total organic carbon analysis. The premise was that the organic carbon would be partly due to antifoam adsorbed onto the particle surfaces.

As a third part of the SB7b-Tank 51 testing, samples of the SRAT dewater condensate were analyzed for silicon. Antifoam molecules terminate in end groups composed of multi-methyl siloxanes, so silicon is a potential marker for volatilized or steam stripped antifoam lost from the SRAT slurry. The test cannot discriminate between silicon derived from antifoam and silicon from the SiO_2 in the slurry, but it can bound potential antifoam losses to the condensate. SB7b-Tank 51 results are in Appendix A. This analysis was also performed on the SRAT dewater condensate samples from the SB7b-Tank 40 testing covered in the main body.

2.2 Simulant Preparation and Characterization

The SB7b simulants were prepared from blends of Tank 4, Tank 7, and Tank 12 simulants originally prepared for SB7a testing plus some leftover blended SB7a simulant. All four simulants were fabricated by the current continuous stirred tank reactor (CSTR) precipitation method.[3] This method involved the following processing steps:

- A slurry of precipitated MnO_2 was prepared.
- An acidic metal nitrate solution was prepared.
- The two were combined and fed to the CSTR along with a 50 wt.% sodium hydroxide solution to produce a slurry of hydrous metal oxide and hydroxide solids in a sodium nitrate solution at a pH of about 9.5.
- The slurry was contacted with sodium carbonate to permit conversion of some of the hydroxides to carbonates.
- The slurry was decanted and washed until the nitrate concentration was below the target supernate nitrate concentration.
- The slurry was concentrated to a point consistent with the targeted total solids value for the final slurry.
- Silica, TiO_2, and sodium salts were added to complete the preparation.

A SB7b batch (Tank 51) simulant was prepared and characterized first (see Appendix A). As discussed earlier, this simulant was intended to support qualification using a washed Tank 51 sample in the Shielded Cells. This qualification approach does not constrain the relative volumes of Tank 51 and Tank 40 at the time of transfer, but carries the implicit assumption that the individual qualifications bound any blend that is actually prepared. A SB7b blend (Tank 40) simulant was prepared to support DWPF flowsheet studies. Subsequently, a decision was made to qualify SB7b using a Shielded Cells prepared blend targeting the Tank 40 composition. This decision rendered the results of the three SRAT/SME simulations with SB7b-batch simulant less significant to the qualification effort, and they are covered in Appendix A.

Frit assessments including glass property predictions for SB7b indicated potential issues with high sulfur, high nickel, and low sodium. A potential fix would have been to add sodium hydroxide to SB7b after washing the sulfur to an acceptable level. A significant caustic addition was indicated, one that would increase the Na_2O content of sludge (on an oxide basis) by up to 4-6% in the waste oxides. Therefore, Phase II SB7b-Tank 40 testing was conducted to bound the processing impacts of a potential caustic addition.

Because of the uncertainty in the path forward for SB7b with respect to a caustic addition, and because of an aggressive schedule and limited quantity of SB7b simulant, a decision was made to bound the acid demand of the simulant be adding caustic equivalent to a ~4.7% increase in Na_2O in the waste oxides. There were also conflicting data concerning insoluble sodium in SB7b. Some results indicated that all sodium was in the supernate phase, while other data indicated some insoluble sodium was present. A small sodium oxalate addition was made along with the sodium hydroxide addition to help increase total sodium in the simulant and to also cover uncertainties in the oxalate acid strike analytical method (typically of order 20-25%). The caustic and sodium oxalate trim additions were made at the start of each SRAT batch. Consequently, most analytical data on the SB7b blend simulant is for the simulant without added caustic and oxalate, i.e. untrimmed. Equivalent values for the trimmed simulant were calculated based on the masses blended with the exception of base equivalents. The base equivalents were measured on a trimmed SRAT receipt sample. This one measurement was selected because it is the major input to the DWPF stoichiometric acid equation. The result was used to check the value obtained by combining the base equivalents of the untrimmed simulant plus the added caustic to predict the base equivalents after trimming. The caustic addition increased base equivalents from 0.51M to 0.77M (calculated) or 0.79M (measured).

Table 1 presents the average elemental results of duplicate analyses of two slurry samples from the SB7b-blend untrimmed simulant calcined at 1100° C. Adjusted results for the simulant following additions of sodium hydroxide and sodium oxalate are also given. These results are compared to the composition of the SB7b blend qualification run in the SRNL Shielded Cells, SC-12.[4] SC-12 SRAT receipt elemental data are given with the radioactive constituents (Hot) and on a renormalized basis after removing the oxides of thorium and uranium. Zirconium is known to be biased low in the SC-12 results (only partially dissolved). A Tank Farm projection for the composition of SB7b is given for comparison to SC-12 and the simulant results. Certain minor elements were not projected (n.p.) for SB7b.

SRAT receipt sample results are also given for the SB7b-10 coupled simulant run in Table 1. The SB7b-10 SRAT receipt sample includes the contribution from the ARP slurry, the most significant of which is from the MST. Results were generally as expected. The simulant was reasonably close to desired values but nickel projections are one exception (raising nickel in the simulant blend much higher than 3.5% was not practical without starting over and making new simulants). Nickel in SB7b will be at the highest concentration in the waste oxides of any sludge batch to date. The significance of the high nickel, however, seems to be primarily in the melter/glass property area rather than in the chemical processing area.

Table 1. Elemental composition of SRAT feeds calcined at 1100° C, wt%

Element	SB7b Untrimmed Simulant	SB7b Trimmed Simulant	SC-12 Receipt Re-scaled	SC-12 Receipt (Hot)	SB7b Projection (Hot)	SB7b-10 Receipt Sample
Al	12.3	11.3	13.2	12.0	12.0	9.76
Ba	0.12	0.11	0.15	0.14	0.10	0.11
Ca	0.84	0.78	0.96	0.87	0.93	0.78
Ce	0.19	0.17	0.36	0.33	0.13	0.12
Cr	0.05	0.05	0.07	0.06	n.p.	0.05
Cu	0.04	0.04	0.12	0.11	0.12	0.05
Fe	23.0	21.2	21.1	19.1	19.6	18.0
K	0.08	0.08	<0.03	<0.03	0.06	0.05
La	0.10	0.09	0.12	0.11	n.p.	0.07
Mg	0.39	0.35	0.42	0.38	0.43	0.43
Mn	4.54	4.18	4.51	4.09	4.68	3.82
Na	16.9	21.4	21.1	19.1	16.0	20.7
Ni	3.80	3.50	4.36	3.96	3.77	2.97
P	<0.10	<0.10	0.15	0.14	n.p.	<0.10
Pb	0.02	0.02	<0.05	<0.05	n.p.	<0.01
S	0.39	0.36	0.69	0.63	0.43	0.42
Si	1.89	1.74	1.65	1.50	1.55	1.41
Sn	0.02	0.02	<0.06	<0.05	n.p.	0.05
Ti	0.02	0.02	0.03	0.02	n.p.	3.53
Zn	0.06	0.06	0.07	0.07	n.p.	0.06
Zr	0.28	0.26	0.21	0.19	0.14	0.25
Th	-	-	-	1.36	1.64	-
U	-	-	-	6.55	6.61	-

n.p. – not projected
SB7b-untrimmed simulant was simulant without added caustic and oxalate
SB7b-trimmed simulant included added caustic and oxalate
SC-12 was the Shielded Cells qualification run of SB7b-Tank 40
SB7b-10 was the coupled simulant run

Table 2 presents results for total, insoluble, soluble and calcined wt.% solids, slurry and supernate density, slurry base equivalent molarity, slurry and supernate total inorganic carbon (TIC), and the slurry anion results from IC. Untrimmed and trimmed SB7b-blend simulant values are compared to SC-12 (updated nitrite, nitrate, slurry TIC, oxalate, and base equivalents from a resample[5]) and to SB7b-10 (post-ARP SRAT receipt).

Table 2. Simulant and Radioactive Feed Properties

	SB7b blend untrimmed	SB7b blend trimmed	SC-12 blend (updated)	SB7b-10 SRAT receipt
Total solids, wt.%	15.4	16.2	16.1	17.0
Insoluble solids, wt.%	9.8	10.0	10.6	8.7
Soluble solids, wt.%	5.6	6.2	5.5	8.3
Calcined solids, wt.%	11.8	12.1	11.8	12.6
Slurry density, g/mL	1.12	1.12	1.12	1.14
Supernate density, g/mL	1.04	1.05	1.06	1.06
Slurry base equiv., mol/kg	0.51	0.78	0.49	0.78
Nitrite, mg/kg slurry	9,490	8,980	10,300	7,990
Nitrate, mg/kg slurry	6,030	5,700	5,570	10,500
Sulfate, mg/kg slurry	1,800	1,700	2,190	2,080
Oxalate, mg/kg slurry	3,100	5,900	3,330	5,820
Chloride, mg/kg slurry	<10	230	<250	270
Slurry TIC, mg/kg slurry	1,240	1,170	972	1,180
Supernate TIC, mg/L supernate	1,100	1,040	1,050	1,040

The SB7b blend tests had 3,320 g of sodium-trimmed starting sludge (before minor trim chemicals and rinse water) except for the ARP/MCU test which started with 2,861 g. The quantity of ARP slurry added to the SB7b-10 simulant had a solids mass equivalent to that in 876 g of trimmed SB7b blend simulant. Therefore, the ARP/MCU test was about 10% larger in terms of solids mass than the other four SB7b blend tests.

Accurate projections for mercury and noble metals in SB7b blend were not available prior to the acid window simulant testing. A weighted average of concentrations from the SB6 and SB7a qualification samples, plus wash endpoint adjusted values from a SB7b-Tank 7 sample, were used to estimate these concentrations. Rhodium was trimmed as a solution of $Rh(NO_3)_3$ containing 4.93 wt.% Rh. Ruthenium was added as the dry trivalent chloride salt at a purity of 41.73 wt.% Ru. Palladium was trimmed as a solution of $Pd(NO_3)_2$ containing 15.27 wt.% Pd. Silver was added as the dry nitrate salt $AgNO_3$. Mercury was trimmed as dry HgO (yellow mercuric oxide, which is more finely ground than red mercuric oxide).

Targets for the SB7b blend testing are given in Table 3 along with the reported values for the SB7a WAPS and SC-12 (SB-7b) SRAT receipt sample from the qualification run for comparison.[6, 7] SB7b was projected to include 71% of its solids from SB7a on a calcined basis. The four SB7b acid stoichiometry window tests all used the same mercury and noble metal concentration targets (in spite of the wording in SRNL-L3100-2011-00176 that says there was a 5% change from the first pair to the second pair).[8] SB7b-10 was trimmed for mercury fairly conservatively, since there were emerging indications that the initial four blend simulant tests had not bound the concentration of Hg, and SB7b-10 used the last of the available SB7b blend simulant. SB7b-10 targets are reported for the blend of sludge and ARP total solids prior to SRAT acid addition (SRAT receipt sample basis), not for the simulated Tank 40 slurry.

Table 3. Noble metal and mercury, wt.% in total solids

	SB7b (Tank 40)	SB7a WAPS	SC-12 (Tank 40/SB7b)	SB7b-10 (with ARP)
Rh, wt%	0.023	0.019	0.021	0.021
Ru, wt%	0.108	0.094	0.100	0.105
Hg, wt%	1.37	1.9	1.34	1.75
Pd, wt%	0.003	0.003	0.002	0.003
Ag, wt%	0.014	<0.02	0.011	0.017

SB7b (Tank 40) is the trimmed starting simulant for the Phase II runs
SB7a WAPS is roughly 71% of SB7b blend in Tank 40-given for comparison
SC-12 is the SB7b-Tank 40 slurry prepared in the Shielded Cells
SB7b-10 is the trimmed blend simulant combined with ARP slurry

SB7b catalytic and mercury stripping behavior was expected to be fairly similar to that of SB7a, assuming the SRAT slurry was concentrated to about 25 wt.% total solids in both cases, but at reduced mercury concentration (reduced stripping time in the SRAT).

2.3 Chemical Process Cell Simulation Details

The trimmed SRAT receipt volume was about 3.0 L for the SB7b-Tank 40 testing. The 4-L lab-scale SRAT equipment was used for these tests. A photo of the 4-L rig is shown in Figure 1.

Figure 1. Lab-scale SRAT apparatus

A modified lab-scale SRAT rig design was used for two scoping runs with generic simulant that were performed to evaluate the impact of adding significant caustic to a characterized slurry in the context of the stoichiometric acid demand. The modified design has off-center agitation in the SRAT and uses two resistance heated rods as the heat source rather than the heating mantle. More details about the new design are in the CPC equipment set-up reference.[9]

Complete integration of the new design into the process control computer was not in place, and SRAT temperature had to be controlled manually. Because the new design was still in evaluation, and because the quantity of SB7b simulants was limited, the SB7b batch and blend tests were performed in the lab-scale equipment design that dates back to SB4. It is anticipated, however, that future sludge batch testing will be done in the modified design. There were no operational issues with the two scoping runs with generic simulants, and other test programs (next generation solvent, mercury chemistry) have also used the modified design successfully.

The reservoir below the ammonia scrubber was charged with a solution of either 749 or 999 g of de-ionized water and 1 g of 50 wt.% nitric acid. (This reservoir is not called the Slurry Mix Evaporator Condensate Tank, or SMECT, because condensates from the SRAT and SME are not drained into it.) The dilute acid reservoir solution was recirculated by a MasterFlex driven Micropump gear pump at about 300 mL per minute to a spray nozzle at the top of the packed section.

A modified SRAT condenser/mercury water wash tank (MWWT) combination was used on the five SB7b blend runs (and two generic simulant scoping runs). The new configuration drops SRAT/SME condensate vertically into the MWWT at a point below the gas-liquid interface inside the MWWT. This significantly reduced the hold-up of mercury and antifoam degradation products in the condenser drain leg that had been seen in various prior test programs.

Initial acid calculations were based on the Koopman minimum acid (KMA) requirement equation.[10]

$$\frac{moles\ acid}{L\ slurry} = base\ equivalents + Hg + soluble\ TIC + .5*Ca + Mg + .0*nitrite + .5*Mn$$

Four different stoichiometric factors were used in the four sludge-only acid calculations, 105%, 110%, 130%, and 140%. The ARP/MCU run was matched to the nominal, or 110%, case. Acid calculations were also performed using the current DWPF algorithm for comparison:[11]

$$\frac{moles\ acid}{L\ slurry} = base\ equivalents + 2*total\ TIC + 0.75*nitrite + 1.2*Mn + Hg$$

The results of these two calculations for the trimmed SB7b blend and SB7b-ARP combination simulants are summarized in Table 4. The table also includes the actual acid additions made based on 110% of the Koopman minimum acid equation (maximum acid) and the equivalent DWPF stoichiometric factors (percent) to go from the DWPF acid equation values to the actual acid additions.

Table 4. Stoichiometric acid calculation results, moles acid/L trimmed slurry

	DWPF Eqn. moles/L	Koopman Min. moles/L	Actual addition at 110%, moles/L	Equivalent DWPF factor
SB7b blend	1.264	1.284	1.413	112%
SB7b-10	1.097	1.123	1.239	113%

Total acid was partitioned between formic and nitric acids using the current RedOx equation.[12] Assumptions of 20-35% formate loss and of 10% to -15% nitrite-to-nitrate conversions were also made to enable this calculation to be performed. The assumptions were based on prior experience with the SB7a[13] and SB7b-Tank 51 simulants (Appendix A). Smaller formate loss and higher nitrite-to-nitrate conversion were assigned to lower acid stoichiometry. These assumptions gave a formic acid fraction of the total acid moles in the range of 0.82-0.87 (or, equivalently nitric acid fraction in the 0.18-0.13 range). The highest formic acid fraction was in the ARP run, because the ARP addition significantly increased the nitrate ion content of the feed.

Scaled design basis DWPF SRAT/SME processing conditions were generally used. The SRAT and SME cycles, however, did not have a heel from a prior batch. R&D directions were prepared for each run and used to supplement the standard SRNL procedure for non-radioactive CPC simulations.[14]

- The SRAT air purge scaled to 230 scfm in DWPF.
- A 100 ppm antifoam addition was made prior to nitric acid addition.
- A 100 ppm antifoam addition was made prior to formic acid addition.
- Nitric and formic acid addition were made at 93 °C.
- Acids were added at two gallons per minute scaled per the discussion below.
- A 500 ppm antifoam addition was made prior to going to boiling following acid addition.
- Boiling assumed a condensate production rate of 5,000 lb/hr at DWPF scale.
- SRAT dewatering took about 3.6-4.0 hours to produce a 25 wt. % total solids slurry.
- Reflux followed dewatering. The end of the 12-hour reflux period defined the end of the SRAT cycle (theoretically this was sufficient to strip mercury to specifications).
- The SME air purge scaled to 74 scfm in DWPF.
- A 100 ppm antifoam addition was made at the start of the SME cycle.
- Canister decontamination water additions and dewaterings were not simulated.
- Two frit 418-water-formic acid additions were made targeting 36% waste loading.
- The SME was dewatered following each frit slurry addition.
- The final SME solids target was 48 wt.%.

Twelve to fifteen samples were taken during each SRAT cycle to monitor the progress of the main reactions. Major cations and anions were checked immediately after acid addition. Samples were pulled during boiling to monitor suspended and dissolved mercury in the SRAT slurry. These samples were pulled directly into digestion vials to eliminate potential segregation of mercury during sub-sampling/aliquoting steps. The SRAT and SME product slurries were sampled similarly once they had cooled to 90° C while the vessel contents were still mixing.

Additional SRAT product samples were taken for compositional and solids analyses after the product had cooled further. The MWWT and FAVC were drained and the condensates weighed after both the SRAT and SME cycles. Elemental mercury was separated from the aqueous phase in the post-SRAT MWWT sample, and the mass of the mercury-rich material determined. Beads

of elemental mercury were also recovered from a few of the SME dewatering condensates and weighed (depending on how big or numerous the bead(s) appeared to be).

Gas chromatograph off-gas data were scaled to DWPF flow rates. The calculation methodology has been previously documented.[15] An internal standard flow is usually established with helium. Other gas flow rates are determined relative to helium by taking the ratio of the two gas volume percentages times the helium standard flow. The result is normally scaled by the ratio of 6,000 gallons of fresh sludge divided by the volume of fresh sludge in the simulant SRAT charge. Several issues with this approach were noted in these tests. The first was that the simulant was lower in total solids than DWPF would likely process (without first caustic boiling it to increase solids concentration). Dividing an inflated simulant charge volume into 6,000 gallons would lead to a non-conservative DWPF gas flow rate. Therefore, scaling was done assuming that a 25 wt. % total solids SRAT product of 4,500 gallons was more appropriate than one assuming an arbitrary solids concentration SRAT receipt slurry of 6,000 gallons. The same scaling was applied to the boil-up rates, air purge rates, and acid addition rates to be consistent.

Second, some of the ACTL GCs are showing signs of aging. The oldest two Agilent 3000's are about eight years old (predate use of Nafion dryers at ACTL by 5-6 years). It was noted that calibration gas results obtained on column A (He, H_2, O_2, N_2) are sometimes fairly sensitive to the line pressure (typically just 2-5 psig, which is well below the column pressure of about 25-30 psig). It has also been noted that oxygen in room air reads in the 16-19 vol% range after calibration, instead of 20-21 vol%. Both observations seem to imply that smaller sample volumes are being injected into column A (injection volume to column B could not be evaluated) at atmospheric pressure (experimental pressure) than at calibration gas pressure. The result is that the absolute values for the He, H_2, and O_2 concentrations could be low. Nitrogen is handled differently because it has a two point calibration with calibration gas and room air. The ratios of H_2/He and O_2/He are sufficient for calculating off-gas species flow rates. The ratios of CO_2/He and N_2O/He, however, may not be unbiased, since species volume percentages from two different columns are being combined (the fraction of nominal sample volume being injected is likely not one-to-one in the A and B columns if one column is partially plugged or otherwise restricted).

Third, the original method developed for the Agilent 3000 has not done as well lately (on repaired GCs) in producing clean chromatographs with baseline separated peaks. The severity of the issue varies from instrument to instrument. Revised methods have been developed for two GCs so far, but not before the SB7b test data were obtained. In the case of SB7b-10 (ARP/MCU) the issue was particularly severe for the He:H_2 split. The data were analyzed two ways, one with H_2/He ratios and one with H_2/N_2 ratios (scaled using the air purge flow). The DWPF-scaled flow rates for hydrogen differ by about 30% from the two calculations. Ideally there would be no variation. Complicating the analysis is the two point calibration for nitrogen which is likely valid near 78 vol% (air at atmospheric pressure) but may be suspect near the calibration gas concentration of about 50 vol% (depending on the severity of the calibration pressure dependence). Parallel testing of the helium and air MKS mass flow controllers indicated that they were performing as expected, i.e. gas mass flow controller behavior cannot explain the differences in the two calculations of off-gas flow. Additional method development and calibration gas pressure impact testing are indicated for some of the GCs.

3.0 Discussion of Process Simulation Results

3.1 SRAT Cycle

The five SB7b-blend simulant SRAT cycles are discussed below. Chemical and physical data from process samples will be presented first followed by off-gas data. SB7b-batch SRAT cycles are discussed in Appendix A, and scoping SRAT studies with caustic spiked simulant are discussed in Appendix B.

3.1.1 *SRAT Cycle Slurry Samples*

Formate loss and nitrite/nitrate results are presented in Table 5 for samples taken a few minutes after formic acid addition was completed and for the SRAT product.

Table 5. SRAT Anion Reactions

	SB7b-6	SB7b-8	SB7b-7	SB7b-9	SB7b-10
KMA stoichiometry, %	105	110	130	140	110
Formate loss, post acid, %	9	9	12	10	5
Nitrite loss, post acid, %	38	0†	45	98	99
Nitrate gain, post acid, %	12	13	19	6	28
Formate loss, SRAT product, %	18	18	35	33	15
Nitrite-to-nitrate, SRAT product, %	15	8	-14	-12	2
Nitrite loss, SRAT product, %	97	100	100	100	100

† SB7b-8 should have had nitrite after acid addition (based on off-gas data), but no detectable amount was reported in the analysis

The broad view is that SB7b-Tank 40 processes like HM-dominated waste similar to SB7a and SB6 (formate loss typical of a fairly catalytically active sludge, some nitrate to ammonia formation, relatively narrow acid stoichiometry window, etc.) The post-acid nitrate gain increased with increasing acid stoichiometry until SB7b-9, while the fraction of nitrite destroyed increased in parallel. It is not clear if nitrate destruction (part of the ammonium ion formation sequence) had started in SB7b-9 before the end of acid addition or if the analytical result should be discounted. SB7b-10, the ARP/MCU run, seemed to be part of a different trend than the other four simulations at the end of formic acid addition. The high nitrite loss after acid addition at 110% acid stoichiometry was unexpected, and it was not confirmed by the N_2O off-gas data.

SRAT product nitrite in SB7b-6, Table 6, met the constraint of <1000 mg/kg slurry at a value of 366, but showed that 105% stoichiometry was essentially the minimum acid that would achieve adequate nitrite destruction. Overall nitrite-to-nitrate conversion fell with increasing acid stoichiometry, which has been typical behavior since SB6 (or earlier) for catalytically active sludges producing ammonia from nitrate. Formate loss generally increased with increasing acid stoichiometry as in the past (the formate mass loss increased with increasing acid even if the percent loss dipped slightly). In all of this analysis the reader should bear in mind that accumulation and propagation of uncertainties put roughly ±10% error bars around the values, e.g. an 18% overall formate loss is probably in the range 8-28%.

Analytical water-soluble slurry anion data for the five SB7b-Tank 40 SRAT products are given in Table 6. Oxalate by acid strike (as) is also given.

Table 6. SRAT Product Anions, mg/kg slurry

Anions	SB7b-6	SB7b-8	SB7b-7	SB7b-9	SB7b-10
F^-	<100	<100	<100	<100	<100
Cl^-	270	270	260	280	330
NO_2^-	370	<100	<100	<100	<100
NO_3^-	27,900	28,800	27,600	29,900	31,300
$SO_4^=$	1,240	1,230	1,310	1,205	2,370
$C_2O_4^=$ (wd)	1,450	1,370	1,100	1,380	2,090
$C_2O_4^=$ (as)	8,050	6,240	8,640	6,160	7,530
HCO_2^-	51,300	54,300	47,800	55,100	59,500
PO_4^{3-}	<100	<100	<100	<100	<100

wd – water dilution, as – acid strike

The higher values of SB7b-10 relative to the other four SRAT products appear to be due to over concentrating the solids in the SRAT product by 10%. A drop in acid strike oxalate from about 8,000 to 6,000 occurred from the first two runs (SB7b-6 and 7) to the second two runs (SB7b-8 and 9). It is uncertain what the significance of these data might be, but on average a small (~10%) loss of oxalate during SRAT processing was indicated in the four sludge-only flowsheet runs. SB7a testing did not indicate much oxalate loss (perhaps 0-5%), but SB3 simulant testing showed a potential for oxalate loss during processing. Noble metal catalyzed wet air oxidation of oxalate was suspected to be splitting oxalate apart at the carbon-carbon bond.

Elemental wt.% data for the five SRAT products calcined at 1100 °C are given in Table 7. Lead, chromium, and the noble metals (not listed) tend to be underreported in SRAT product calcined solids. General consistency in values for the first four SRAT products is seen as desired. The fifth SRAT product is from the ARP/MCU run and should have a different composition. The 3.4 wt.% Ti primarily relates to the monosodium titanate in this slurry. Sodium was also increased by the introduction of MST.

Table 7. SRAT Calcined Elements at 1100 °C-wt.%

Rnn ID	SB7b-6	SB7b-8	SB7b-7	SB7b-9	SB7b-10
Al	11.5	11.4	11.4	11.6	9.9
B	<0.10	<0.10	<0.10	<0.10	<0.10
Ba	0.11	0.11	0.10	0.11	0.12
Ca	0.74	0.75	0.75	0.74	0.79
Ce	0.16	0.16	0.16	0.16	0.15
Cr	0.05	0.05	0.05	0.05	0.06
Cu	0.04	0.04	0.02	0.03	0.05
Fe	20.1	20.0	20.4	20.4	18.0
K	0.07	0.07	0.06	0.09	0.06
La	0.08	0.08	0.07	0.08	0.07
Li	<0.10	<0.10	<0.10	<0.10	<0.10
Mg	0.34	0.35	0.33	0.34	0.42
Mn	4.3	4.2	4.2	4.2	3.8
Na	19.0	18.8	18.9	18.8	20.8
Ni	3.5	3.5	3.5	3.5	3.0
P	<0.10	<0.10	<0.10	<0.10	<0.10
Pb	<0.010	<0.010	<0.010	<0.010	<0.010
S	0.39	0.39	0.38	0.39	0.44
Si	1.7	1.6	1.7	1.6	1.5
Sn	0.02	0.02	0.02	0.02	0.05
Ti	0.02	0.02	0.02	0.02	3.4
Zn	0.06	0.06	0.06	0.06	0.06
Zr	0.25	0.25	0.24	0.26	0.26

SRAT product solids data, densities, and pH are given in Table 8. The wt.% insoluble and soluble solids were calculated from the measured total slurry and supernate (dissolved) solids. The density measurements were made at 25 °C.

Table 8. Additional SRAT Product Properties

Run ID:	SB7b-6	SB7b-8	SB7b-7	SB7b-9	SB7b-10
Wt. % total solids	26.1	25.9	24.4	25.4	28.3
Wt. % insoluble solids	14.5	13.5	13.3	13.4	13.1
Wt. % soluble solids	11.6	12.4	11.1	12.0	15.2
Wt. % dissolved solids	13.4	14.4	12.8	13.9	17.5
Wt. % calcined solids	16.9	16.8	16.1	16.6	18.5
Slurry density, g/mL	1.19	1.19	1.18	1.20	1.20
Supernate density, g/mL	1.09	1.09	1.08	1.09	1.10
Product pH at 25 °C	7.44	7.39	8.72	8.03	8.33

The first four tests ended near the target of 25 wt.% total solids. Supernate density correlated well with the wt.% dissolved solids as expected. The pH data trended counter intuitively as in some previous catalytically active sludges, i.e. increasing the acid addition moles led to higher, rather than lower, SRAT product pH values. Some more discussion is given in the next section near Table 10.

The sample results for SB7b-10 found here and elsewhere consistently indicate that this slurry was concentrated past the target amount in the SRAT cycle. The SRAT receipt sample results indicate that it was most likely during the ARP addition and boiling period prior to the analytical sample. Removal of about 325 g of excess condensate prior to acid addition is indicated by the sample and mass balance data to explain the SRAT receipt and SRAT product results. This is significantly more than the tare weight of the collection vessel and is difficult to attribute to a single operator error. A check using the average reported boil-up rate times the total ARP boiling time indicated that (very) roughly 200 extra grams of condensate might have been produced (2305 g versus 2102 g), but much of the boiling time lacks a recent boil-up rate determination (in particular, no measurement after ARP addition completed). Therefore, the calculated condensate by this approach could be significantly higher than 200 g off from the 2102 g target (the cold ARP addition reduces the boil-up rate at a given heating load setting, so when it ends the boil-up rate typically goes up). Direct confirmation by reweighing the condensate is no longer possible, since the condensate was transferred to residue. In any event, the mass loss could have been partially or totally as uncondensed water vapor through a leak. There might have been a leak associated with the ARP addition tubing that was not included in the system at leak check time. (The system is checked for leaks in the normal operating configuration before and after the run, but the ARP addition configuration is not usually checked.)

3.1.2 *Mercury and Ammonia*

Mercury suspended/dissolved in the SRAT/SME slurry was tracked as a function of time during the process simulations. Mercury recovered in the MWWT was weighed. Noteworthy accumulations of mercury at other times were sometimes weighed as well, for example in some of the SME dewatering condensates. Condensate samples were not analyzed for mercury during the SB7b study, since prior tests have shown fairly low solubility (typically less than 5% of all added mercury has been found in a dissolved state in the overhead condensates).

SB7b-6 and 8 were the low acid simulations of the baseline flowsheet. They behaved similarly. Figure 2 shows the mass of mercury accounted for by the measured slurry concentration times the slurry mass relative to the initial grams of mercury as a function of time at boiling (SRAT and SME boiling time combined into one scale).

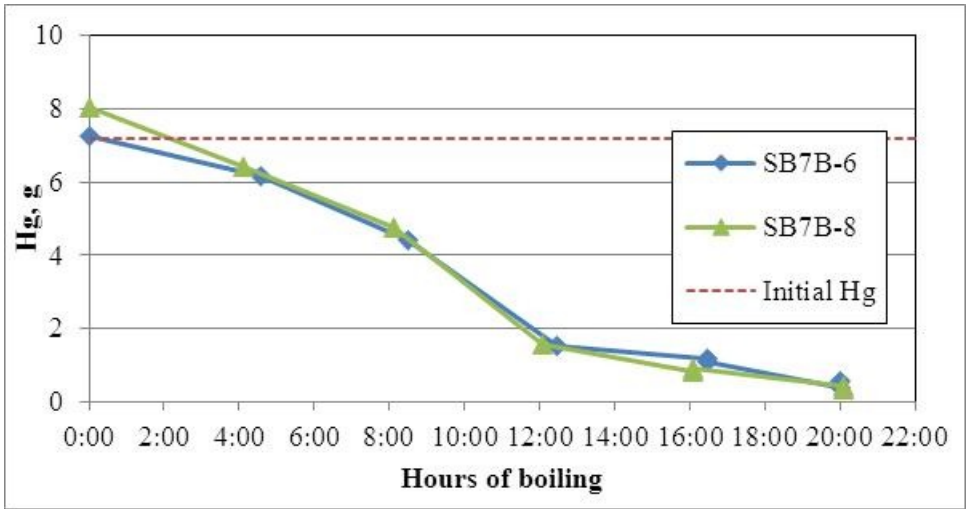

Figure 2. Low acid slurry mercury versus boiling time

The results from these two simulations, performed in different weeks in different hoods, are nearly identical. Although it appears that 90+% of the mercury was removed from the two SME product slurries (points near 20 hours), the recovery of elemental mercury in the MWWT was only 45-50%. Over 40% of the mercury is unaccounted for in this pair of runs. It is believed to have pooled at the bottom of the SRAT/SME vessel.

SB7b-7 and 9 were the two higher acid stoichiometry runs, and the slurry mercury behavior differed from the low acid runs as seen in Figure 3.

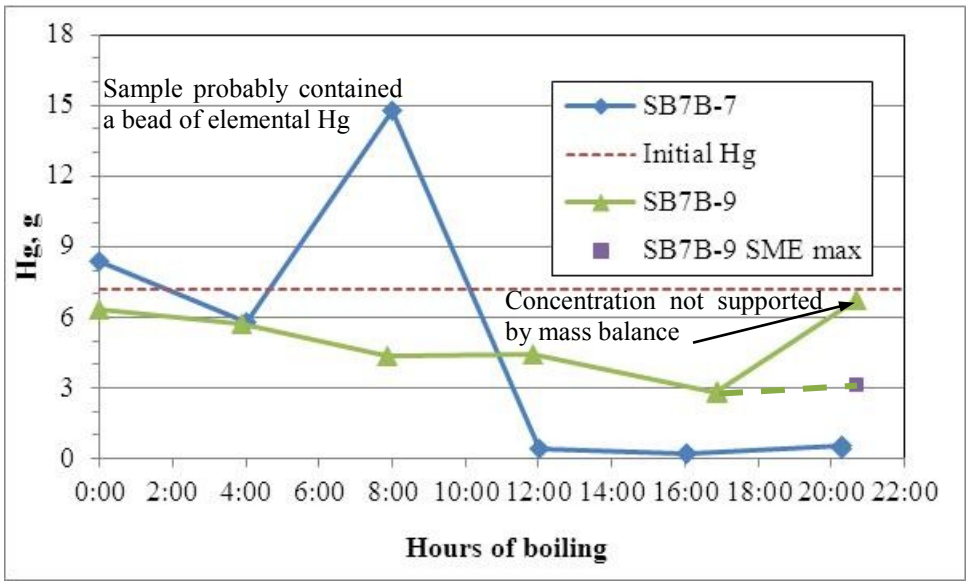

Figure 3. High acid slurry mercury versus boiling time

The data obtained confirm the presence of samples enriched in Hg above what could possibly be present in a well-mixed slurry sample. The likelihood of such samples was investigated during CPC simulations of the SB7b batch simulant which are discussed in Appendix A. SB7b-7 appeared to capture a bead of elemental mercury that caused the result to spike at 8:00 of boiling time. Subsequent samples indicated less than 0.5 g in the slurry, but only 35% of the 7.2 g added were recovered as elemental Hg, or 2.55 g.

The timing of the mercury spike in the middle of the SB7b-7 SRAT boiling period is intriguing, since prior to the spike the Hg concentration looked normal, and following the spike the very low Hg concentrations signaled that the Hg had dropped out of the slurry or was in some other manner difficult to sample. If mercury was actively coalescing and falling to the bottom prior to 12 hours of boiling, then there could have been a window of time during which falling beads were more prone to being sampled, i.e. the timing of the spike may not have been purely random but may have coincided with the settling out of most of the elemental mercury beads.

In the case of the SB7b-9 SME product, it was possible to determine a maximum (upper bound) well-mixed slurry Hg concentration using the mass of mercury added and masses recovered overhead. The upper bound is shown as the purple square at 21:00. In this case, 3.49 g was recovered in the SRAT MWWT, and 0.29 g was recovered in both the first and second SME dewaterings. Therefore, the SME product could have at most 3.12 g of mercury (by difference relative to the starting Hg). The two SME product slurry results, however, indicated 6.7 g and

32.7 g of mercury (the second result was graphically excluded to keep the trace on scale). The upper bound is fairly similar to the SRAT product slurry quantity of 2.82 g based on the measured concentration. The SME product results also indicate that slurry sampling managed to collect one or more beads of mercury that were not homogeneously dispersed in the slurry. There appears to be a fairly low probability that both samples of a pair would do this based on the mercury slurry sampling data to date (if there were a 20% chance of getting one bead-enriched sample, then there would only be a 4% chance of both samples of a pair being bead-enriched, that is, it would be unlikely, but not completely impossible).

Mercury recovered from SB7b-6 (low acid) covered a wide range of bead sizes, while that recovered from SB7b-7 (high acid) had a single large bead combined with many very small beads, Figure 4.

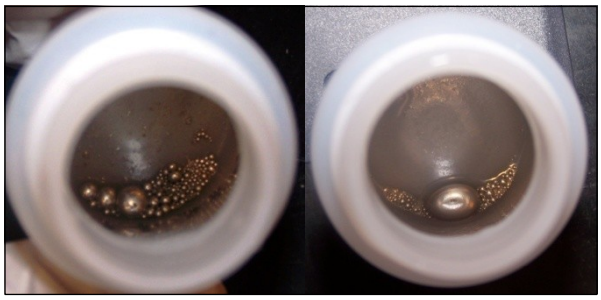

Figure 4. Mercury recovered in the initial tests (low acid left, high acid right)

Several other visual observations were made. There was a gray film around the center drain of the MWWT in the 130% and 140% stoichiometry runs that was quite distinct (more distinct at 140% than 130%). Mercury wanted to stick to the walls more in the 140% run than in others. The film also formed, and there was some stickiness, in the coupled flowsheet run, SB7b-10. The condensate removed from the MWWT in SB7b-10 at the end of the SRAT cycle was initially a milky gray. After time, what must have been a very fine dispersion of mercury-rich beads (perhaps micron-sized in diameter) was observed to settle to the bottom of the sample, and the supernate cleared and became transparent. The initial MWWT condensate had a density of 1.12 g/mL and contained 150 mg/L of Hg apparently as a slurry. After settling the aqueous phase had a density of 1.03 g/mL and contained 5.4 mg/L of Hg.

The coupled flowsheet run, SB7b-10 or ARP/MCU run, was expected to be qualitatively similar to the two low acid runs, since it was also a low acid run, Figure 5.

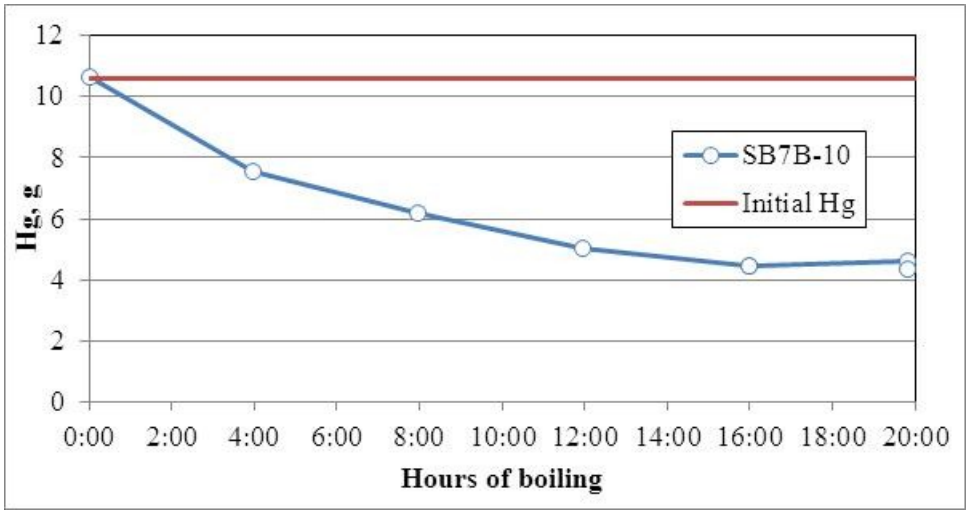

Figure 5. Coupled flowsheet slurry mercury versus boiling time

The elemental recovery was 4.8 g out of 10.6 g (45%) which was comparable to the two low acid runs. Several non-trivial Hg beads in the SME condensates were discarded before they were weighed which could have accounted for another several tenths of a gram (based on previously weighed bead masses). The SRAT and SME product slurries were holding about 4.5 g of mercury suspended per the sample results. Consequently, the fate of the majority of mercury in this run was known.

The status of suspended (slurried) mercury at the end of the SRAT cycle is summarized in Table 9 in order of increasing acid except for the coupled run, SB7b-10. The reported concentration comes from an average for two samples each run in duplicate. This result was converted to a wt. % total solids basis in the SRAT product using SRAT product slurry data given in Table 8.

Table 9. SRAT Product Mercury

Run ID:	SB7b-6	SB7b-8	SB7b-7	SB7b-9	SB7b-10
Concentration, mg Hg/kg slurry	439	333	72	1,035	1,863
Wt. % Hg in product solids	0.17	0.13	0.03	0.41	0.66

The mercury material balances indicate that these values are lower bounds for the amount of mercury remaining in the SRAT vessel at the end of the SRAT cycle (with the possible exception of SB7b-9 where the sum of mercury recovered plus mercury in the SRAT product is close to the mass of mercury added in the simulant). The 3% higher wt. % total solids of SB7b-10 during the SRAT (28 vs. 25) may have helped to better suspend the mercury compared to the other four simulations.

Ammonia/ammonium ion formation and associated by-products (NO_x, CO_2, enhanced formate loss, negative nitrite-to-nitrate conversion) have been seen in the last several sludge batches. The actual formation of ammonium ion from nitrate ion has been found to occur as the slurry pH returns to the vicinity of seven in systems with significant catalytic activity and/or mercury concentration coupled with excess formic acid. The evolution of slurry pH during the SRAT cycle is shown in Figure 6.

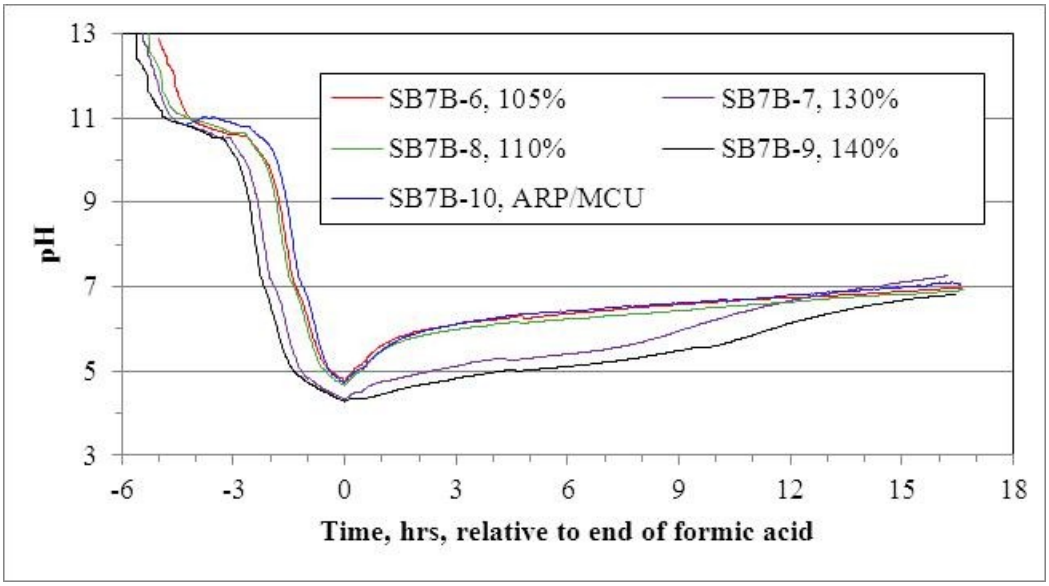

Figure 6. SRAT vessel pH readings versus time

The five traces of pH all ended in the neighborhood of seven by the end of reflux. Values within the vessel at boiling tend to differ somewhat from the room temperature values of the SRAT product samples. Table 10 shows the data listed in order of increasing acid except for the coupled run, SB7b-10.

Table 10. SRAT Product pH Comparison

Run ID:	SB7b-6	SB7b-8	SB7b-7	SB7b-9	SB7b-10
In vessel at 101 °C	6.97	6.92	7.26	6.82	7.08
Product pH at 25 °C	7.44	7.39	8.72	8.03	8.33

The SB7b-7 vessel probe was reading about 0.4 units low following the SME cycle when checked against the standard buffer solutions (4, 7, 10), so the 7.26 may be low, but is probably not high.

Samples of the ammonia scrubber reservoir were taken mid-reflux, at the end of the SRAT cycle, and at the end of the SME cycle. The quantity of total ammonia recovered as ammonium ion was calculated. SB7b-8 was the only run where ammonia was found five hours into reflux, and it is believed that this may have been due to a small heel from a previous run. The ammonium ion concentration in the scrubber during SB7b-8 stayed constant suggesting that there was no actual formation of fresh ammonia vapor occurring in the SRAT/SME vessel. Analyzed results are given in Table 11.

Table 11. Ammonia Scrubber Collection

Run ID:	SB7b-6	SB7b-8	SB7b-7	SB7b-9	SB7b-10
Stoichiometric factor	105%	110%	130%	140%	110%
After SRAT cycle, g	<0.01	0.06	0.09	0.42	<0.01
After SME cycle, g	<0.01	0.06	0.34	0.48	<0.01

The data in Table 10 and Table 11 seem to indicate that acid stoichiometry rather than SRAT product pH control ammonia evolution into the off-gas. The results in Table 11 are shown graphically in Figure 7. Results are at approximately 1/8,000 scale for the SRAT cycle and 1/8,600 scale for the SME cycle.

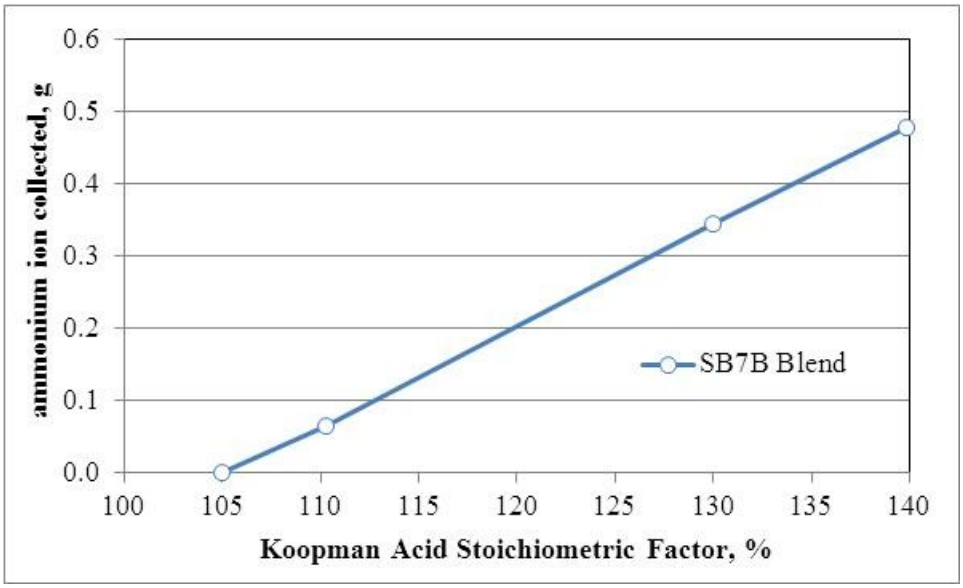

Figure 7. Ammonia scrubber recovery as a function acid stoichiometry

Overall, ammonia generation was not that high based on recovery in the scrubber (less than half of SB6 levels). The amount in the SME product was not measured (analytical issues). SB7b-9 at 140% acid lost 13 g of nitrate relative to the feed plus nitric acid, as well as all of the nitrate formed from conversion of nitrite to nitrate (about 4 g based on the sample at the end of acid addition), but only off-gassed less than 0.5 g of ammonia. This indicates that much of the destroyed nitrate did not make it all of the way through the reaction sequence to ammonia, and there should be some NO_x formation during boiling to account for the lost nitrate in the higher acid stoichiometry tests. GC measurements indicated about 1 g of N_2O was made after the feed nitrite was destroyed which presumably came from 2.8 g of destroyed nitrate. Unfortunately, current GC data cannot estimate NO or NO_2 at low concentrations, so the amount of nitrate that was destroyed to produce these two gases is unknown. Historically, nitrite destroyed during acid addition goes less than 50% to N_2O.

3.1.3 *SRAT Element Solubility*

Several supernate samples were taken between acid addition and the end of the SRAT cycle to track soluble cations in each run. Sodium and potassium in simulated waste generally stay ionized and dissolved in the supernate throughout processing. Zirconium, titanium, and cadmium are generally below detection limits in SRAT supernate samples. Iron and aluminum stay mostly insoluble. Other cations, such as Ba, Ca, Cu, Mg, Mn, Ni, S, Si, and Zn exhibit a range of solubilities during processing. The percentages of selected total elements found in the supernate phase following formic acid addition are given in Table 12. The results are presented as grams of an element in the supernate phase divided by grams of the element in the slurry (supernate plus insoluble solids) times 100%.

Table 12. Dissolution percent of elements following formic acid

Run ID:	SB7b-6	SB7b-8	SB7b-7	SB7b-9	SB7b-10
Stoichiometric factor:	105%	110%	130%	140%	ARP/MCU
Al	0.2	0.3	1.0	1.4	0.5
Ba	1.7	1.0	1.9	1.5	0.4
Ca	31	30	47	56	22
Cu	7.4	8.0	26	20	7.8
Fe	0.02	0.03	0.09	0.14	0.02
Mg	23	21	30	32	45
Mn	66	57	81	73	74
Ni	5.4	6.0	11	14	5
S	89	84	92	89	100
Si	1.1	1.1	44	21	2.7
Sn	8.5	11	14	18	4.5
Zn	1.7	<0.2	4.7	<0.2	1.3

Extent of dissolution generally was higher at higher acid stoichiometry in the samples taken immediately after acid addition. The slurry pH was also lower at higher acid stoichiometry at this point in the SRAT cycle. Calcium solubility has been higher in other simulants. It is believed that the moderately high oxalate concentration inhibits calcium and magnesium solubilities by forming low solubility precipitates after the initial carbonate and hydroxide insoluble forms enter solution during acid addition. The zinc data are suspicious. Results from the first pair of runs are completely different from the second pair. Some zinc solubility, especially at higher acid stoichiometries, is not unusual. Sulfur presumably represents the sulfate in the simulant which was expected to be mostly soluble.

The next set of supernate samples were taken three hours after dewatering. This was three hours into reflux in SB7b-6 through 9, and three hours into MCU addition in SB7b-10. Results are given in Table 13.

Table 13. Dissolution percent of elements after three hours reflux

Run ID:	SB7b-6	SB7b-8	SB7b-7	SB7b-9	SB7b-10
Stoichiometric factor:	105%	110%	130%	140%	ARP/MCU
Al	0.01	0.01	0.01	0.03	<0.01
Ba	0.3	0.2	0.5	0.6	0.2
Ca	5.0	7.4	22	37	3.1
Cu	0.2	0.2	0.6	0.3	0.5
Fe	0.02	0.01	1.5	7.1	<0.01
Mg	18	20	35	34	35
Mn	15	22	69	63	22
Ni	0.1	0.1	1.4	6.3	0.3
S	80	82	90	85	100
Si	1.7	1.0	2.2	1.1	1.2
Sn	1.3	3.3	6.9	8.6	1.1
Zn	<0.1	<0.1	0.3	<0.1	<0.1

Solubilities generally fell during dewatering and the early part of reflux as the supernate phase was concentrated and the pH rose. Mn and S, however, stayed near their end of acid addition levels. Differences between sludge-only and coupled operation appeared inconsequential.

Table 14. Dissolution percent of elements after seven hours reflux

Run ID:	SB7b-6	SB7b-8	SB7b-7	SB7b-9	SB7b-10
Stoichiometric factor:	105%	110%	130%	140%	ARP/MCU
Al	0.04	0.01	0.01	0.01	0.01
Ba	0.3	0.11	0.3	0.3	0.1
Ca	3.7	4.2	7.4	12	1.7
Cu	0.2	<0.1	1.2	0.2	0.2
Fe	0.08	0.02	0.02	0.4	<0.01
Mg	15	17	27	24	26
Mn	11	14	26	35	14
Ni	0.1	0.04	0.07	0.4	0.08
S	76	80	83	57	100
Si	41	10	14	0.7	2.0
Sn	0.09	2.4	2.6	5.3	0.5
Zn	<0.1	<0.1	<0.1	<0.1	<0.1

After dewatering plus seven hours of reflux (or MCU addition), most of the initially soluble calcium had reprecipitated as had much of the Mg and Mn. The SRAT cycle ended after twelve hours of reflux. By the SRAT product, Table 15, there was not much left in the supernate besides K and Na and small quantities of select other cations (S is probably sulfate, an anion).

Table 15. Dissolution percent of elements after twelve hours reflux

Run ID:	SB7b-6	SB7b-8	SB7b-7	SB7b-9	SB7b-10
Stoichiometric factor:	105%	110%	130%	140%	ARP/MCU
Al	<0.01	<0.01	<0.01	<0.01	<0.01
Ba	0.1	<0.1	0.1	<0.1	<0.1
Ca	1.9	2.0	1.5	3.2	1.1
Cu	<0.1	<0.2	0.7	3.3	0.1
Fe	<0.01	<0.01	<0.01	<0.01	<0.01
Mg	11	13	7.1	27	23
Mn	5.5	9.0	2.8	20	6.6
Ni	0.01	0.01	<0.01	0.02	0.02
S	84	89	87	89	100
Si	0.4	0.5	0.7	0.7	0.7
Sn	<0.2	1.7	<0.2	3.0	0.2
Zn	<0.1	<0.1	<0.1	<0.1	<0.1

Some data were obtained for the two major catalyst noble metals for hydrogen generation, Rh and Ru. The percentages in Table 16 were calculated relative to the masses of the two noble metals added, since the 1100 °C calcination of the SRAT product loses most of these two noble metals. Some variation in the ICP-AES detection limit impacted what could be learned from sample to sample.

Table 16. Dissolution percentage of key noble metals

Run ID:	SB7b-6	SB7b-8	SB7b-7	SB7b-9	SB7b-10
Stoichiometric factor:	105%	110%	130%	140%	ARP/MCU
Rh after acid add'n	45	42	46	23	42
Rh after 3 hrs reflux	<0.2	0.55	0.8	0.66	<3
Rh after 7 hrs reflux	<0.2	0.49	1.3	0.57	<3
Rh-SRAT product	<2	<3	2.0	<3	<3
Ru after acid add'n	3.8	5.5	10.2	7.8	4.6
Ru after 3 hrs reflux	<0.5	0.13	0.6	1.4	<0.5
Ru after 7 hrs reflux	<0.5	0.12	0.6	1.2	<0.5
Ru-SRAT product	<5	<0.5	0.9	1.3	<0.5

Generally the peak solubility period for the noble metals appeared to have already occurred by the end of acid addition consistent with earlier studies on noble metal chemistry during SRAT processing.[15] Rhodium was still fairly soluble at the end of formic acid addition. This is the period where a nitro-rhodium complex tends to be catalytically active for hydrogen generation. By three hours into reflux, most of the Rh had precipitated out of the supernate. Hydrogen generation during reflux was probably primarily due to Ru catalysis.

3.1.4 *SRAT Off-gas Data*

The discussion in Section 2.3 indicated that there were some issues with the simulant solids, with the GC data, and with the scaling of the GC data to DWPF equivalent generation rates. Individually these issues appeared to have less than 10% impact on the calculation of DWPF-scale gas generation rates. In this case, however, the impacts were generally cumulative, rather than off-setting, in determining the maximum hydrogen generation rate. Before continuing with this section, it should also be recalled that these tests were performed with significant added caustic that increased the baseline acid demand and, in stoichiometric factor percentage space, tended to reduce the allowable operating window between nitrite destruction and allowable hydrogen generation.

The issue with the SB7b blend simulant was the lower total and insoluble solids concentrations relative to the August 2011 SB7b blend projections. The caustic-trimmed simulant was 16.2 wt% total solids and 10.0 wt.% insoluble solids. The August projection for caustic trimmed SB7b in Tank 40 was 17.2 and 11.7 wt.% respectively. Historically, scaling has been done assuming that the charge of simulant to the SRAT was the scaled equivalent of 6,000 gallons of SB7b slurry from Tank 40. For SB7b the scaling was done assuming the SRAT product was 25 wt.% total solids at a scaled equivalent to 4,500 gallons (the heel volume is neglected in simulant scaling calculations). Table 17 shows that the impact was 3-7% for the baseline flowsheet tests, but rose to almost 16% for the ARP/MCU run, assuming a 25 wt% total solids SRAT product was made. Physically, a scale factor of 8,000 means that the lab-scale SRAT was at roughly 1/8,000 DWPF scale on a volumetric basis.

Table 17. Impact on scaling factor

Run ID:	SB7b-6	SB7b-8	SB7b-7	SB7b-9	SB7b-10
Stoichiometric factor:	105%	110%	130%	140%	ARP/MCU
SRAT receipt	7,591	7,591	7,591	7,591	7,045
SRAT product	8,124	8,090	7,812	7,881	8,160†
Scaling impact	7.0%	6.6%	2.9%	3.8%	15.8%

† SB7b-10 was subsequently changed to 7,211 (see below)

SB7b-6 through 9 all received identical sludge charges, so the SRAT receipt scale factor did not change. It was subsequently found that SB7b-10 produced a 28.3 wt% total solids SRAT product. Therefore, the 8,160 scaling factor was adjusted down to 7,211 to dilute the product back to an equivalent basis of 25 wt.% total solids slurry. (SME scale factors are equal to the SRAT scale factors multiplied by the ratio of the SRAT product mass before samples to the product mass after samples).

The He:H_2 separation of the GC used for SB7b-6, 9, and 10 deteriorated before method adjustments could be implemented to restore the separation. This was not an issue for SB7b-6 which produced virtually no hydrogen. There were signs of potential other issues, perhaps related to an off calibration mass flow controller for either air or helium on one of the two hoods. The established 0.5 vol% helium in air using the mass flow controllers gave actual GC helium readings of 0.49, 0.47, and 0.42 for SB7b-6, 9, and 10 respectively. The first two are within 10%, but the third is off 20%. The other GC gave a helium reading of 0.55 for SB7b-7 and 8. This is within 10% but in the opposite direction. In all five runs, however, the GCs appeared to hold their calibration quite well (based on before and after checks with calibration gas). Except for SB7b-10, all of the helium readings were within 10% of the expected value. Consequently, only SB7b-10 data were given special treatment.

The mass flow controllers used on SB7b-10 were checked after the run against other calibrated mass flow controllers. The helium flow controller used for SB7b-6 and 9 reached the end of its calibration period and was exchanged for an alternate flow controller prior to SB7b-10. As-found calibration results will be reported at a future date by the SRNL calibration shop. The air mass flow controller appeared to be within 1% of setpoint and the helium flow controller was perhaps passing several percent more gas at setpoint (not an explanation for a lower than expected helium vol%). Consequently, the issue with the helium volume percent was attributed to the GC performance. The GC calibration was found to be sensitive to the calibration gas pressure, but this test is not done enough to know the normal likelihood of this observation.

Two possibilities exist for scaling the off-gas flows in SB7b-10. They can be scaled assuming that the helium vol% is approximately correct (if off, it is off in the same proportions as the hydrogen and oxygen gas vol% are off, since they are all injected on the same column; therefore ratios of H_2/He and O_2/He are still good). The data from column B for CO_2 and N_2O, however, may not have the same injection issue, so calculated CO_2 and N_2O flow rates could be off. The other possibility is to scale off the nitrogen flow as determined by the air flow and known vol% of nitrogen in dry air.

The GC read atmospheric purge gas as 78-80 vol% nitrogen which is virtually the correct value. One reason this might occur is that nitrogen is calibrated using calibration gas to cover the region from 0-51 vol% and room air to cover the region from 51-80 vol%. Therefore, the GC should read nitrogen correctly at atmospheric pressure when not significantly diluted by other gases. However, as generation rates of CO_2 and NO_x increase, diluting the nitrogen (the minimum

observed reading was 55.5 vol%), then the reading moves closer to the calibration gas point which may be in error by perhaps (0.50-0.42)/0.50*100% = 16% or so, the approximate magnitude of the bias due to helium. The positive side would be that the nitrogen read less than 72 vol% for only about 1.3 hours of the SRAT/SME, and never during hydrogen generation. Therefore, hydrogen generation rate values for SB7b-10 will be derived from the ratio to nitrogen, while the other four runs will stay with the normal convention of ratio to helium.

The DWPF-scale hydrogen generation rates during the SRAT cycle are given in Figure 8. The N_2 on the legend for SB7B-10 denotes that the data were scaled from nitrogen rather than helium. The He-scaled gas generation rates are about 30% higher for all SB7b-10 off-gas data. They would bound the N_2-scaled rates. Nevertheless, the N_2-scaled gas generation rates are given in the figures below, because the off-gas data are more nearly consistent with the majority of other data.

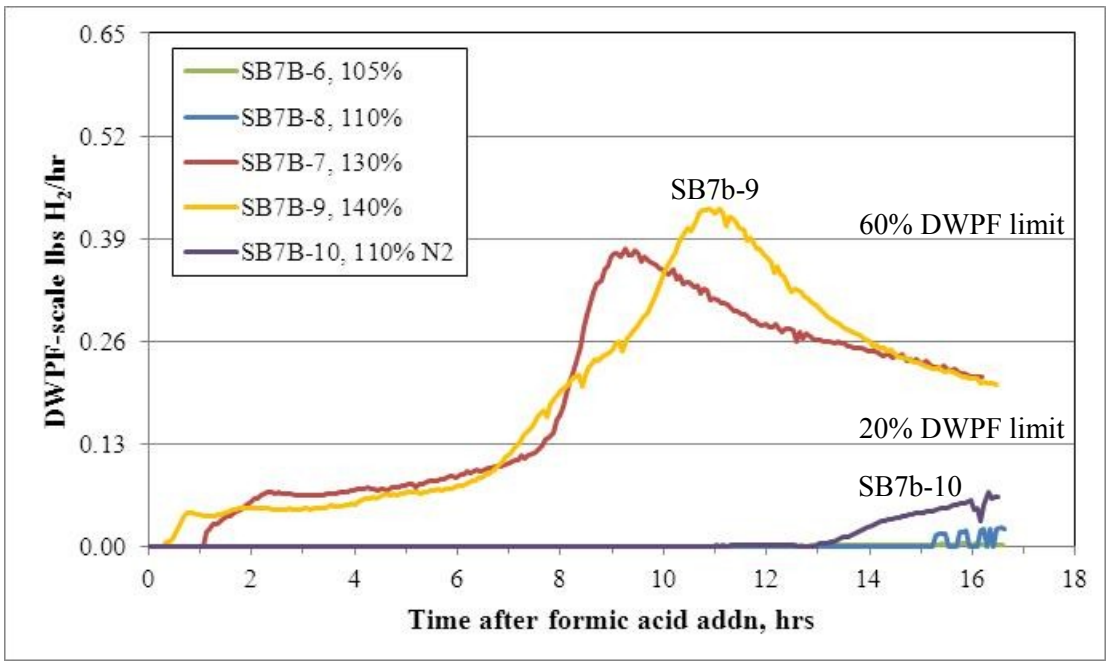

Figure 8. SRAT cycle hydrogen generation rates

The three lower acid runs had little hydrogen generation except for the ARP/MCU run, SB7b-10. Hydrogen generation rates began to rise as the addition of the acidic MCU stream concluded. Even though the stoichiometric factor was only 110% (including the MCU), the hydrogen generation rate increased to over 10% of the DWPF SRAT limit during the last 3-4 hours of boiling, Table 18. SRAT product data indicate that some of this behavior may be attributable to the higher total solids content (28.3 wt.% vs. 25% target) which increased the concentrations of the available noble metals and the remaining free acid. Some of this behavior, however, should probably be attributed to the combination of fairly high noble metal concentrations with relatively low mercury concentrations.

Table 18. SRAT Cycle Hydrogen Generation

Run ID:	SB7b-6	SB7b-8	SB7b-7	SB7b-9	SB7b-10
Stoichiometric factor:	105%	110%	130%	140%	ARP/MCU
Peak hydrogen, lb/h	0.004	0.024	0.38	0.43	0.085
% of SRAT limit	0.6	3.7	58	66	10
Total hydrogen, mg	0.8	1.0	166	176	13

SB7b-7 and 9 had similar hydrogen generation rate profiles in Figure 8. Based on some of the issues discussed earlier in this section, the two runs could even have been closer. Helium ran high in SB7b-7 and low in SB7b-9 relative to expectations. The hydrogen generation rate is the hydrogen concentration divided by the helium concentration times the helium flow rate and a set of scaling and unit conversion constants. So, if for some reason the hydrogen was not similarly impacted as the helium, then the SB7b-7 rates would increase and the SB7b-9 rates would decrease. The concentration endpoints were also close, but not identical, following dewatering.

Cumulatively, the hydrogen data suggest that much further concentration of this feed slurry during the SRAT cycle (for example, by bringing in three transfers and concentrating while caustic, or running 8,000-9,000 gallon SRAT batches) has the potential to push the hydrogen generation rates over the DWPF SRAT limit at formerly moderate acid stoichiometries in the 130-140% range. This caution for potential operating strategies with SB7b is complicated by the addition of caustic to increase waste loading window flexibility. Caustic addition increases the baseline moles of acid needed per liter of sludge without increasing the moles of excess acid per liter that can be handled without producing excessive hydrogen. In other words, increasing the baseline acid demand shrinks the stoichiometric percentage window.

Large swings in ARP content of the SRAT receipt slurry could impact the choice of acid stoichiometric factor. Generally, as the ARP content of the receipt slurry goes up, the chosen stoichiometric factor needs to go down using the DWPF-Hsu stoichiometric acid equation. The acid content of any large volume of MCU to be processed in a single sludge batch should also be considered. Simulant testing was at 0.033M acid in 8,000 gallons equivalent of MCU. This equated to 2.6% of the total acid (2.8% of the stoichiometric acid). If a comparable volume were processed at a higher molarity, then neglecting the acid content could push the process past the acid window upper limit depending on the stoichiometric factor.

The noble metal concentrations in the simulant during reflux at 25 wt.% total solids are believed to be very close to what the analytical data indicates will be the case for SB7b. Normally the simulant runs target 110% noble metals (based on the latest projections), but in this case the composition estimates changed as new data became available in July and August. The revised estimates appear to have eliminated the targeted excess. Therefore, simulant tests may not have bound the noble metal concentrations in SB7b because of potential analytical uncertainty in the sample results. Experiences dating back to Sludge Batch 2, however, argue against performing CPC simulations using 25-30% or higher conservatism in the noble metal concentrations, since the resulting simulant flowsheet data did not translate as well to the real waste. The consequence in this case is that the SB7b blend simulant flowsheet window results do not contain much, if any, conservatism if the decision is made to add 3,500-7,000 gallons of 50% caustic to the batch.

The carbon dioxide gas generation rates are split into two graphs. The first, Figure 9, is a high range graph covering the period during and immediately after acid addition. The second, Figure 10, is a low range graph covering the boiling period. There is a three hour overlap between the two graphs. CO_2 in SB7b-10 matches the other four runs at the initial peaks found from -1 to -2.5

hours relative to the end of formic acid using the nitrogen scaling. This was expected based on the analyses for carbonate in the SB7b-10 sludge-ARP feed. The helium-scaled CO_2 generation rate peaked near 690 lb/h, or over 16% higher than any of the other runs. This seems to indicate that the nitrogen scaling was more realistic than the helium scaling during this period. A 15-20% higher carbonate loading for the ARP/MCU run is not credible.

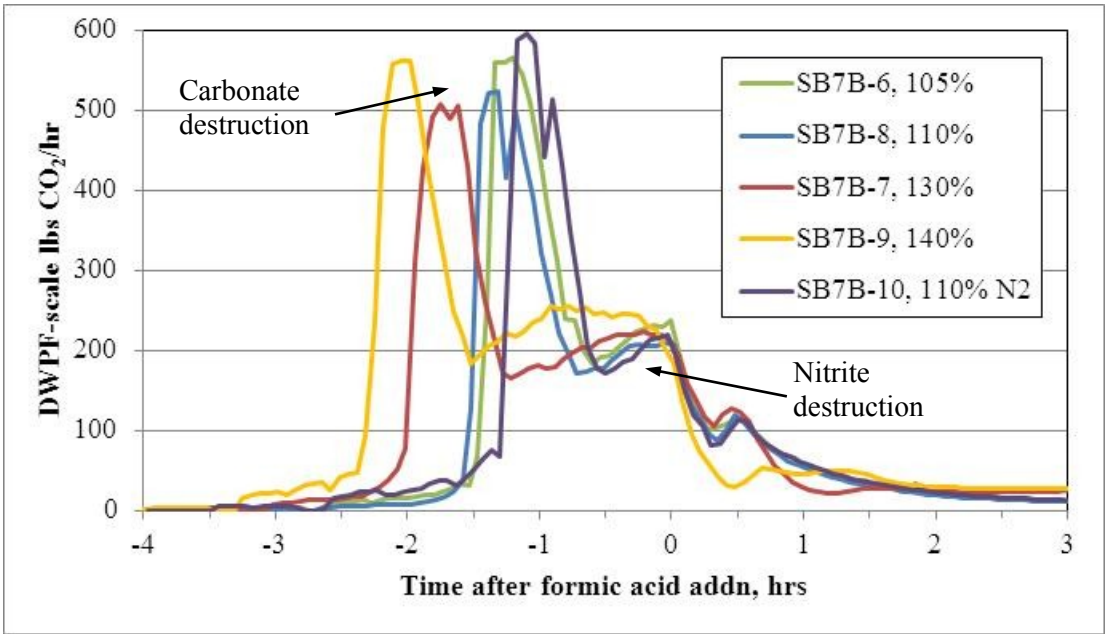

Figure 9. SRAT cycle CO_2 during and immediately after acid addition

The longer duration acid additions of the 130% and 140% runs are clearly evident by the earlier peak times for carbonate destruction at about -2 hours compared to about -1 hours for the three low acid runs. The presence of added caustic had no visible impact on the magnitude of the carbon dioxide generation rates.

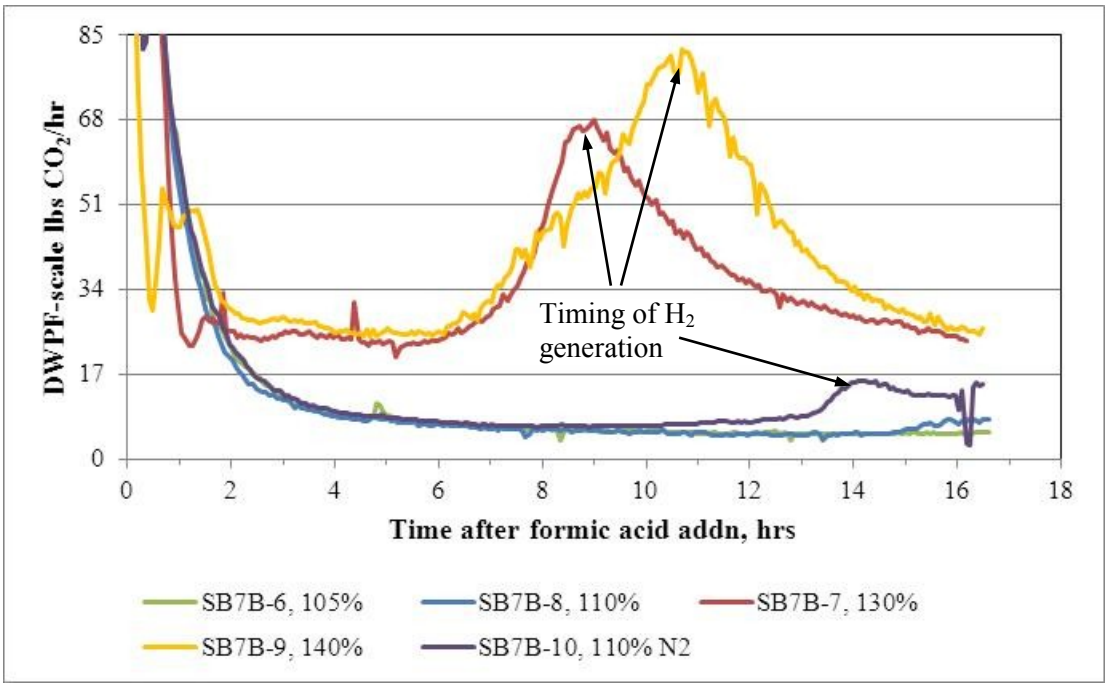

Figure 10. SRAT cycle CO_2 during boiling

Peaks in CO_2 during boiling align with peaks in H_2. Following acid addition the CO_2 traces for the 105% and 110% baseline flowsheet runs are nearly identical. Data come from two different GC's, so relative scaling and conversion to DWPF-scale lb/h at least was consistent. At about 15 hours after acid addition there was a slight increase in the 110% case relative to the 105% case. The coupled flowsheet tracked both of the low acid runs for about the first nine hours after acid addition before starting to drift to higher rates. (The nine hours included about five hours of heat-up and dewatering with no MCU addition, followed by four hours of dewatering with MCU addition). The coupled run off-gas CO_2 then began a more rapid rise coinciding with the onset of noticeably increased hydrogen generation at about 13.5 hours after acid addition. MCU addition was occurring simultaneously during the post-dewatering period until about the last 45 minutes of the SRAT cycle.

Some numerical results for carbon dioxide generation are given in Table 19. The table gives the maximum volume %, the calculated peak lb/h generation rate (which occurred simultaneously with the max vol% in all five cases), and the Simpson's Rule integrated total mass of CO_2 produced. SB7b-10 started with more solids mass (more TIC) than the other four, so a slightly higher total CO_2 production at low acid should be expected relative to SB7b-6 and 8.

Table 19. SRAT Cycle Carbon Dioxide Generation

Run ID:	**SB7b-6**	**SB7b-8**	**SB7b-7**	**SB7b-9**	**SB7b-10**
Stoichiometric factor:	105%	110%	130%	140%	ARP/MCU
Peak CO_2, lb/h	566	523	508	561	595
Max vol%	24.4	25.2	25.0	24.2	24.2
Total CO_2, g	41	39	68	80	46

Catalytic activity apparently drove the formation of 30-40 additional grams of CO_2 in the high acid runs compared to the low acid runs. There is a few percent difference between the peak vol% in SB7b-6 and 9 compared to SB7b-7 and 8 which could be related to the condition of the two different GCs used. A reverse difference (lower vol% = higher lb/h) is seen in the peak lb/h results. This difference relates to the variations in helium behavior on the two A columns, and to the conversion from vol% to lb/h using He as an internal standard. A potential systematic uncertainty in the peak CO_2 rate of ~50 lb/h could be inferred independent of random factors from these results (8-9%).

Off-gas data for N_2O are presented in a similar manner to the data for CO_2. A high range graph covering the period around acid addition is given in Figure 11.

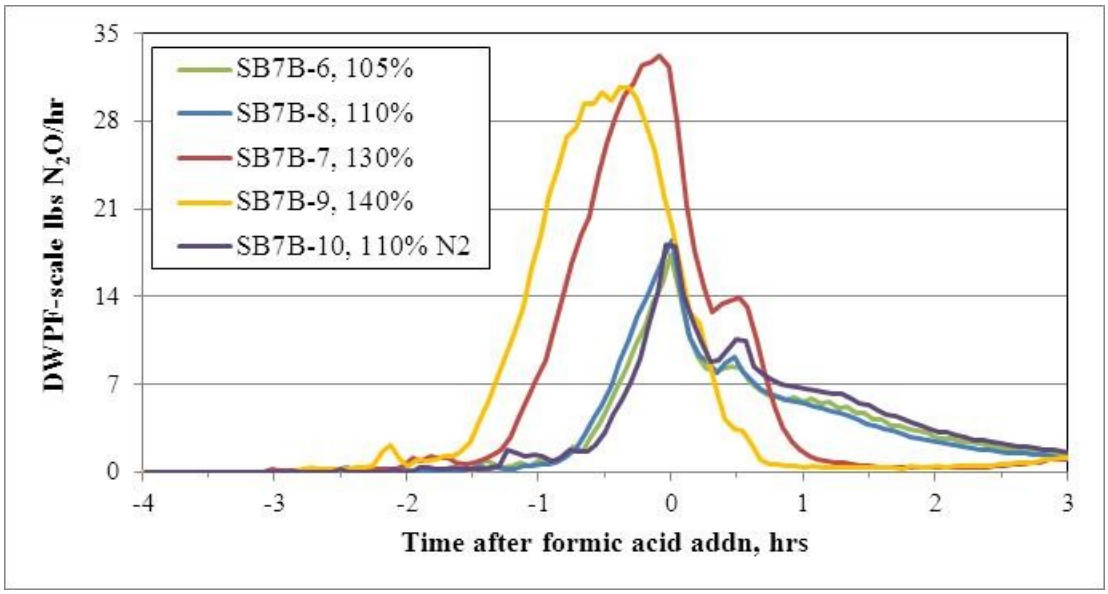

Figure 11. SRAT cycle N_2O near the end of acid addition

The amount of N_2O formed was a strong function of the acid stoichiometry. The total quantity of N_2O produced nearly doubled with increased acid stoichiometry. Some numerical N_2O results are given in Table 20.

Table 20. SRAT Cycle Nitrous Oxide Generation

Run ID:	SB7b-6	SB7b-8	SB7b-7	SB7b-9	SB7b-10
Stoichiometric factor:	105%	110%	130%	140%	ARP/MCU
Peak N_2O, lb/h	17.4	18.5	33.2	30.6	18.2
Max vol%	0.9	1.1	2.0	1.6	0.9
Total N_2O, g	1.8	1.8	3.1	3.2	2.2

Low range N_2O data for the period following acid addition are given in Figure 12.

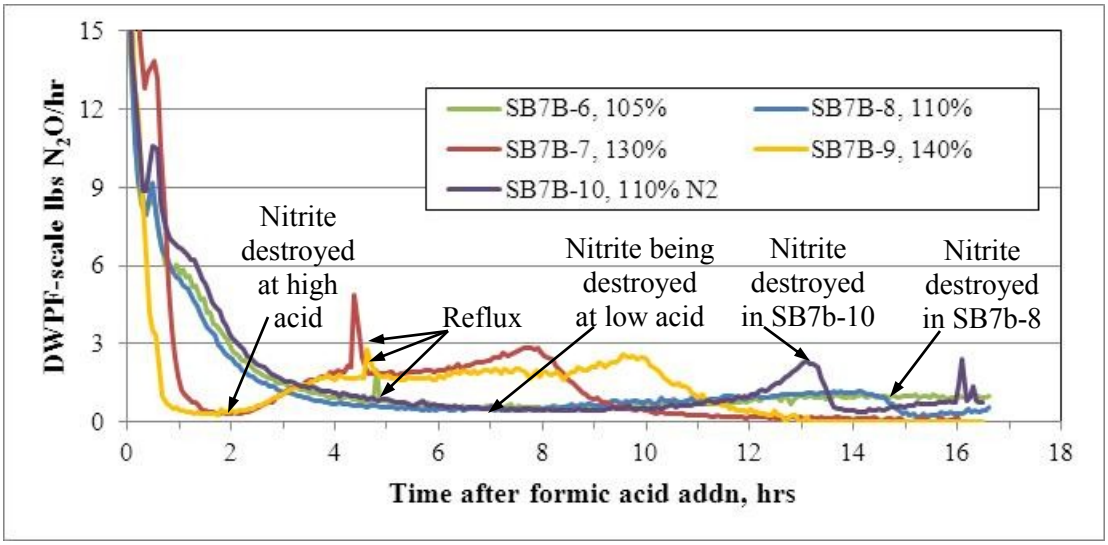

Figure 12. SRAT cycle N_2O during boiling

The N_2O data contain many interesting features. The two high acid runs likely completed nitrite destruction within the first two hours after formic acid addition completed based on the N_2O data. The 140% run was about 30 minutes ahead of the 130% run in the first hour or so after acid addition, and hydrogen generation in the higher acid run started about 30 minutes sooner as well. Both runs, nevertheless, have a sustained period of N_2O generation later that cannot be attributed to nitrite in the feed slurry. This period is likely the time during which the pH was not favorable for ammonium ion formation, and the ammonium formation reaction sequence effectively stopped after converting nitrate back to nitrite. The nitrite desorbed and then reacted with excess acid to form N_2O and presumably NO. After about ten hours, the N_2O generation fell off, and presumably ammonium ion formation occurred during the period from then until the end of the SRAT cycle. (See below for data on ammonia collection in the scrubber in these two runs.)

Conversely, in the three low acid runs, the sustained N_2O generation was most likely due to the continuing destruction of the feed nitrite that continued well into reflux (and had not yet completed by the end of the SRAT at 105%). SB7b-8 N_2O generation dropped to nearly zero between 14 and 15 hours after acid addition which likely corresponds to the end of nitrite destruction. SB7b-10 had acid coming in with MCU solution during most of the boiling period. Once a critical amount of acid had been added there seemed to be an acceleration in the destruction of nitrite (at about 12 hours) finally leading to essentially a zero N_2O generation rate just prior to 14 hours due to no more nitrite ion. This same period correlated with the onset of hydrogen generation.

Some small spikes are seen in the N_2O data, three between 4 and 5 hours and one at 16 hours. These are due to small changes in processing and do not reflect unusual chemistry. The three between 4 and 5 hours show a short-lived burst in N_2O generation immediately following the onset of reflux and the return of accumulated MWWT nitrite ion to the SRAT. There was also a small measurable spike in the fourth flowsheet run at this same time, though it was too small to be obvious on the graph. The coupled flowsheet did not go to reflux at this time, and it had no spike since no nitrite was refluxed into the slurry. The coupled run continued dewatering while simultaneously starting the MCU solution addition to maintain constant volume in the SRAT. The spike at 16 hours in the coupled run occurred because the mantle power was shut off, boiling stopped, but then the mantle was turned back on for a short time. (Although the coupled run went

to reflux following dewatering of the MCU addition mass, there was virtually no nitrite ion remaining in the MWWT at that time to trigger a surge in N_2O generation.)

3.1.5 *SRAT Condensate Analysis*

A sample of SRAT dewater condensate from each run was submitted for analysis. Results are summarized in Table 21. Samples were analyzed in duplicate for Al, K, Na, S, and Si by ICP-AES, in duplicate for nitrite, nitrate, sulfate, and formate by IC, and also for pH. Since pH fell outside the standard calibration solution range of 4-10, an independent calculation of pH was made assuming that nitrate was nitric acid, the formate did not contribute to pH, and that pH = $-\log_{10}[H^+]$, where [H+] equaled the nitrate ion molarity by IC, $[NO_3^-]$. Al, K, Na, and S were all below the detection limits (Al<0.1 mg/L, K<10 mg/L, and Na and S both <0.1 mg/L). Nitrite and sulfate were also below the IC detection limit of 100 mg/L. A calculation was made assuming that Si was 100% derived from antifoam at 14 wt.% Si in antifoam, and the percentage of added antifoam that could have been stripped to the condensate was calculated and given in the last row.

Table 21. SRAT Dewater Condensate Analyses

Run ID:	**SB7b-6**	**SB7b-8?**	**SB7b-7**	**SB7b-9?**	**SB7b-10**
Stoichiometric factor:	105%	110%?	130%	140%?	ARP/MCU
Condensate mass, g	1,112	1,122	1,060	1,045	1,313
Si, mg/L	114	468	346	142	130
Nitrate, mg/L	2,900	1,070	3,260	3,140	1,730
Formate, mg/L	350	2,020	1,750	310	370
pH by probe	1.56	1.40	1.31	1.42	1.78
pH by $[NO_3^-]$	1.33	1.77	1.28	1.30	1.55
Max. % antifoam lost	40	160	110	45	39

There is a better than 50% probability that the SB7b-8 and 9 condensate sub-samples were swapped (relative to their labels) when they were prepared by pouring them up from the bulk dewater condensates. Note that SB7b-10 was also at 110% acid stoichiometry, but its ratio of formic acid to total acid was different due to the different feed composition. SB7b-10 has low formate which is the expected result for a low acid run, like SB7b-6 and not like SB7b-8. Nitrate should fall with increasing acid stoichiometry and formate tends to increase simultaneously. If that is so, then the Si, as well as % antifoam lost, increase with increasing acid stoichiometry. A similar trend was seen in the SB7b batch simulant testing, Appendix A. The condensate mass values are correct for the column heading. The nitrate data appear to be difficult to explain in either sequence.

Switching the analytical results between SB7b-8 and 9 would change the maximum percent antifoam lost, since the condensate mass is a factor in the calculation. Since some values cannot simply be transposed, an alternate version of Table 21 is given below switching the SB7b-8 and 9 analytical results and recalculating the maximum percentage of antifoam lost into the condensate.

Alternate version of Table 21

Run ID:	SB7b-6	SB7b-8?	SB7b-7	SB7b-9?	SB7b-10
Stoichiometric factor:	105%	110%?	130%	140%?	ARP/MCU
Condensate mass, g	1,112	1,122	1,060	1,045	1,313
Si, mg/L	114	142	346	468	130
Nitrate, mg/L	2,900	3,140	3,260	1,070	1,730
Formate, mg/L	350	310	1,750	2,020	370
pH by probe	1.56	1.42	1.31	1.40	1.78
pH by [NO_3^-]	1.33	1.30	1.28	1.77	1.55
Max. % antifoam lost	40	49	110	145	39

While the alternate version still has a difficult line for nitrate, it does have the three low acid runs with 300-400 mg/L of formate and Si < 145 mg/L, while the two high acid runs have 1,750-2,020 mg/L of formate and Si > 345 mg/L.

In either version of the table, there is the potential for a significant loss of antifoam to the dewater condensate. Please note that the dewater condensate mass was a significant fraction of the SRAT vessel contents, and that this does not happen in every sludge batch. Dewatering decreased the amount in the vessel from roughly 3,700 g to 2,700 grams of slurry in SB7b-6 to 9, while SB7b-10 was from approximately 4,140 to 2,830 grams of slurry, i.e. about 30% of the post-acid addition mass was removed as dewatered condensate in all five runs. A more modest dewatering would be expected to remove less antifoam regardless of the actual fraction of the Si that is due to antifoam in the MWWT dewater condensate. Some additional considerations regarding the fate of antifoam are discussed in the Appendix A summary of scoping results using hexane to extract antifoam from samples and equipment.

3.2 SME Cycle

The five SB7b-blend simulant SME cycles are discussed below. Chemical and physical data from process samples will be presented first followed by off-gas data.

3.2.1 *SME Cycle Slurry Samples*

Formate and nitrate loss are presented in Table 22 for samples taken of the SME product slurry. The combined loss in oxalate for the SRAT+SME cycles is also given based on the acid strike analytical results.

Table 22. SME Anion Reactions

Run ID:	SB7b-6	SB7b-8	SB7b-7	SB7b-9	SB7b-10
Acid stoichiometry, %	105	110	130	140	110
Formate loss, %	-6	4	-3	8	12
Nitrate loss, %	1	3	4	4	5
Composite oxalate loss, %	0	24	20	24	23

Negative formate losses occur when the SME formate material balance indicates a gain in formate mass. Formate losses between -10% and +10% cannot be significantly distinguished from zero. CO_2 generation was seen in all five SME cycles, which indicates the loss of formate and/or oxalate ion. CO_2 production in SB7b-7 and 9 are consistent with about a 4% formate loss,

while CO_2 production in SB7b-6 and 8 are consistent with a 2% formate loss. The presumption, however, is that CO_2 is derived solely from formate ion which may not be valid in the presence of significant dissolved oxalate ion.

In SB3 simulant tests there were occasional signs of a small formate gain in the presence of an oxalate loss. The SB7b oxalate concentration data are fairly uncertain at ±20%, but it appears that there may have been some oxalate loss in the block of four acid window runs. There were no increases in SME product oxalate relative to SRAT product oxalate that would be expected for random errors distributed about no net change in oxalate. Oxalate loss could be responsible for some CO_2 formation and also for some formate production.

Analytical anion data for the five SB7b-Tank 40 SME products are given in Table 23 as mg anion/kg slurry. Both water dilution and acid strike oxalate values are given. The first gives oxalate present in a water soluble form, while the difference indicates oxalate tied up as water insoluble oxalate solids.

Table 23. SME Product Anions, mg/kg

Run ID:	SB7b-6	SB7b-7	SB7b-8	SB7b-9	SB7b-10
F^-	<100	<100	<100	<100	<100
Cl^-	237	231	231	250	285
NO_2^-	370	<100	<100	<100	<100
NO_3^-	24,100	23,700	24,400	25,700	25,300
$SO_4^=$	1,150	1,150	1,120	1,110	2,170
$C_2O_4^=$ (wd)	1,370	1,130	1,390	1,390	2,250
$C_2O_4^=$ (as)	7,170	5,470	5,410	5,440	6,460
HCO_2^-	53,000	48,800	49,000	48,400	49,500
PO_4^{3-}	<100	<100	<100	<100	<100

wd – water dilution, as – acid strike

The SME product oxalate concentrations from the acid strike preparation in SB7b-7, 8, and 9 were nearly identical. It appears that over 70% of the oxalate in the feed precipitated as water insoluble oxalate compounds. That is sufficient oxalate to precipitate all of the calcium in the system as calcium oxalate and still have about a third of the precipitated oxalate anions left over for other cations.

The higher values of SB7b-10 relative to the other four SRAT products appear to be due to over concentrating by 10%. A drop in acid strike oxalate from about 8,000 to 6,000 occurred from the first two runs (105%, 130% acid) to the second two runs (110%, 140%). It is uncertain what the significance of these data might be, but on average a small (~10%) loss of oxalate during CPC processing was indicated. SB7a testing did not indicate much oxalate loss, but SB3 simulant testing showed a potential for oxalate loss during processing.

Elemental wt.% data for the five SME products after calcining at 1100 °C are given in Table 24. General consistency in values for the first four SME products is seen as desired. The fifth SME product is from the ARP/MCU run and should have a distinctly different composition. The 1.2 wt.% Ti primarily relates to the monosodium titanate in this slurry. Sodium was also increased by the introduction of MST.

Table 24. SME Calcined Elements at 1100 °C-wt.%

Run ID:	SB7b-6	SB7b-7	SB7b-8	SB7b-9	SB7b-10
Al	4.3	4.3	4.1	4.2	3.6
B	1.4	1.4	1.3	1.3	1.5
Ba	0.04	0.04	0.04	0.04	0.04
Ca	0.30	0.30	0.29	0.34	0.31
Ce	0.07	0.07	0.07	0.07	0.05
Cr	0.03	0.03	0.03	0.04	0.02
Cu	0.02	0.02	0.02	0.03	0.03
Fe	7.6	7.4	7.2	7.3	6.4
K	0.05	0.05	0.06	0.06	0.04
La	0.03	0.03	0.03	0.03	0.03
Li	2.1	2.1	2.1	2.1	2.2
Mg	0.14	0.14	0.14	0.15	0.15
Mn	1.6	1.6	1.5	1.6	1.3
Na	11.2	11.1	10.9	11.1	11.8
Ni	1.3	1.3	1.2	1.3	1.0
P	<0.1	<0.1	<0.1	<0.1	<0.1
Pb	<0.01	<0.01	<0.01	<0.01	<0.01
S	0.13	0.13	0.14	0.14	0.17
Si	23.4	23.4	23.5	23.5	23.4
Sn	<0.01	<0.01	<0.01	<0.01	0.02
Ti	0.04	0.04	0.05	0.05	1.2
Zn	0.03	0.03	0.02	0.03	0.02
Zr	0.17	0.17	0.18	0.18	0.10

SME product solids data, densities, and pH are given in Table 25. The SME targeted 48 wt% total solids. The wt.% insoluble and soluble solids were calculated from the measured total slurry and supernate (dissolved) solids. The density measurements were made at 25 °C.

Table 25. Additional SME Product Properties

Run ID:	SB7b-6	SB7b-7	SB7b-8	SB7b-9	SB7b-10
Acid Stoichiometry %	105	130	110	140	110
Wt. % total solids	47.6	47.1	48.2	49.1	52.4
Wt. % insoluble solids	36.0	36.6	35.8	38.2	39.9
Wt. % soluble solids	11.6	10.5	12.4	10.9	12.6
Wt. % dissolved solids	18.2	16.6	19.4	17.7	20.9
Wt. % calcined solids	39.9	39.5	40.6	41.0	44.1
Slurry density, g/mL	1.38	1.38	1.37	1.37	1.44
Supernate density, g/mL	1.11	1.10	1.11	1.11	1.13
Product pH at 25 °C	8.13	8.41	7.66	7.55	8.61

The first four tests ended near the target of 48 wt.% total solids. The wt.% dissolved solids did not follow a consistent trend (up-down-up) with stoichiometry suggesting potential small sample homogeneity issues. The pH data trended randomly as well (down-up-down) with acid stoichiometry.

3.2.2 *SME Off-gas Data*

SME cycle hydrogen generation rates are presented at DWPF scale in Figure 13. The y-axis is marked in increments of 20% of the DWPF SME hydrogen limit of 0.223 lb/h. Dewatering after the first frit addition occurred roughly 18-20 hours after SRAT formic acid addition, while dewatering after the second frit addition occurred roughly 20-23 hours after formic acid addition.

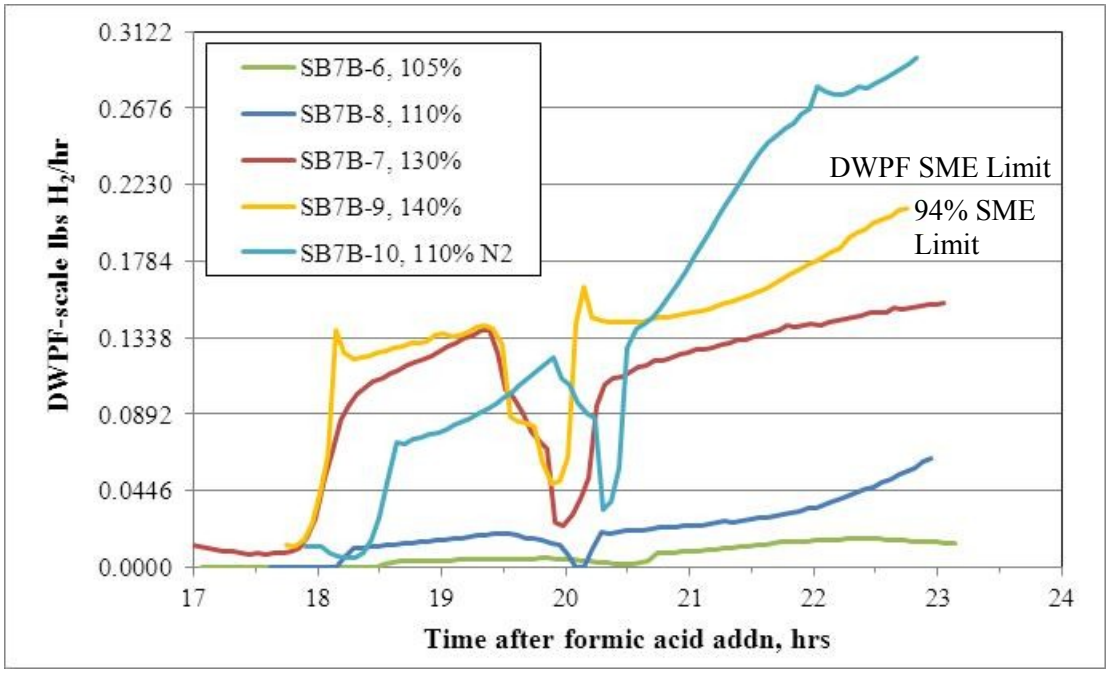

Figure 13. SME Cycle Hydrogen

The five SRAT cycles transitioned into the boiling period following the first frit-formic acid slurry addition without issues. The formic acid in the second frit slurry addition added to that in the first addition, however, triggered increases in hydrogen generation rates in all five SME cycles. The frit formic acid caused a 5.4% increase in the stoichiometric acid added, e.g. 105% became 110.4% in the SME cycle. The increases were tolerable at low acid stoichiometry and low solids concentration. The 140% acid stoichiometry test (145.4% SME) nearly reached the DWPF SME cycle limit.

The coupled flowsheet run, SB7b-10, was significantly different in the SME cycle from the low acid stoichiometry sludge-only flowsheet runs that it was supposed to mimic. The coupled run exceeded the SME hydrogen limit by over 30% and made four times more hydrogen than the sludge-only run at the same stoichiometry. This was likely due in part to the higher than targeted wt.% total solids (52% vs. 48%) that concentrated the noble metals and formic acid, made the slurry more viscous, and may have led to locally hotter regions near the heated vessel wall.

Carbon dioxide generation rates for the SME cycle are given in Figure 14.

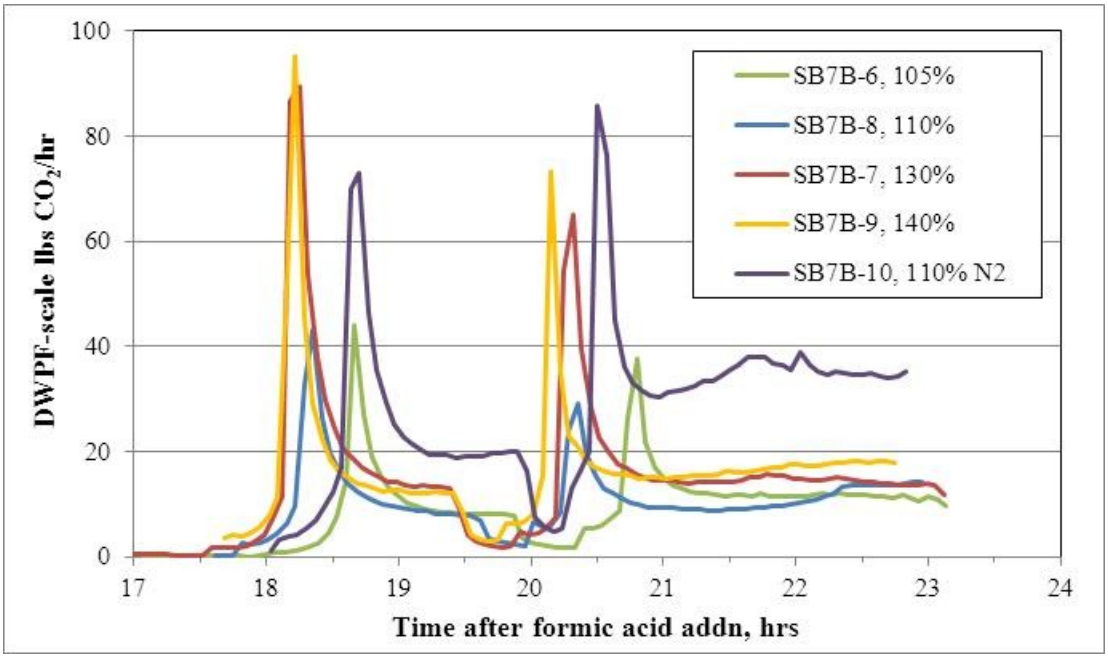

Figure 14. SME Cycle Carbon Dioxide

The correlation between hydrogen and CO_2 is fairly weak in these SME cycles. All four sludge-only flowsheet runs finished the SME cycle at about the same CO_2 generation rate of roughly 15 lb/h. The coupled flowsheet run was at much higher CO_2 generation rates. One might hypothesize that the wt.% solids of the SME product was dominating the amount of CO_2 production rather than the acid stoichiometry.

The SME cycle CO_2 production is compared to the SME cycle formate loss in Table 26. These results are in the context of 120-130 g of formate present in the SME slurry.

Table 26. SME Formate Loss and CO_2 Made

Run ID:	SB7b-6	SB7b-8	SB7b-7	SB7b-9	SB7b-10
Acid stoichiometry, %	105	110	130	140	110
CO_2 in SME cycle, g	2.8	2.9	4.9	4.6	8.1
Formate loss in SME, g	-7.6	4.7	-3.6	10.5	18

The correlation between formate loss and CO_2 formation is not good (it is expected to be fairly good). The changes in formate are only a few percent of the total formate and are difficult to extract accurately from mass balances combined with IC formate analyses. Results hint that there may have been some issues with the SB7b-6 and 7 SRAT and/or SME slurry formate analyses which were run as a block.

Often, hydrogen and CO_2 are the only SME off-gas graphs to report. That was not the case for SB7b. Significant (readily measureable) N_2O formation was seen in four of the five SME cycles, Figure 15. The exception was the high acid run, SB7b-9.

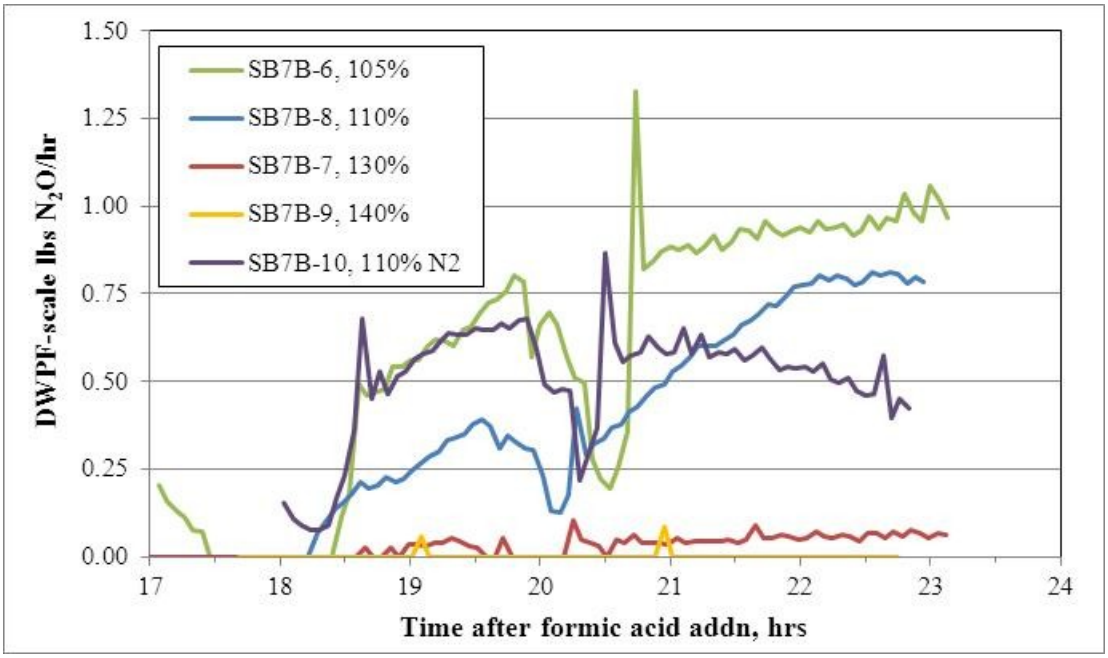

Figure 15. SME Cycle Nitrous Oxide

SB7b-6 could be showing the destruction of the nitrite remaining in the SRAT product. The interpretation of the off-gas data, e.g. hydrogen, would indicate, however, that there was no nitrite ion remaining in any of the other four runs (either feed nitrite or nitrite formed from nitrate and excess acid). The N_2O could be from further incomplete conversion of nitrate to ammonium ion. The two high acid runs were making ammonium ion and made very little N_2O, while the low acid runs put very little ammonia into the off-gas and managed to make some N_2O. If this is the correct interpretation, then it is another piece of data indicating that SB7b is a particularly active system catalytically.

3.2.3 *SME Product Waste Loading and Redox*

Calcined solids based waste loadings were calculated for the SME products. The mass of calcined solids in the SME product (before samples) was compared to the mass of frit added. The mass of calcined solids in the SRAT product fed to the SME was also compared to the mass of frit added. This approach gave two independent estimates of the waste loading. The target was 36% waste loading. Frit 418 was used. These were compared to nominal Li and B based waste loadings assuming 8 wt.% B_2O_3 and Li_2O in the frit.

Table 27. SME Waste Loading

Run ID:	SB7b-6	SB7b-8	SB7b-7	SB7b-9	SB7b-10
Acid stoichiometry, %	105	110	130	140	110
SRAT waste oxides, % in glass	37	37	37	36	38
SME waste oxides, % in glass	35	35	34	36	32
B-based waste loading, %	44	48	44	49	39
Li-based waste loading, %	44	44	45	45	40

SB7b-10 missed the target by more than the normal variation seen in prior tests. The reason is a lack of agreement between the SRAT product calcined solids mass and the SME product calcined solids mass minus the frit mass. The element based waste loadings are difficult to explain without invoking 7% for the B_2O_3 and Li_2O in the frit.

The RedOx calculations ($Fe^{2+}/\Sigma Fe$) are compared to the measured RedOx[16] in Table 28. The four individual SME product inputs to the RedOx equation are given as well (there was no coal).

Table 28. SME RedOx

Run ID:	SB7b-6	SB7b-8	SB7b-7	SB7b-9	SB7b-10
Acid stoichiometry, %	105	110	130	140	110
Formate, gmol/kg SME product	1.174	1.088	1.083	1.075	1.100
Oxalate, gmol/kg SME product	0.081	0.061	0.062	0.062	0.074
Nitrate, gmol/kg SME product	0.389	0.396	0.381	0.414	0.408
Manganese, gmol/kg SME product	0.115	0.112	0.112	0.116	0.106
Calculated RedOx	0.26	0.22	0.23	0.19	0.22
Measured RedOx	0.22	0.19	0.20	0.16	0.30

The four baseline blend flowsheet runs ran close to the expected RedOx value (delta of 0.03-0.04). The expected values were consistently higher for the four baseline runs rather than randomly distributed about the measured values. Oxalate contributed about 10-12% of the reducing potential of the melter feed (formate and oxalate contribution). A 20% uncertainty in oxalate concentration would only have a ±2% impact on the reducing potential which should not present a problem for RedOx control.

4.0 Conclusions

Simulant flowsheet studies were completed for SB7b as it will be processed from Tank 40. The testing only considered the case where caustic was added to increase sodium relative to other species. Four lab-scale SRAT/SME simulations were performed using the sludge-only flowsheet. The tests covered the range of 105-140% of the Koopman minimum acid equation (106.6-142% DWPF-Hsu equation). One lab-scale SRAT/SME simulation was performed using the coupled (ARP/MCU) flowsheet at 110% KMA.

Nitrite was present in the SRAT product at 105% KMA at 366 mg/kg slurry, while SME cycle hydrogen reached 94% of the DWPF SME cycle limit at 140% KMA. A suitable process window appears to be 107-130% for the DWPF acid equation for sludge-only processing allowing some conservatism for the mapping of lab-scale simulant data to full-scale read waste processing. This window should be usable with or without the addition of up to 7,000 gallons of caustic to the batch.

DWPF process simulations of the CPC using SB7b-Tank 40 simulant spiked with caustic indicate the potential for processing challenges in DWPF. SB7-Tank 40 will continue to have high noble metal concentrations following the transfer of SB7b from Tank 51. In addition, the mercury concentration will fall somewhat. Mercury appears to be mitigating some of the catalytic hydrogen generation, while perhaps promoting ammonium ion formation in its stead. SME cycle hydrogen generation seemed particularly sensitive to the wt.% total solids concentration target

and to the additional formic acid added with the frit slurries. DWPF should not concentrate past 48 wt.% total solids if moderate hydrogen generation is occurring simultaneously.

The coupled flowsheet simulation made more hydrogen in the SRAT and SME cycles than the sludge-only run with the same acid stoichiometry. The slow acid addition in MCU seemed to alter the reactions that consumed the small excess acid present such that hydrogen generation was promoted relative to sludge-only processing. The coupled test reached higher wt.% solids and this likely contributed to the SME cycle hydrogen limit being exceeded at 110% KMA. It is clear from the trends in the processing GC data, however, that the frit slurry formic acid contributed to driving the hydrogen generation rate above the SME cycle limit.

The impact of bounding quantities (up to 9,000 gallons) of ARP on DWPF study for SB3 indicated that the best approach was to reduce the stoichiometric acid factor as the volume of ARP combined into the SRAT receipt slurry increased.[17] The factor correction is necessary to offset certain biases in the coefficients of the current DWPF stoichiometric acid equation related to the acid demand in the insoluble sludge solids that are essentially absent in ARP. Catalytically active sludges that produced significant hydrogen, like SB7b, were the ones that were most at risk.

5.0 Recommendations

DWPF should process SB7b with caution. Further concentration of the insoluble solids beyond the projections of August 2011 could invalidate the testing in this report by increasing noble metal concentrations to untested levels. The potential addition of caustic (not finalized as of this draft) has reduced the stoichiometric acid factor window relative to SB7a. Neglecting the acid content of the MCU solution could be an issue for hydrogen generation, though it is probably only an issue for large MCU volumes and acid molarities in excess of 0.04M.

For processing SB7b:

- The DWPF should initiate processing by targeting an acid addition stoichiometry of 115% based on the current DWPF (Hsu) equation for processing the blend of SB7a with SB7b.

- The DWPF should discontinue the addition of formic acid with the frit-water slurry in the SME cycle. SRNL studies indicate that formic acid is probably not needed to slurry Frit 418 or avoid gel formation (some simple tests may be needed to confirm). The additional formic acid added with the frit appears to be largely responsible for pushing the hydrogen generation rates near or over the SME cycle limits.

- The acid stoichiometric factor for SRAT batches with greater than 1,000 gallons of ARP incorporated into the SRAT receipt slurry should be reduced to 110% for the initial batches and only increased if warranted by processing results (both SRAT and SME cycle hydrogen generation).

- At the recommended acid stoichiometry (115% DWPF equation), DWPF should initiate operations by assuming the following parameters for the SRAT as a starting point for DWPF acid calculations:

    - 100% nitrite destruction

- 20% formate destruction
- 15% nitrite-to-nitrate conversion

A small amount of formate and nitrate (~5%) may also be destroyed in the SME, and these amounts should be estimated after the first couple of SME batches. The combined SRAT/SME oxalate losses during testing ranged from 0-25%, which is nearly the range of uncertainty on the product slurry analyses, but the result was not centered about zero loss. Therefore 10% oxalate destruction should be assumed during the acid calculation REDOX balance until DWPF process data are available.

- IIT 747 antifoam appeared to be adequate to control foaming during the simulant testing using existing protocols for addition amounts. The additional antifoam every 8 hours during boiling was not required. Nitric acid addition was completed using 100 ppm in the simulant tests rather than 200 ppm. The existing protocols for the SRAT and SME cycles should be reviewed to determine whether selected additions can be eliminated or reduced. The review should consider the results of SC-12, the real waste run, since they are more indicative of foaming tendencies than simulant tests. Caustic boiling was not performed during the testing except in the coupled flowsheet run; existing protocols should be followed for caustic boiling.

6.0 Acknowledgements

The author would like to acknowledge the assistance of the Process Science Analytical Lab personnel and the Analytical Development group for their support with sample analysis. The technical analysts, both at Aiken County Technology Laboratory, and those loaned from the main SRNL campus, were instrumental in setting up the test equipment and conducting the process simulations which required round-the-clock coverage. The author also acknowledges the technical review assistance of M. E. Stone, who reviewed acid calculations and simulation R&D directions in addition to the review of this report. S. L. Crump's work with volatile and semi-volatile organic analysis is also acknowledged in the context of examining samples for antifoam and/or antifoam decomposition products.

7.0 References

[1] Stone, M. E., *Task Technical and Quality Assurance Plan for Sludge Batch 7b Simulant Flowsheet Studies*, SRNL-RP-2011-00270, SRNL, Aiken, SC, 29808 (February 2011).

[2] Coleman, C. J., *Method to Determine Oxalate in High-Level Sludge by Ion Chromatography,* WSRC-TR-2002-00497, Westinghouse Savannah River Company, Aiken, SC 29808, 2002.

[3] Newell, J. D., *Simulant Development for Sludge Batch 6*, SRNL-STI-2010-00219, SRNL, Aiken, SC, 29808 (April 2010).

[4] Pareizs, J. M., *Chemical and Fissile Characterization Results of the SRNL-Prepared Sludge Batch 7b Tank 51 and Tank 40 Samples*, SRNL-L3100-2011-00128, SRNL, Aiken, SC, 29808 (July 2011).

[5] Pareizs, J. M. and D. P. Lambert, *Data and Observations from the SB7b Qualification SRAT and SME Cycle*, SRNL-L3100-2011-00141, SRNL, Aiken, SC, 29808 (July 2011).

[6] Reboul, S. H. and D. R. Click, *Stable Constituents in SB7a Tank 40 WAPS Sample*, SRNL-L3100-2011-00133, SRNL, Aiken, SC, 29808 (June 30, 2011).

[7] Pareizs, J. M., *Tank 51 SB6 Qualification SRAT Receipt Characterization*, SRNL-L3100-2010-00027, Savannah River Site, Aiken, SC, 29808 (March 11, 2010).

[8] Fox, K. M., D. K. Peeler, M. E. Stone, D. C. Koopman, J. M. Pareizs, and D. R. Click, *Summary of SRNL Sludge Batch 7b Testing and Recommendations for DWPF Processing*, SRNL-L3100-2011-00176, SRNL, Aiken, SC, 29808 (September 2011).

[9] Stone, M. E., *Lab-scale CPC Equipment Setup*, SRNL-L3100-2011-00127, SRNL, Aiken, SC, 29808 (July 2011).

[10] Koopman, D.C., A. I. Fernandez, and B. R. Pickenheim, *Preliminary Evaluations of Two Proposed Stoichiometric Acid Equations*, SRNL-L3100-2009-00146, Savannah River Site, Aiken, SC 29808 (2009).

[11] Marek, J. C. and R. E. Eibling, *Calculational Algorithms for Nitric Acid Sludge Adjustment*, SRTC-PTD-92-0050, Savannah River Site, Aiken, SC, 29808 (September 1992).

[12] Jantzen, C. M. and M. E. Stone, *Role of Manganese Reduction/Oxidation (RedOx) on Foaming and Melt Rate in High Level Waste Melters*, WSRC-STI-2006-00066, Savannah River Site, Aiken, SC, 29808 (March 2007).

[13] Fernandez, A. I. and D. C. Koopman, *Sludge Batch 7 Qualification and Flowsheet Chemical Process Cell Simulations*, SRNL-STI-2011-00006, Rev. 1, SRNL, Aiken, SC, 29808 (May 2011).

[14] SRNL L29 Manual, Procedure ITS-0094, Rev. 4, *Laboratory Scale Chemical Process Cell Simulations*, SRNL, Aiken, SC, 29808.

[15] Koopman, D. C., *Noble Metal Chemistry and Hydrogen Generation during Simulated DWPF Melter Feed Preparation*, WSRC-STI-2008-00002, SRNL, Aiken, SC, 29808 (June 2008).

[16] Newell, J. D., *Defense Waste Processing Facility (DWPF) Sludge Batch 7b (SB7B) RedOx Evaluation*, SRNL-L3100-2011-00178, SRNL, Aiken, SC, 29808 (August 2011).

[17] Koopman, D. C., C. C. Herman, M. A. Baich, D. R. Best, T. K. Snyder, M. F. Williams, *Impact of a Bounding Quantity of ARP Waste on the DWPF Process Flow Sheet*, WSRC-TR-2003-00403, SRNL, Aiken, SC, 29808 (September 2003).

Appendix A
SB7b-Tank 51 Process Simulations

Introduction

Two sets of simulations were performed to support SB7b flowsheet development in addition to the testing discussed in the main body of the report. The first of these was testing with a simulant targeted to the SB7b-Tank 51, or batch, composition. The second set of tests investigated the impact of significant added caustic on the acid requirement for nitrite destruction using a well-characterized simulant from storage. This appendix covers the SB7b-Tank 51 results.

Three SRAT/SME simulations were performed at lab-scale using a simulant that targeted the projected composition of SB7b-Tank 51 slurry. These simulations were performed in April 2011 when it was still assumed that SB7b qualification in the SRNL Shielded Cells would be done using a washed sample from Tank 51. Subsequently, a decision was made to qualify the blend of SB7b with SB7a, in which SB7a accounts for over two-thirds of the blend on a solids basis.

Simulant

Simulants of Tank 4, Tank 7, and Tank 12, originally prepared for SB7a, were combined to prepare the SB7b simulant. A SB7b-Tank 51 slurry was also prepared in the Shielded Cells. The radioactive slurry was combined with SB7a Tank 40 WAPS sample slurry to prepare the SB7b blend simulant used in qualification. The simulant composition for SB7b-Tank 51 is compared to the slurry made in the Shielded Cells on both a radioactive and non-rad basis in Table 29 as well as to an early August 2011 projection for the composition in Tank 51 prior to transfer to Tank 40. The elemental data are derived from an oxide basis (calcined basis) composition. Mercury is not retained in calcined oxides and is not in the table. An equivalent non-rad Shielded Cells composition was obtained by subtracting the uranium and thorium oxides from 100%, and then renormalizing the remaining oxides back to 100% total.

Table 29. SB7b-Tank 51 Calcined Elemental Comparison

	SB7b Tank 51 Simulant	Shielded Cells Tank 51-non rad	Shielded Cells Tank 51 – rad	SB7b Tank 51 Tank Farm Projection
Al	9.78	9.21	8.32	8.89
Ba	0.15	0.19	0.17	
Ca	1.16	0.91	0.82	0.93
Ce	0.19	0.26	0.24	
Cr	0.06	0.06	0.05	0.13
Cu	0.04	0.11	0.10	
Fe	28.2	25.1	22.6	24.8
K	0.06	<0.03	0.08	0.27
La	0.11	0.15	0.14	
Mg	0.32	0.28	0.25	0.27
Mn	4.22	3.32	3.00	3.43
Na	14.5	20.5	18.5	13.1
Ni	6.23	6.50	5.87	5.88
P	<0.1	<0.1	<0.1	
Pb	<0.01	0.05	0.05	
S	0.58	0.92	0.83	0.59
Si	1.64	1.43	1.29	1.55
Ti	0.02	0.03	0.02	
Zn	0.05	0.05	0.05	
Zr	0.35	0.22	0.20	
Th	-	-	0.80	0.68
U	-	-	7.46	8.44

The Tank Farm projection for Tank 51 only included comparatively major species, so there are many blank entries that do not indicate the absence of those species in the slurry. The main difference between the simulant and the Shielded Cells slurry was in sodium content. The higher sodium in the Cells slurry tended to reduce the wt.%'s of the other elements. A similar effect was seen with the SB7b blend compositions (the Shielded Cells blend had sufficient sodium to not require a caustic addition to achieve high waste loadings with frit 418, unlike the projection for SB7b in the Tank Farm).

Some additional compositional and physical property results are given in Table 30.

Table 30. Simulant and Radioactive Feed Properties

	SB7b Batch simulant	SB7b Tank 51 Cells
Total solids, wt%	16.5	17.9
Insoluble solids, wt%	11.7	14.4
Soluble solids, wt%	4.8	5.7
Calcined solids, wt%	12.5	14.4
Slurry density, g/mL	1.13	1.14
Supernate density, g/mL	1.04	1.05
Slurry base equiv., mol/L slurry	0.42	Note 1
Nitrite, mg/kg	12,000	8,850
Nitrate, mg/kg	8,500	5,700
Sulfate, mg/kg	2,300	2,300
Oxalate, mg/kg	1,400	1,300
Chloride, mg/kg	<100	<180
Slurry TIC, mg/kg slurry	1,410	-
Supernate TIC, mg/L supernate	1,070	750

1 – hydroxide plus carbonate plus aluminate (1:1:1) gives 0.42M slurry base

Slurry TIC was not measured on the Cells sample. The Cells slurry was more washed than the simulant slurry as seen by the nitrite and nitrate concentrations. This seems to stand in contradiction to the Cells calcined sodium being higher than the simulant. The Cells slurry was also more concentrated in total solids and insoluble solids. This is not an off-setting effect to the higher sodium in the calcined elements if the sodium is primarily in the supernate phase.

Mercury and noble metals in the SB7b Tank 51 simulant are compared to those in the SB7b-Tank 51 blend prepared in the Shielded Cells and to the SB7a WAPS sample in Table 31.

Table 31. Noble metal and mercury, wt.% in total solids

	SB7b Sim (Tank 51)	SB7a WAPS	SB7b-Tank 51 Cells
Rh, wt%	0.036	0.019	0.027
Ru, wt%	0.17	0.094	0.13
Hg, wt%	0.66	1.9	0.71
Pd, wt%	0.006	0.003	0.002
Ag, wt%	0.017	<0.02	0.011

The simulant target noble metal concentrations bound the Cells slurry in a wt.% total solids sense, but also in a mg noble metal/kg slurry sense (which required the simulant wt.%'s to be at least 9% higher than the radioactive slurry values). Both the simulant and the Cells Tank 51 blend are considerably higher in Rh and Ru than the SB7a WAPS sample. Consequently the blend of SB7b with SB7a will cause an increase in the Rh and Ru concentrations. The simulant mercury concentration did not bound the mercury in the Cells blend. Both, however, are much lower than the mercury in SB7a, so Tank 40 mercury concentration will decrease after SB7b is added.

Process Simulation Results
SRAT Cycle Data

Three lab-scale SRAT/SME process simulations were performed:

SB7b-1 at 105% Koopman minimum acid (111% Hsu)
SB7b-2 at 145% Koopman minimum acid (153.5% Hsu)
SB7b-3 at 115% Koopman minimum acid (122% Hsu)

Twelve hour reflux periods followed dewatering in the SRAT, since the mercury was predicted to strip to below the SRAT product specification in this time. SME product-based melter RedOx targeted 0.2 $Fe^{2+}/\Sigma Fe$.

Formate loss and nitrite/nitrate results are presented in Table 32 for samples taken a few minutes after formic acid addition was completed and for the SRAT product.

Table 32. SB7b-Batch SRAT Anion Reactions

	SB7b-1	SB7b-3	SB7b-2
Acid stoichiometry, %	105	115	145
Formate loss, post acid, %	12	18	†
Nitrite loss, post acid, %	48	64	†
Nitrate gain, post acid, %	31	20	†
Formate loss, SRAT product, %	25	34	39
Nitrite-to-nitrate, SRAT product, %	10	14	0
Nitrite loss, SRAT product, %	100	100	100

† - Results for SB7b-2 immediately after acid addition were suspicious, and it is possible that a non-representative sample was obtained, or that caustic quench dilution information was improperly recorded (expected results: ~20-25% formate loss, data show gain; <20% nitrate gain, data show 42% gain; a 42% gain is not credible for any stoichiometry).

Analytical anion data for the three SRAT products are given in Table 33.

Table 33. SB7b-Batch SRAT Product Anions, mg/kg

	SB7b-1	SB7b-3	SB7b-2
F^-	<100	<100	<100
Cl^-	430	410	390
NO_2^-	<100	<100	<100
NO_3^-	19,900	22,000	22,100
$SO_4^=$	630	730	590
$C_2O_4^=$ (wd)	<100	<100	<100
TIC* (ins)	446	274	473
HCO_2^-	41,400	39,200	42,700
PO_4^{3-}	<100	<100	<100

wd – water dilution
* – see insoluble TIC discussion below

Some variation in the results for SB7b-2 compared to the other two is due to this SRAT product being somewhat less concentrated, e.g. chloride and sulfate analyzed lower not because there was less present, but because the sample was more dilute. For each run, about 40 g of SRAT product slurry was diluted with DI water to about 700 g, centrifuged, decanted, and a new sample of about 60 g produced containing the insoluble solids in the SRAT product. These samples were analyzed for TIC-TOC. It was determined after the runs that the single wash did not remove enough formate ion to unambiguously detect antifoam bound with the insoluble solids (as TOC). TOC results ranged from 1100-1300 mg/kg. While the absolute concentrations are only accurate within a factor of 1.5-2 because the washes were only semi-quantitative, the insoluble solids in all three SRAT products contained inorganic carbon (carbonate or bicarbonate) at an intermediate concentration. These may be associated with the precipitated Ca, Mg, or Mn formed during boiling.

Elemental wt.% data for the three SRAT products after calcining at 1100 °C are given in Table 34. Lead, chromium, and the noble metals (not listed) tend to be underreported in SRAT product calcined solids. General consistency in values for the three SRAT products is seen as desired.

Table 34. SB7b Batch SRAT Calcined Elements at 1100 °C-wt.%

	SB7b-1	SB7b-3	SB7b-2
Al	9.1	8.8	9.1
Ba	0.15	0.15	0.16
Ca	0.98	1.0	0.99
Ce	0.22	0.21	0.22
Cr	0.06	0.06	0.06
Cu	0.04	0.03	0.03
Fe	26.6	29.3	26.7
K	0.08	0.05	0.07
La	0.11	0.10	0.11
Mg	0.32	0.31	0.32
Mn	3.9	3.9	3.9
Na	14.3	13.4	14.4
Ni	5.9	6.3	5.8
P	<0.10	<0.10	<0.10
Pb	<0.010	<0.010	<0.010
S	0.53	0.64	0.55
Si	2.0	2.0	2.0
Sn	0.03	0.02	0.03
Ti	0.02	0.02	0.02
Zn	0.06	0.06	0.06
Zr	0.34	0.34	0.35

SRAT product solids data, densities, and pH are given in Table 35. The wt.% insoluble and soluble solids were calculated from the measured total slurry and supernate (dissolved) solids. The density measurements were made at 25 °C. There is pH data from the probe present in the SRAT vessel when the mantle was turned off at the end of the SRAT cycle as well as an independent pH measurement made on the sample of the SRAT product at room temperature.

Table 35. Additional SB7b Batch SRAT Product Properties

	SB7b-1	SB7b-3	SB7b-2
Wt. % total solids	23.4	23.7	22.7
Wt. % insoluble solids	14.1	14.4	14.4
Wt. % soluble solids	9.3	9.3	8.3
Wt. % dissolved solids	10.9	10.9	9.7
Wt. % calcined solids	16.8	17.2	15.8
Slurry density, g/mL	1.13	1.14	1.13
Supernate density, g/mL	1.06	1.07	1.06
Product pH at 25 °C	7.45	8.41	7.96
Product pH in vessel at 101 °C	7.30	7.11	6.64

The tests ended near the target of 24 wt.% total solids. The pH data taken from the probes in the slurry during processing (at 101 °C) seem to make more sense than the room temperature data taken later on samples of the SRAT products. The result for SB7b-2, however, may be low. The graph of pH versus time below, Figure 16, shows an unexplained shift down in pH for SB7b-2 of several tenths that appears to have been sustained over the last ten hours of reflux.

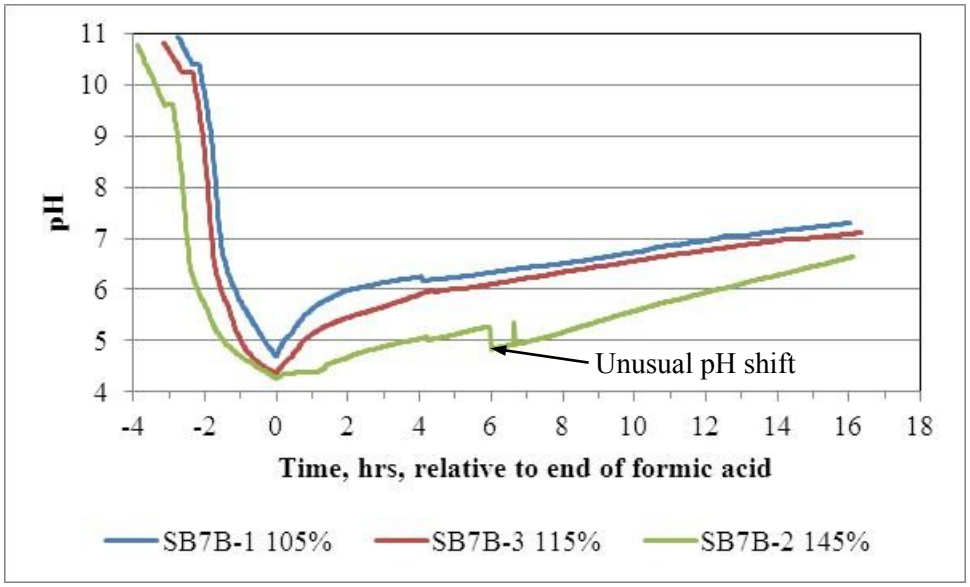

Figure 16. Batch simulant SRAT cycle pH data

SRAT Off-gas Data

SRAT cycle hydrogen generation rates converted to DWPF scale are given in Figure 17.

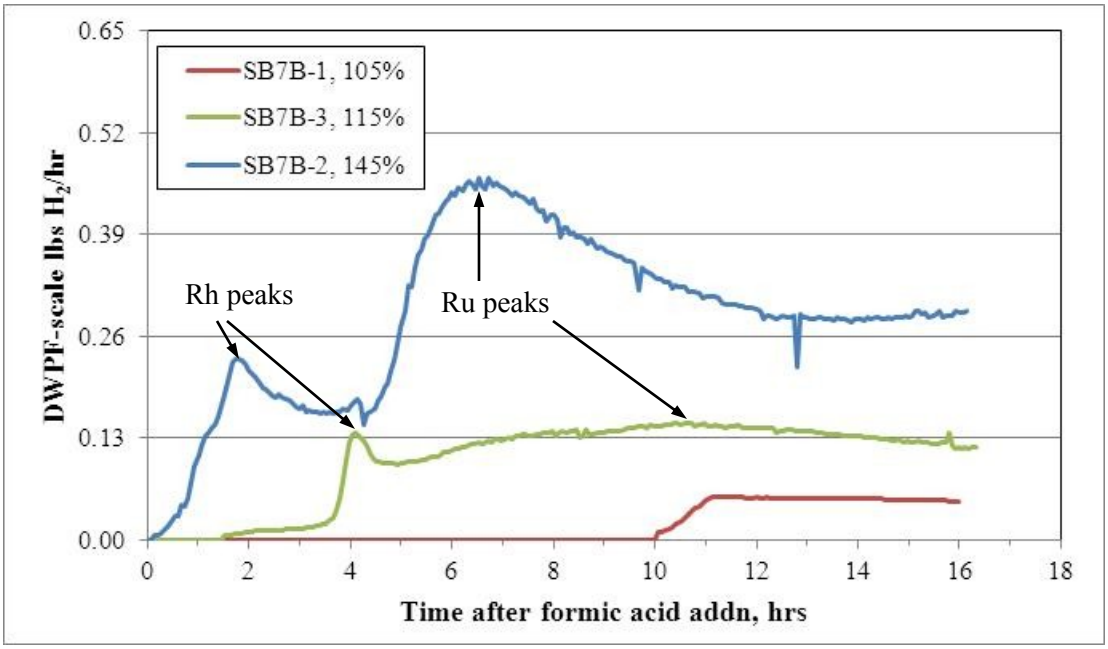

Figure 17. SB7b Batch SRAT hydrogen generation

The data for SB7b-2 and 3 seem to indicate a Rh driven peak at 2 and 4 hours after acid addition respectively, followed by a Ru driven peak at 6 and 11 hours respectively. The second peaks gave the maximum generation rates for the SRAT cycle. While the initial Rh peak in hydrogen generation seems to be nearly entirely due to Rh, the second, or "Ru", peaks seem to combine Ru catalysis with a background level of Rh catalysis. SB7b-2 reached 71% of the DWPF SRAT limit. The onset of hydrogen at ten hours in SB7b-1 likely signals the completion of nitrite destruction in that run.

Carbon dioxide generation rates during and immediately following acid addition are shown in Figure 18. The remaining SRAT CO_2 data are shown in Figure 19 using an expanded scale.

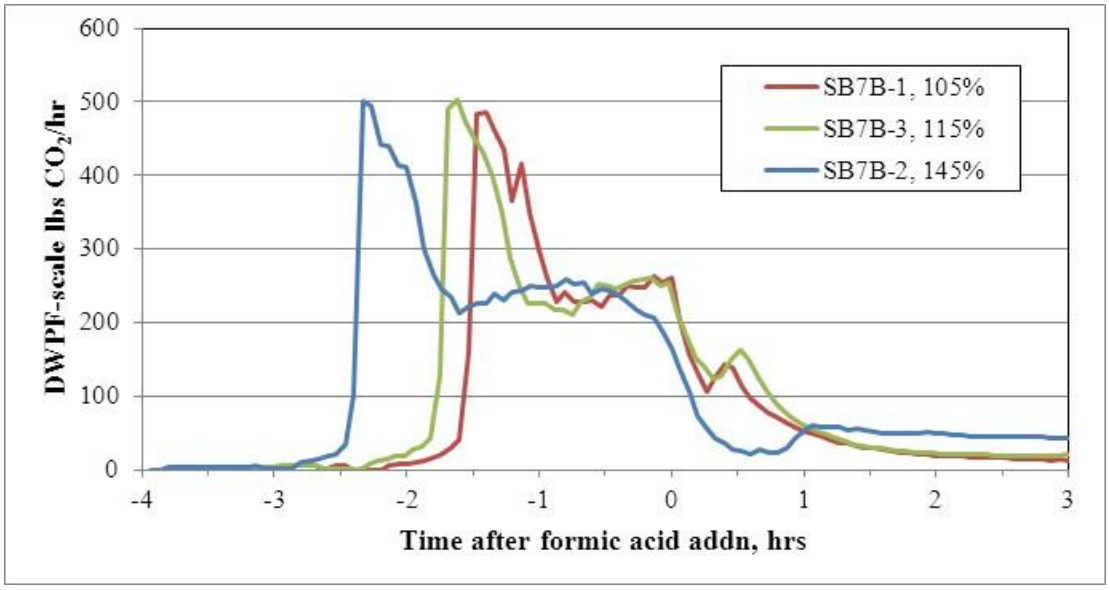

Figure 18. SB7b Batch CO_2 generation rates

The three runs were very similar except for the differences due to the initiation and duration of acid addition as stoichiometry changed.

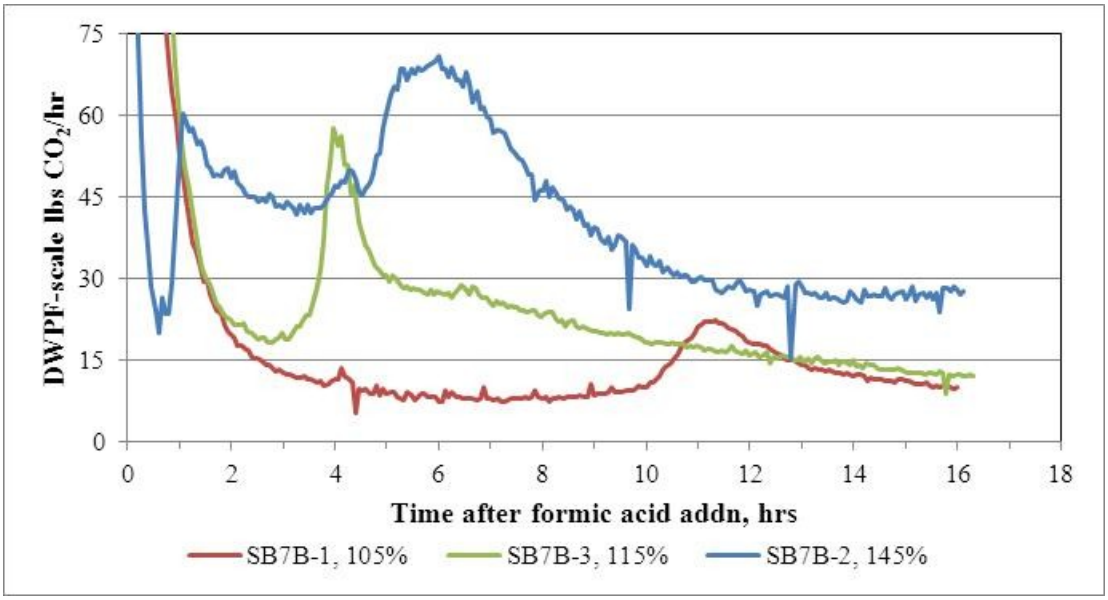

Figure 19. SB7b Batch CO_2 during boiling

CO_2 profiles for SB7b-2 and 3 were only weakly correlated with the hydrogen generation rates. Timing was somewhat matched but relative peak shapes were quite different. SB7b-1 had an increase in CO_2 at 10 hours corresponding to the onset of hydrogen in that run.

The nitrous oxide data during primary nitrite destruction is shown in Figure 20

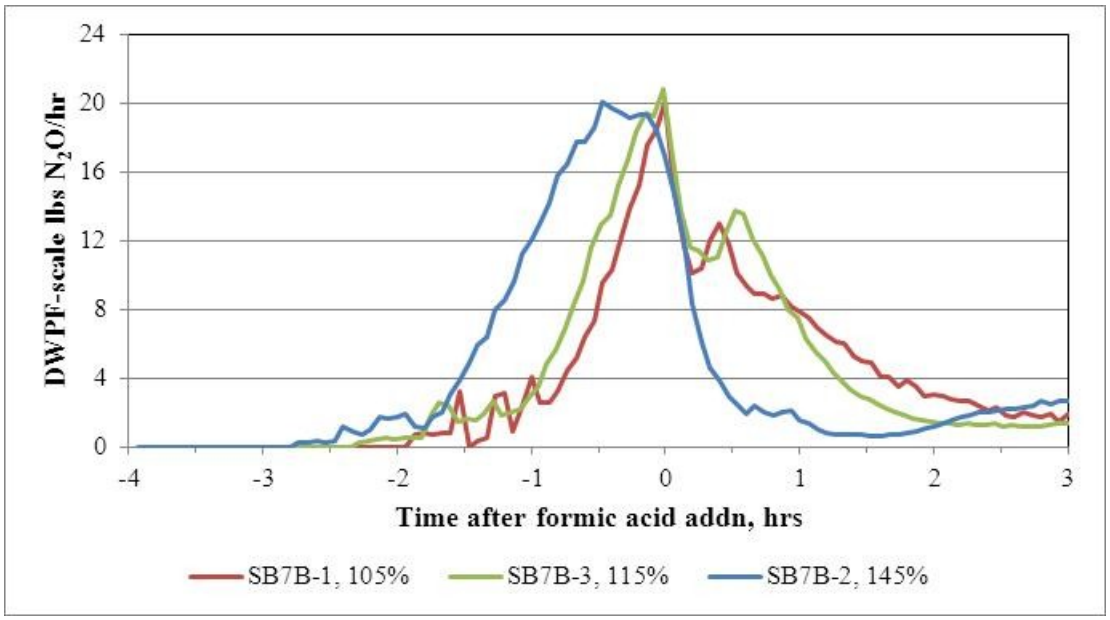

Figure 20. SB7b Batch N_2O generation rates

The data are fairly well aligned while acid is being added (the slopes up are virtually identical in the period from -2 to 0 hours). This indicates a reaction rate proportional to the acid addition rate. An early end to nitrite destruction is indicated for SB7b-2, probably less than 30 minutes after the end of formic acid addition. SB7b-3 appears to have nearly completed nitrite destruction by 1.5-2 hours after formic acid addition. Data for the remainder of the SRAT cycle are given Figure 21.

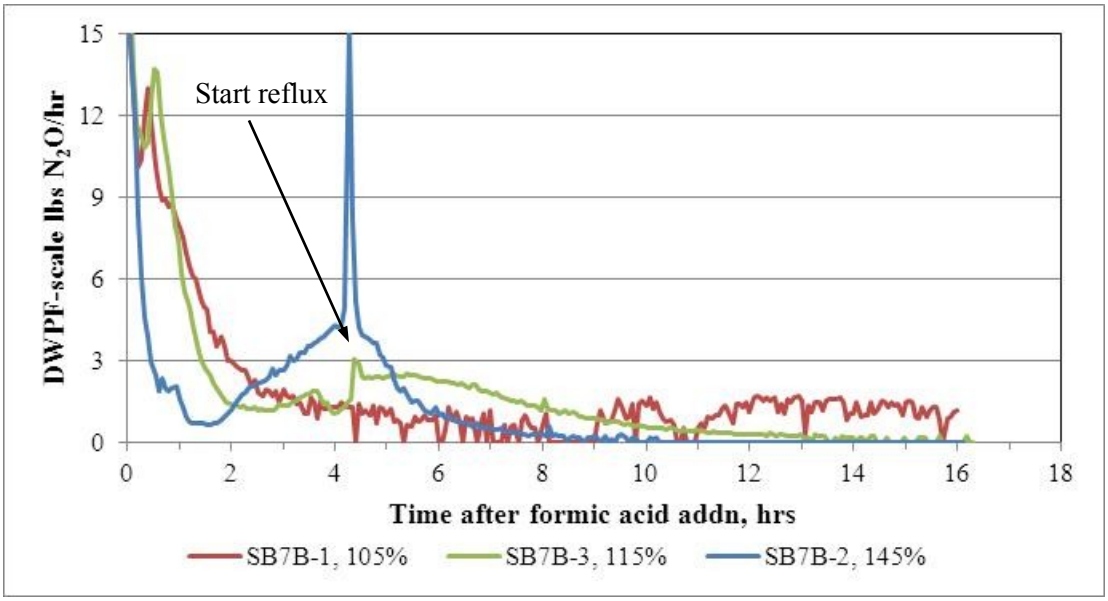

Figure 21. SB7b Batch N_2O during boiling

The spike at four hours for SB7b-2 occurred at the onset of reflux. There was a smaller spike in SB7b-3. SB7b-1 showed signs of continuing nitrite destruction during most of the SRAT, but the signal was close to the detection limit. A peak of 0.2 vol% was almost not detectable.

Consequently, the trace for SB7b-1 appears ragged, or noisy, because the data are at the lower end of the detection range.

Supplemental SRAT Cycle Data

Samples of the SRAT dewater condensate were analyzed to support several on-going studies. The samples were analyzed for nitrite, nitrate, formate, mercury, and silicon. Silicon was assumed to be present as antifoam at 14 wt.% Si. The fraction of antifoam that could have been lost during dewatering was calculated from the dewater condensate mass, Si concentration, and mass of antifoam additions in the SRAT. The fraction of mercury present in solution in the dewater condensate was also calculated with respect to the mass of mercury added as the HgO trim chemical. An abbreviated summary is given in Table 36.

Table 36. SB7b Batch SRAT Dewater Condensate

	SB7b-1	SB7b-3	SB7b-2
Acid Stoichiometry	105%	115%	145%
Condensate mass, g	1,163	1,209	1,046
Nitrite, mg/L	<100	<100	<100
Nitrate, mg/L	6,100	3,400	2,900
Formate, mg/L	260	310	1,500
Potential antifoam loss	27%	66%	83%
Dissolved mercury loss	6.4%	5.7%	0.4%

Si mass in the dewater condensate increased with increasing acid stoichiometry. This increase implies more potential antifoam loss to the MWWT with increasing acid stoichiometry. Potentially a very high percentage of antifoam could have been lost during dewatering. The dewatered condensate mass was fairly large for a 4-L lab-scale SRAT run in all three cases (there were roughly 4,000 g in the SRAT at the start of dewatering and just under 3,000 g after dewatering). The large dewater mass may have inflated the potential antifoam loss. The maximum stripped antifoam mass, assuming all Si is associated with antifoam at 14% Si in antifoam, only amounts to 2.4 g of antifoam or less than a quarter percent of the collected condensate mass. The reader should be aware that these are bounding calculations. The Si in the condensate could as easily be disilicic acid from stripping some of the chemically dissolved SiO_2.

Nitrate and formate can be taken as nitric and formic acid respectively. Therefore, higher concentrations of these species implies that the condensate is more acidic. The amount of nitrate collected historically depends on how much nitrite is destroyed during dewatering versus during formic acid addition (nitrate and nitrite form from the NO_2 produced during nitrite destruction that gets absorbed into water droplets in the SRAT condenser, and nitrite subsequently converts to nitrate under fairly acidic conditions in the MWWT).

The concentration of condensate formate typically depends on the acid stoichiometry (higher stoichiometry, more formate in both SRAT and condensate). The formate concentration in the MWWT tends to decline over time as the SRAT pH slowly increases due to catalytic decomposition of formic acid/formate in the SRAT slurry. Dissolved mercury decreased with increasing acid stoichiometry. The anion data imply a rising pH of the condensate with increasing acid stoichiometry which should impact mercury solubility. The magnitude of the dissolved Hg drop from SB7b-3 to SB7b-2, however, seems to indicate that more than simply pH may be impacting Hg solubility.

Scoping samples were obtained in an attempt to learn more concerning the fate of antifoam during the CPC process. These samples included the SRAT dewater condensates analyzed for Si as discussed in Table 36. In addition, hexane extractions were performed on SRAT and SME dewater condensates, the MWWT and FAVC condensates removed following the SRAT and SME cycles (for SB7b-1 and 2 only), the SME product slurry, and the ammonia scrubber solution. Following the extractions, and draining of liquids and slurries from the lab equipment, the SRAT, SRAT lid, SRAT agitator, SRAT off-gas line, SRAT sample tube, SRAT pH probe, SRAT condenser, MWWT, SRAT condenser to FAVC line, and FAC were subjected to hexane rinses to recover any soluble organic material. A sample of SRAT product was also taken, diluted about 17 to 1 with de-ionized water, and centrifuged. The majority of the diluted supernate was discarded to remove formate (soluble total organic carbon, TOC). The remaining sample (primarily insoluble SRAT product solids) was analyzed for TOC.

Various compounds potentially related to antifoam were found using semi-volatile organic analysis and volatile organic analysis on the hexane extractions and hexane rinses. These included siloxanes, triimethyl silanol, methoxy trimethyl silane, hexamethyl disiloxane, aliphatic hydrocarbons, dioctyl phthalate, and emulsifiers. Cumulatively, these species amounted to less than 3% of the antifoam mass in all three runs when the measured concentrations were worked back through material balances. This small contribution in all three runs, however, came more than 50% from rinsing the MWWT with hexane.

The TOC results on the SRAT solids could explain as much as 40-80% of the antifoam mass assuming antifoam is 48% carbon. The hypothesis was that the antifoam, or at least the organic part of the antifoam, might be held on the surfaces of the insoluble solids. In that form, the organic material was potentially difficult to extract into solution with hexane.

The SRAT dewater condensate Si results presented in Table 36 could be derived from antifoam at 27-83% of the total antifoam. Combined with the TOC results on the SRAT product, the pair of results could nearly close an antifoam material balance.

Table 37. SB7b Batch Antifoam Balance

	SB7b-1	SB7b-3	SB7b-2
Acid Stoichiometry	105%	115%	145%
SRAT insoluble TOC as antifoam	80%	39%	48%
Dewater Si loss as antifoam loss	27%	66%	83%
Miscellaneous organics as antifoam	2%	<1%	2%
Sum	110%	106%	133%

There are several unproven assumptions in the antifoam balance, however, so these results should be taken as preliminary and scoping rather than definitive. A decomposed antifoam molecule could show up multiple places, such as a low molecular weight siloxane in the dewater condensate and as an adsorbed organic chain on the SRAT solids. The hexane rinses and extractions seemed to give rather uneven results, suggesting that lab technique is likely a factor. The TOC analysis required removal of TOC due to residual formate. The original plan was to dilute the formate such that its contribution to TOC would be less than 10% of any significant TOC due to antifoam, but the actual samples were potentially 50-75% TOC due to formate which had to be subtracted from the measured TOC to obtain the TOC potentially due to antifoam.

During the organic analyses of the above hexane rinses and extractions, there were two condensate samples (from SB7b-1) that were found to contain very low concentrations of dimethyl mercury (of order 1-3 ppb; SRNL's working threshold for dimethyl mercury is in ppm's). Some dimethyl mercury was found draining the MWWT condensate following the SRAT cycle, and some was found in the final SME dewater condensate. Concentration was estimated from peak area alone, since Analytical Development did not have a dimethyl mercury standard to use for calibration. The analytical signature, however, was sufficient for a conclusive identification of dimethyl mercury in the two samples.

Various samples of a more routine nature were taken to check for unexpected deviations in the SRAT processing chemistry. SRAT slurries were checked for dissolved elements following acid addition, after dewatering, after four hours of reflux, and in the SRAT product. Sodium and potassium are not reported but are close to 100% in solution. Results for the minimum acid stoichiometry run are given in Table 38.

Table 38. Dissolution percent of elements in SB7b-1

Element:	Post acid	Post dewatering	4 hours reflux	SRAT product
Al	0.02	0.01	0.01	<0.01
Ba	0.5	0.5	0.4	0.2
Ca	89	70	64	49
Cu	3	0.6	0.6	0.6
Fe	<0.01	<0.01	<0.01	<0.01
La	1.8	0.3	0.3	0.2
Mg	25	23	21	10
Mn	67	20	15	3
Ni	10	0.11	0.04	<0.01
Rh	61	0.85	0.50	<1
S	51	44	41	37
Si	1.7	1.8	3.5	1.9
Sn	6.0	2.2	<2	<2
Zn	4.5	<0.1	<0.1	<0.1

A general decline in solubility of elements versus processing time was observed following acid addition. The pH climbed steadily during this period which likely explains the behavior of Al, Ba, Cu, Ni, Sn, and Zn. The precipitated forms of Ca, Mg, and Mn are speculated to be oxalates mixed with carbonates or bicarbonates formed from absorbed CO_2 produced from formic acid decomposition. Sulfur (sulfate is the only source of sulfur in the simulant preparation recipe) was indicated to be significantly precipitated in this and the other run data. This is different than the behavior seen in the SB7b blend testing. Nearly indistinguishable results were obtained for SB7b-3 at 10% higher acid stoichiometry, Table 39.

Table 39. Dissolution percent of elements in SB7b-3

Element:	Post acid	Post dewatering	4 hours reflux	SRAT product
Al	0.07	0.01	0.01	<0.01
Ba	0.7	0.6	0.3	0.1
Ca	83	68	65	47
Cu	4.4	1.1	0.9	0.3
Fe	0.02	0.03	<0.01	<0.01
La	2.4	0.3	0.2	0.2
Mg	28	26	22	11
Mn	69	37	20	3.6
Ni	12	0.15	0.03	<0.01
Rh	65	0.54	0.61	1.7
S	39	32	31	32
Si	1.0	19	19	3.2
Sn	7.3	3.8	2	<2
Zn	7	<0.1	<0.1	<0.1

Higher extents of dissolution were found in SB7b-2 at the highest acid stoichiometry, and dissolution was sustained longer and at higher levels than in SB7b-1 and 3, Table 40.

Table 40. Dissolution percent of elements in SB7b-2

Element:	Post acid	Post dewatering	4 hours reflux	SRAT product
Al	0.55	0.03	0.01	<0.01
Ba	0.5	0.5	0.4	0.2
Ca	92	84	76	74
Cu	14	5	2	1
Fe	0.02	5.9	0.59	<0.01
La	5.0	1.7	0.7	0.3
Mg	33	34	35	29
Mn	90	85	63	18
Ni	24	7	1	0.01
Rh	24	2.0	1.1	2.1
Ru	6.1	0.5	0.4	0.9
S	58	50	45	37
Si	1.5	4.0	2.9	0.7
Sn	9	7	6	2
Zn	12	3.8	0.2	<0.1

Note that Ca and Mn were over 90% dissolved following acid addition in SB7b-2. This confirms the significance of these two insoluble species to the stoichiometric acid requirement. Mg never reached the same level of dissolution as Ca and Mn in the samples, although it may have already dissolved and undergone some precipitation by the end of acid addition. A somewhat different behavior for Mg compared to Ca has been seen in several of the sludge batch studies performed since the work on the SRAT chemistry timeline. Mg contributed 2.7% to the stoichiometric acid demand, so even a large uncertainty in its true chemical significance to the acid demand would have a minimal impact on the calculated value for the minimum stoichiometric acid requirement. The low sulfur solubility was unlike that in the high acid SB7b blend tests at 130 and 140% KMA.

Ca sustained a 30% higher extent of dissolution through to the SRAT product than in the two lower acid runs. More of the starting insoluble Ni (presumably as $Ni(OH)_2$) was dissolved during acid addition and neutralized than in the two lower acid runs. This nickel was able to consume some of the excess acid added to SB7b-2. La and Zn may have exhibited similar behavior to Ni, but they were present at less than 2% the total concentration of Ni and would not have a detectable impact on acid consumption.

Less Rh, but more Ru, was in solution at the end of acid addition compared to the two lower acid runs. A significantly higher percentage of Rh stayed dissolved during boiling, however, than in the two lower acid runs. SRAT noble metal chemistry studies showed that the dissolution behavior of Ru during the SRAT cycle is more complicated than that for most species. Detectable Ru was found in the supernate of all four SB7b-2 samples, but only in the end of acid addition samples for SB7b-1 and 3. Ru catalysis is the most likely explanation for the majority of the hydrogen made in the SRAT and SME cycles.

Iron went through an intermediate period of dissolution in SB7b-2 which was not detected (if it even occurred) in the two lower acid runs. Iron is the major insoluble species in SB7b batch simulant (about 3x by mass and 1.4x by moles relative to Al, the next most abundant insoluble element). More moles of iron are dissolved at 6% compared to 24% of the Ni. The dissolved iron, assuming it acts like $Fe(OH)_3$, could have consumed about 7% of the actual acid addition, or 10% of the minimum acid demand, i.e. iron dissolution was not a trivial piece of process chemistry. It is possible that the iron dissolution was driven by the formation of an iron oxalate complex. Formation of iron oxalates has been suspected since the early SB3 testing of high oxalate sludges.

SB7b-Tank 51Mercury Data

SRAT slurry samples were taken for mercury after acid addition. Samples were also taken at several different times once acid addition was complete (after dewatering, after 4 hours reflux, and after 8 hours reflux). SRAT and SME product slurries were also sampled for mercury. The mass of mercury in the vessel based on the measured slurry concentration is plotted as a function of processing time after formic acid addition had completed in Figure 22.

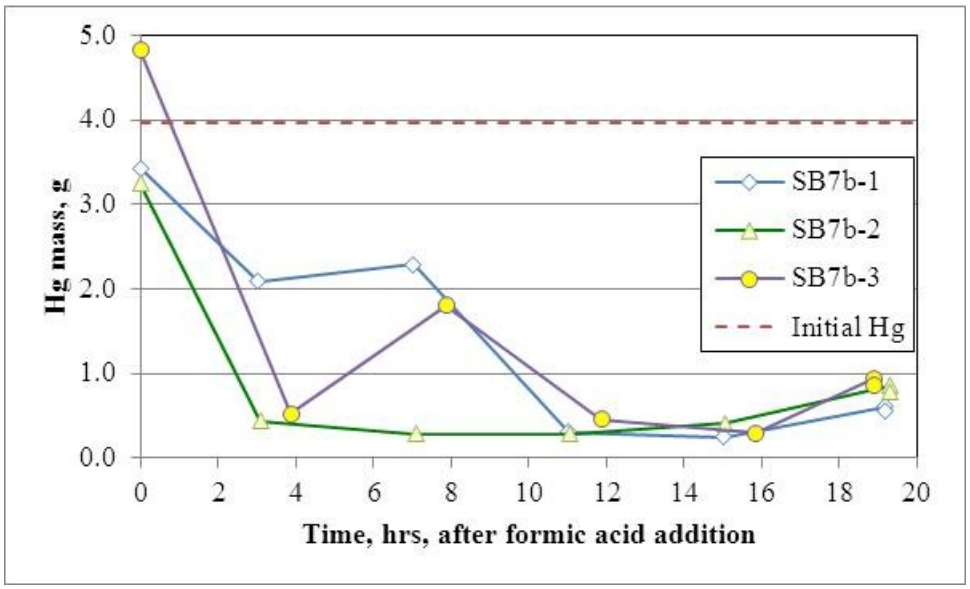

Figure 22. SB7b-Batch Slurry Mercury Content

The highest acid run, SB7b-2, showed behavior seen in many recent high acid runs. Mercury effectively dropped out of the slurry samples before dewatering was completed. The lowest acid run, SB7b-1, conversely, seemed to have suspended mercury at least for 8-9 hours after acid addition. SB7b-3 is harder to characterize. If the 8 hours after formic sample was artificially enriched by a Hg bead, then SB7b-3 generally followed SB7b-2. Conversely, if the 4 hour after formic sample was a bad sample, then SB7b-3 might have generally followed SB7b-1. Material balance results below indicate that SB7b-3 generally followed SB7b-1. There are indications in all runs that mercury fell to the bottom, and was partially resuspended in the SME cycle, since all three SME products appeared to have more mercury dispersed in the slurry then their corresponding SRAT products.

Mercury material balances were attempted for the three runs. Closure was best at lower acid stoichiometries, Table 41.

Table 41. SB7b Batch Mercury Balance

	SB7b-1	SB7b-3	SB7b-2
Acid Stoichiometry	105%	115%	145%
Recovered elemental Hg, g	1.735	1.461	0.641
Hg in SRAT dewater condensate, g	0.252	0.224	0.017
Hg in SME, g	0	0.196	0
Sum, g	2.549	2.741	1.440
% of added Hg	64%	69%	36%

Recovered elemental Hg was collected following the SRAT cycle when the MWWT was drained of all contents in preparation for the SME cycle. Mercury in the SB7b-3 SME came from some elemental Hg that was not drained after the SRAT and could not be removed for weighing until the SME was completed. None of the three runs had any visible beads in the SME condensate bottles. The SRAT dewater condensate mercury was determined from the mass of condensate times the concentration of mercury measured analytically in a sub-sample.

Data were obtained for mercury dissolved in the SRAT supernate on the samples after acid addition, after dewatering, and after four hours reflux for runs SB7b-1 and SB7b-2. These data are plotted along with the slurry data and the hydrogen generation rate (scaled to fit on the graph) in Figure 23 and Figure 24.

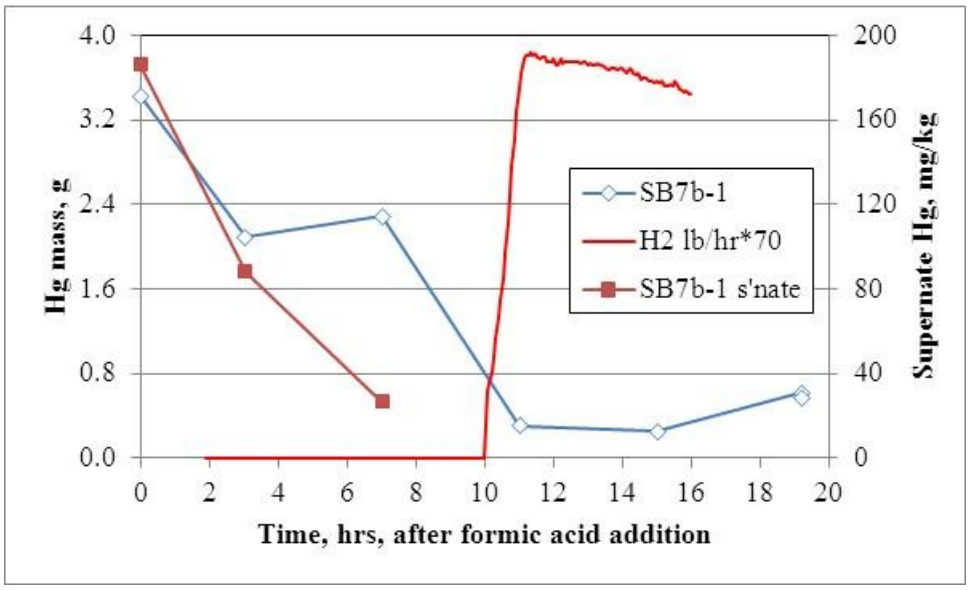

Figure 23. Timing of Hg and H2 in SB7b-1

The mercury dissolved in the SB7b-1 SRAT supernate immediately following acid addition was not trivial (of order 0.8 g or 20% of the starting Hg). Dissolved mercury seemed to fall roughly as slurry mercury fell. Hydrogen generation was minimal until the mercury had dropped significantly in both the supernate and slurry.

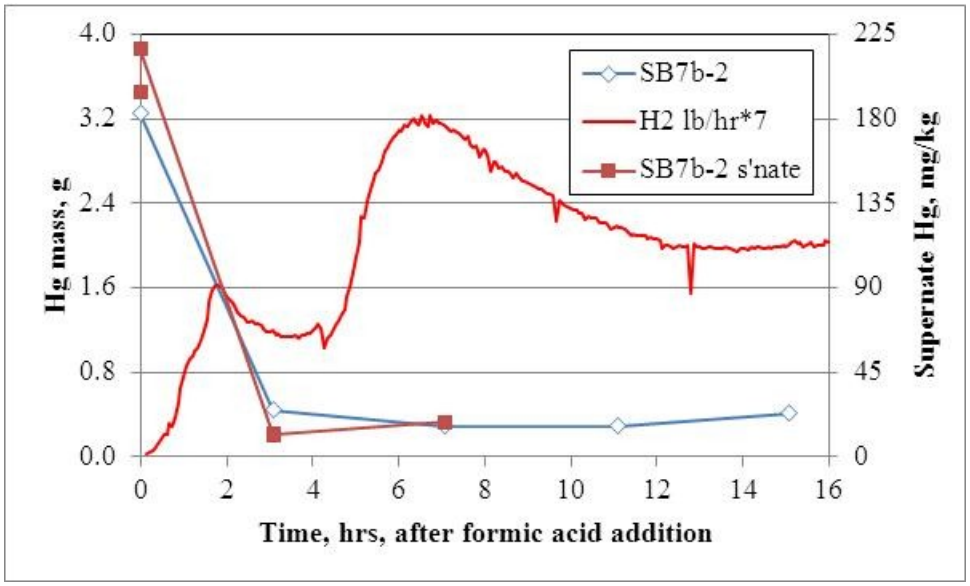

Figure 24. Timing of Hg and H2 in SB7b-2

It was somewhat surprising that the dissolved Hg in the SB7b-2 supernate generally tracked the slurry Hg. The slurry mercury data presumably indicate mercury beads or particles dropping to the bottom of the SRAT and no longer getting sampled in addition to stripped Hg loss. Dissolved mercury, however, is not going to settle like dense particles. An alignment between low slurry and supernate Hg with the onset of hydrogen is seen in SB7b-2 as well.

Data for SB7b-3 are given in Figure 25. Supernate Hg was not characterized for this run, but it could easily be similar to that for SB7b-1, since other processing results paralleled that run.

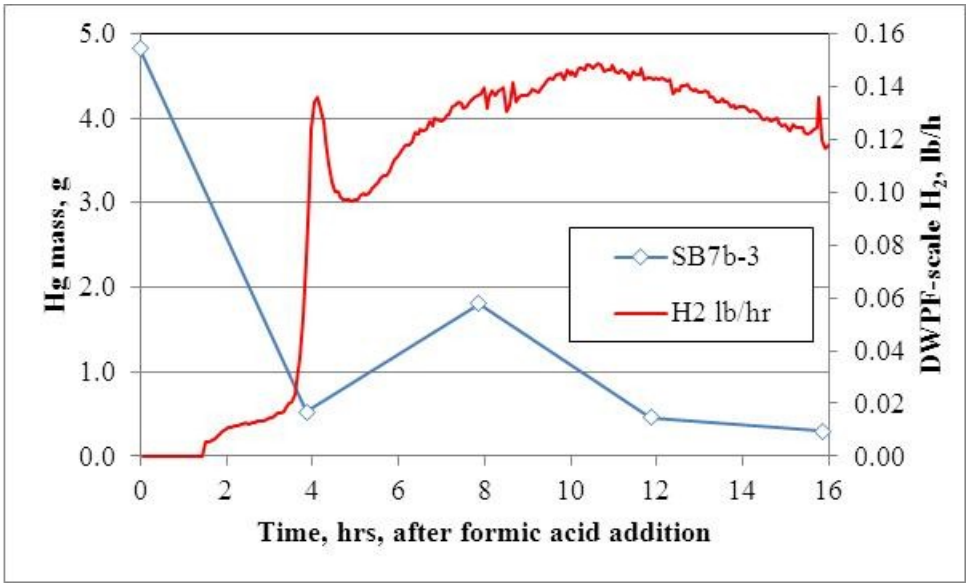

Figure 25. Timing of Hg and H2 in SB7b-3

For the third time, it appeared that once the slurry mercury mass dropped to roughly less than one gram (~350 mg/kg) that hydrogen generation increased in significance. Various mechanisms could be postulated, including nitrite stabilized mercury complexes, to explain the apparent relationship (nitrite is a candidate for a complex, since hydrogen generation also correlates with the destruction of nitrite ion).

SME Cycle Data

Formate and nitrate loss are presented in Table 42 for samples taken of the SME product slurry.

Table 42. SB7b Batch SME Anion Reactions

	SB7b-1	SB7b-3	SB7b-2
Acid stoichiometry, %	105	115	145
Formate loss, %	12	6	15
Nitrate loss, %	7	4	8

Analytical anion data for the three SME products are given in Table 43 as mg anion/kg slurry. SB7b-3 was not concentrated as much as the other two due to rheological and mixing issues, so many anion values should tend to be lower than in the other two runs.

Table 43. SB7b Batch SME Product Anions, mg/kg

	SB7b-1	SB7b-3	SB7b-2
F^-	<100	<100	<100
Cl^-	390	330	370
NO_2^-	<100	<100	<100
NO_3^-	16,900	17,300	19,500
$SO_4^=$	760	600	700
$C_2O_4^=$ (wd)	<100	<100	<100
HCO_2^-	36,600	33,400	38,100
PO_4^{3-}	<100	<100	<100

wd – weighted water dilution

Oxalate was present (theoretically in the 1,000-2,000 mg/kg range), but apparently mostly in forms that were not water soluble in the SME product slurry. An acid strike preparation was not performed on these SME products to draw oxalate into solution. Elemental wt.% data for the three SME products after calcining at 1100 °C are given in Table 44.

Table 44. SB7b Batch SME Calcined Elements at 1100 °C-wt.%

	SB7b-1	SB7b-3	SB7b-2
Al	3.3	3.2	3.4
B	1.6	1.7	1.6
Ba	0.06	0.06	0.06
Ca	0.36	0.37	0.36
Ce	0.07	0.08	0.07
Cr	0.03	0.03	0.03
Cu	0.02	0.02	0.01
Fe	9.2	10.4	9.4
K	0.05	0.03	0.04
La	0.04	0.04	0.04
Li	2.2	2.3	2.2
Mg	0.11	0.11	0.11
Mn	1.34	1.35	1.38
Na	8.4	9.4	8.7
Ni	1.9	2.0	2.0
P	<0.1	<0.1	<0.1
Pb	<0.01	<0.01	<0.01
S	0.18	0.20	0.17
Si	25.0	23.6	24.2
Sn	<0.01	<0.01	<0.01
Ti	0.02	0.02	0.01
Zn	0.02	0.02	0.02
Zr	0.13	0.13	0.13

The elemental break down of the three SME products was very similar. SME product solids data, densities, and pH are given in Table 45. The wt.% insoluble and soluble solids were calculated from the measured total slurry and supernate (dissolved) solids. The density measurements were made at 25 °C.

Table 45. Additional SB7b Batch SME Product Properties

	SB7b-1	SB7b-3	SB7b-2
Acid Stoichiometry %	105	115	145
Wt. % total solids	48.6	44.8	48.4
Wt. % insoluble solids	39.7	37.3	40.0
Wt. % soluble solids	8.9	7.5	8.4
Wt. % dissolved solids	14.8	11.9	14.1
Wt. % calcined solids	42.7	39.5	42.3
Slurry density, g/mL	(1.27)†	1.32	1.43
Supernate density, g/mL	1.08	1.07	1.09
Product pH at 25 °C	6.99	7.55	7.66

† - the SB7b-1 SME slurry density is unrealistic for 48.6 wt% total solids unless the sample contained trapped air bubbles or other low density foreign material

The first two tests ended near the concentration target of 49 wt.% total solids, but the SME products were very viscous and difficult to mix. The target for SB7b-3 was dropped to 45 wt.% total solids. The actual slurry density for SB7b-1 is unlikely to be less than 1.3 g/mL. Density generally tracks the total and insoluble solids content of the SME product. Measurement exceptions can occur if there is entrained gas (air bubbles) or if there is some other low density material held up in the instrument chamber.

The ammonia scrubber reservoir was sampled after the SRAT cycle and after the SME cycle to check for ammonium ion accumulation.

Table 46. Ammonium ion accumulation in scrubber reservoir

	SB7b-1	SB7b-3	SB7b-2
Acid Stoichiometry %	105	115	145
After SRAT, mg/L	<5	402	186
SRAT pH	7.5	8.4	8.0
After SME, mg.L	<5	433	243
SME pH	7.0	7.6	7.7

The lack of appreciable ammonium ion at low acid stoichiometry has been observed repeatedly once lab-scale testing incorporated an ammonia scrubber. The relatively high SRAT product pH in SB7b-3 may have driven more ammonia into the off-gas system compared to SB7b-2 (SB7-2 would be predicted to form more ammonium ion than the other two runs due to the higher acid, but the ammonium may have still been in the slurry due to the higher solubility at lower pHs).

SME Off-gas Data

Hydrogen generation rate data from the SME cycle are reported at DWPF scale in Figure 26. The y-axis is scaled in 20% increments relative to the DWPF SME limit of 0.223 lb/h.

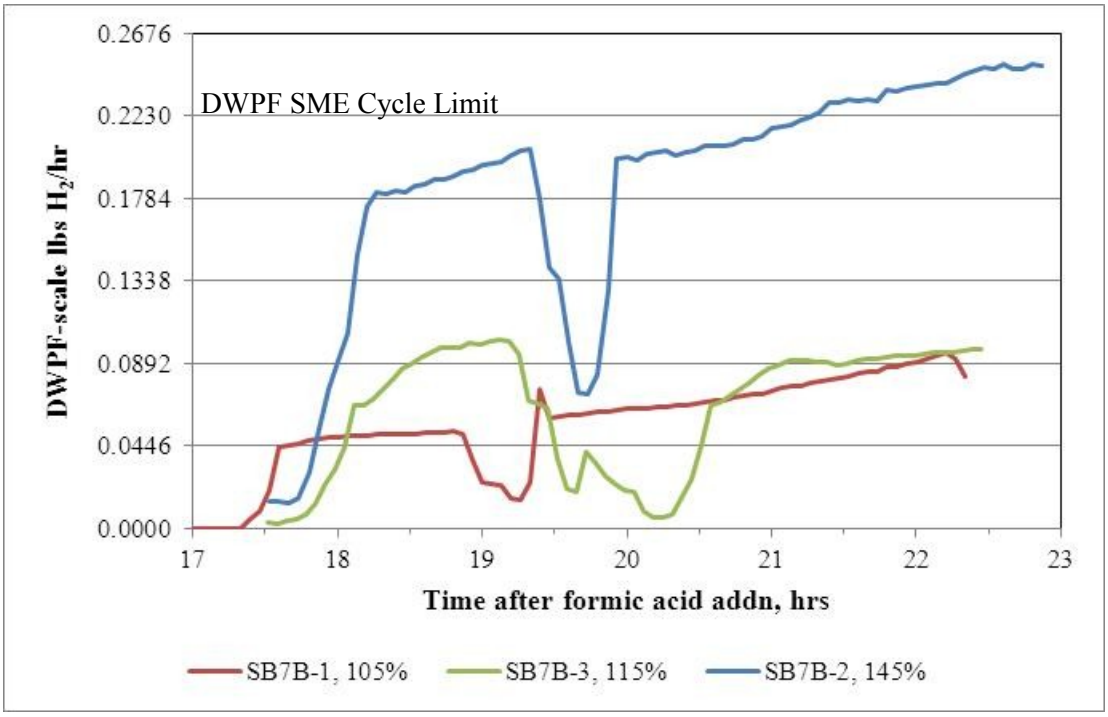

Figure 26. SB7b Batch SME cycle hydrogen generation

The 145% acid stoichiometry test exceeded the SME cycle hydrogen limit of 0.223 lb/h as it was concentrated past 45 wt.% total solids. Mixing also became an issue during this period which may have led to hotter vessel wall temperatures enhancing the hydrogen generation rate. Hydrogen generation rates following the first frit addition were generally lower than the ending SRAT cycle rates by 0-30%.

SME cycle carbon dioxide generation rate data are presented in Figure 27.

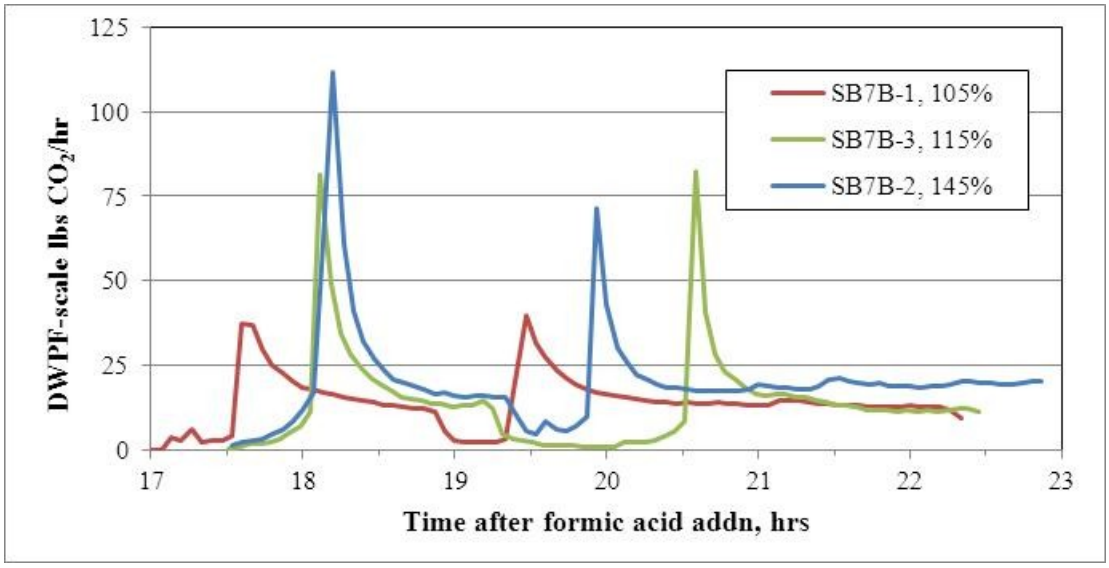

Figure 27. SB7b Batch SME cycle CO_2 generation

The principle features in the generation rates are due to the release of accumulated CO_2 at the onset of boiling following the first and second frit-formic acid slurry additions. Note that the CO_2 generation rate in SB7b-2 was not increasing as sharply as the hydrogen generation rate was toward the end of the SME cycle.

Summary

The SB7b batch studies were the first phase of the SB7b simulant work. The feed slurry was not trimmed with additional caustic, unlike the later SB7b tests covered in Appendix B and the main body of the report. An acid stoichiometry of 105% destroyed nitrite in the SRAT. SB7a simulant studies failed to destroy nitrite at 100% stoichiometry for the Tank 51 (batch) simulant, but succeeded at 110%. Above detection limit nitrite of 175 mg/kg was found, however, in the run at 110% stoichiometry with added oxalate (roughly double the oxalate). Data are accumulating that indicate that oxalate concentrations above 5,000 mg/kg in the SRAT feed slurry are impacting the minimum acid stoichiometry being predicted by the Koopman acid equation.

An acid stoichiometry of 150% in SB7a-batch simulant led to hydrogen generation rates of 80% of the DWPF SRAT limit and 81% of the SME limit. With SB7b at an acid stoichiometry of 145%, hydrogen generation peaked at 71% of the DWPF limit, while the SME cycle peak exceeded the DWPF SME limit by 12%. This is a sign that control of acid stoichiometry will be more of an issue for SB7b than it was for SB7a. SB7a-Tank 51 required 1.18 moles acid/L SRAT receipt compared to 1.04 moles acid/L SRAT receipt for SB7b-Tank 51. SB7a could handle up to 0.59 moles/L more acid, while SB7b could only handle 0.47 moles/L more acid. Maximizing the ratio of SB7a to SB7b in the blend will tend to partially mitigate this situation.

Scoping recovery studies of antifoam seemed to indicate that the slurry insoluble solids and the SRAT condensate were the leading candidates for finding antifoam. Hexane extraction and rinsing may not be selective enough or effective enough to track antifoam or its decomposition products.

Appendix B
SB7b Caustic Addition Scoping Simulations

Introduction

Two 4-L lab-scale process simulations were performed using a generic blend of the A, B, and C simulants prepared at Clemson during preparations for Sludge Batch 3. The testing came after a decision to qualify the blend of SB7b with SB7a in Tank 40 had been made. The purpose of the two tests was to assess the impact of two levels of caustic addition on the stoichiometric acid equation at estimated SB7b levels of oxalate, mercury, and noble metals. The testing was driven by the small quantity of SB7b-Tank 40 simulant available (barely enough for the five runs in the main body and none for scoping studies). Generic ABC blend simulant has been used to support the beaded frit program and various studies related to DWPF process chemistry (hydrogen, SRAT chemistry, minimum formic acid, early alternate reductant tests, and next generation solvent tests).

Scope

SB7B-4 simulated a 0.49M increase in base equivalents via caustic addition (roughly a 6 wt.% increase in Na_2O in calcined SRAT product or 21,000 gallons of 50% caustic). SB7B-5 simulated a 0.32M increase in base equivalents via caustic addition (roughly a 4 wt.% increase in Na_2O in calcined SRAT product or 14,000 gallons of 50% caustic). This corresponded to additions of 3.42 g 50% NaOH solution/100 g ABC simulant and 2.21 g 50% NaOH solution/100 g ABC simulant respectively. The caustic addition calculations were based on the expected SB7b blend calcined oxide composition rather than on the actual ABC simulant calcined oxide composition. Both cases bound the 0.28M increase in base equivalents tested in the SB7b-Tank 40 blend simulations (see Section 3.0 of main body) on the high side of acid requirement (are conservative with respect to impact of caustic on the ability to target a SRAT product with barely destroyed nitrite ion).

Sodium oxalate was also added since ABC simulant slurry has fairly low oxalate (1,400 mg/kg), while SB7a and SB7b have considerably more oxalate (likely over 8,000 mg/kg in SB7a). The addition targeted 7,800 mg oxalate/kg SRAT receipt slurry (ABC oxalate plus trim oxalate combined in ABC + caustic + sodium oxalate + trim mercury and noble metals). An addition of 0.68 g oxalate/100 g ABC simulant was made to both runs. The main significances of sodium oxalate are that it has an impact on the excess acid, and thus on the required acid stoichiometry for nitrite destruction, that it has an impact on RedOx, and thus on the split of added acid between nitric acid and formic acid, and that it impacts the solubilities of certain species that distribute between the soluble and insoluble solids during SRAT/SME processing.

Both runs targeted 110% stoichiometry based on the Koopman minimum acid equation (KMA). ABC simulant processing data were a significant component in the development of the KMA. The SRAT cycles presumed a 30% formate loss, 10% nitrite-to-nitrate conversion, 100% nitrite destruction, and 3% oxalate destruction. The SRAT product targeted 25 wt.% total solids. The SME cycle assumed an additional 2% formate loss, 36% waste loading, and targeted 47 wt.% total solids for the final product slurry.

The noble metal and mercury concentrations in the total solids are compared to the SB7a Tank 40 WAPS sample results and the SB7b rad waste qualification (SC-12) results in Table 47.

Table 47. Noble metal and mercury, wt.% in total solids

	SB7B-4 SB7B-5	SB7a WAPS	SC-12 (Tank 40/SB7b)†
Rh, wt%	0.0237	0.019	0.021
Ru, wt%	0.1135	0.094	0.100
Hg, wt%	1.4435	1.9	1.34
Pd, wt%	0.0034	0.003	0.002
Ag, wt%	0.0144	<0.02	0.011

† - SC-12 is the rad waste Shielded Cells qualification run

Mercury and noble metal concentrations in the solids were about 10% higher than the SC-12 values.

The lab-scale simulations were conducted in the newly designed lab-scale 4-L SRAT with off-center mixing, two heating rods instead of a mantle, and the direct vertical condensate drop configuration from the SRAT condenser to the MWWT.

SRAT Results

Since the main purpose of the two runs was to test the impact of caustic on the suitability of the KMA, these results will be discussed first. SB7B-4 (max caustic) had 1450 mg nitrite/kg in its SRAT product, while SB7B-5 (65% max caustic) had 109 mg nitrite/kg. Both nitrite results were higher than expected assuming oxalate was inactive during processing (~105% KMA typically leads to a <100 mg nitrite/kg SRAT product result, and the runs were at 110% KMA).

The ABC nitrite results drove a decision to start the SB7b blend simulant tests at 105% KMA instead of 100% KMA (100% KMA was used in SB6 and SB7a simulant tests as a low acid stoichiometry test for identifying the acid window). SB7b blend simulant was given a smaller increase in acid demand due to added caustic, and SB7b blend simulant was trimmed to a lower oxalate concentration than the ABC simulant. The second change was in the direction that suggested the stoichiometric acid factor could be partially dropped from 110% toward 100%. The caustic change was thought to be neutral to the stoichiometric factor when processing at minimum acid for nitrite destruction. SB7b-6, actually run at 105% KMA, had 366 mg nitrite/kg in the SRAT product which seems to confirm the logic of the above argument.

The SRAT anions reactions were broken down into the usual percentage conversions and are summarized in Table 48 compared to the pre-run projections.

Table 48. SRAT Anion Reactions

	Target	SB7B-4	SB7B-5
Acid stoichiometry, % KMA		110	110
Formate loss, full SRAT, %	30	22	17
Nitrite-to-nitrate, full SRAT, %	10	12	18
Nitrite loss, full SRAT, %	100	91	99

SRAT formate destruction was lower than projected because there was not 5-10% excess acid following acid addition that was available for catalytic reactions that destroy formate. Nitrite-to-

nitrate conversion was slightly higher than projected because there was no excess acid to attack nitrate ion via the reaction sequence responsible for ammonium ion generation.

Analytical anion data for the two SRAT products are given in Table 49.

Table 49. SRAT Product Anions, mg/kg slurry

	SB7B-4	SB7B-5
F^-	<100	<100
Cl^-	530	560
NO_2^-	1,450	109
NO_3^-	26,500	26,200
$SO_4^=$	1,070	1,100
$C_2O_4^=$ (wd)	650	680
HCO_2^-	50,600	50,200
PO_4^{3-}	<100	<100

wd – water dilution

The anion concentrations are remarkably similar in spite of different caustic, nitric acid, and formic acid additions. The formic acid addition to SB7B-4 was 8% larger than the addition to SB7B-5, and the nitric acid addition, on a nitric acid plus trimmed sludge nitrate basis, was 12% larger in SB7b-4 than in 5. The extra caustic in SB7B-4, however, meant that less mass was removed during dewatering. The greater SB7B-4 SRAT product slurry mass brought the SB7B-4 slurry anion concentrations close to those in SB7B-5 in spite of the somewhat larger anion masses.

Table 50. Additional SRAT Product Properties

	SB7B-4	SB7B-5
Wt. % total solids	24.1	24.1
Wt. % insoluble solids	12.8	13.1
Wt. % soluble solids	11.3	11.0
Wt. % dissolved solids	13.0	12.7
Wt. % calcined solids	15.7	15.8
Slurry density, g/mL	1.14	1.15
Supernate density, g/mL	1.08	1.08
Product pH at 25 °C	6.8	7.1
Vessel pH at 101 °C	†	6.7

† - ground fault problem – no electronic pH data

SB7B-4 with more nitrite would be expected to have a higher pH (less acid remaining) than SB7B-5, but the results do not confirm this in the cooled SRAT product samples. The vessel pH readings for SB7B-4 were corrupted by a ground fault which prevented electronic data collection, but manually recorded pH readings indicated about 6.71 at the end of the SRAT cycle.

Dissolution of Ca, Mg, and Mn occurred during the SRAT. Mg solubility exceeded Ca in both absolute concentration and percent of total species in the SRAT product. Mg solubility exceeded Mn in percent of total species (both runs), as well as in absolute concentration in SB7B-4 but not in SB7B-5. There was twice as much Mn as Mg overall in the simulant. Results for the extent of solubility were comparable to low acid tests with SB7b-blend simulant.

Off-gas data were developed from the GC readings. Hydrogen was not detected in either SRAT cycle. This is not surprising when >100 mg/kg nitrite remains, although there may have been one or two instances where a little hydrogen was produced in spite of a small amount of residual nitrite ion. Carbon dioxide generation data are given in Figure 28.

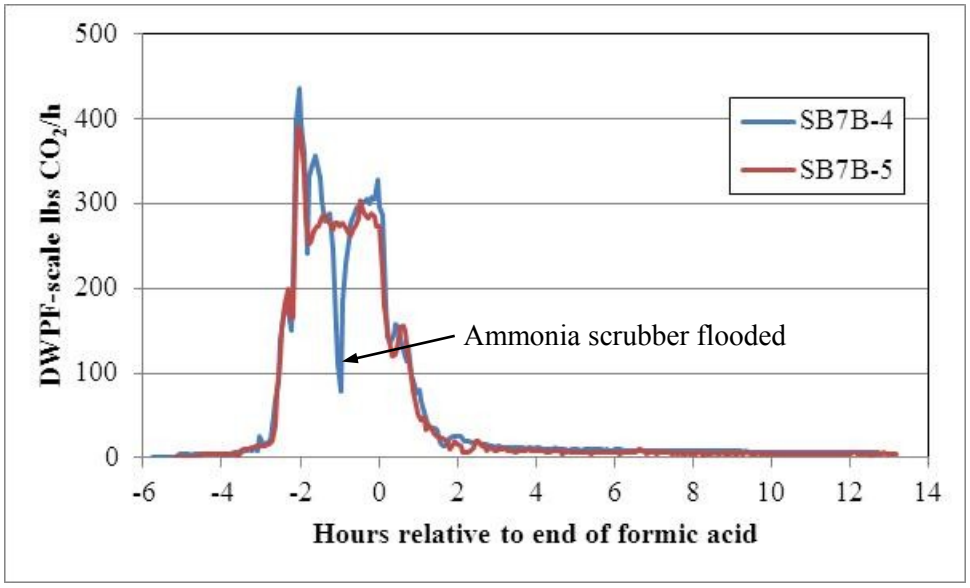

Figure 28. SB7b caustic spike SRAT CO_2 results

The CO_2 results are very similar. A dip in generation occurred at -1.3 hours in SB7B-4. This was the result of the ammonia scrubber flooding which prevented the CO_2 being produced in the SRAT from reaching the GC downstream of the FAVC. SB7B-4 produced 52 g versus 49 g in SB7B-5 (the same mass approximately within the uncertainty of the GC calibrations and numerical integration scheme). The profiles indicate that the two runs were generally in step in terms of the timing of the major CO_2 producing reactions (TIC destruction at about -2 hours, followed by most of the nitrite destruction and Mn reduction from -1 to +3 hours). Once the majority of nitrite that would be destroyed was destroyed, or about 4-6 hours after the end of formic acid addition, the rate of CO_2 generation was less than 3% of the peak values that occurred during acid addition.

N_2O data for the two caustic scoping runs are given in Figure 29.

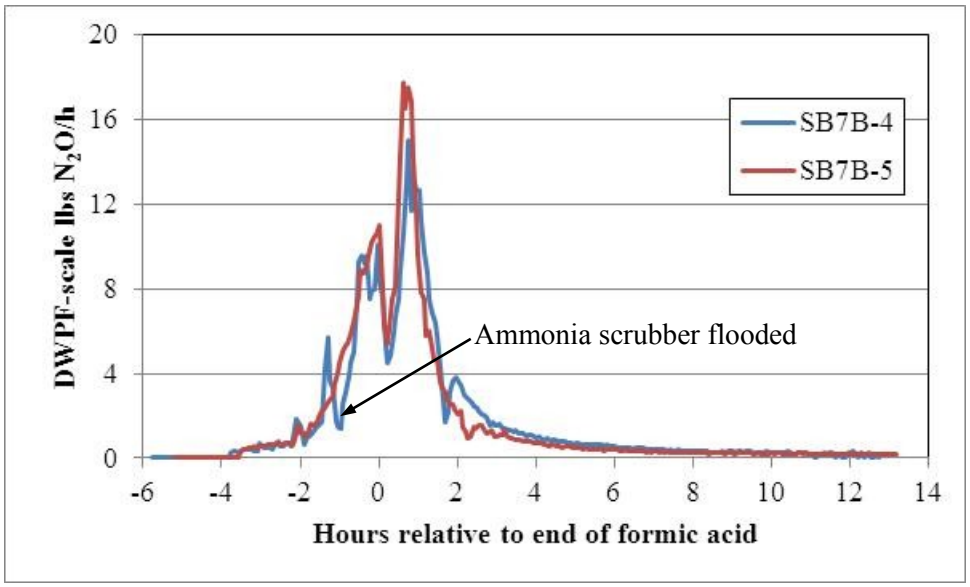

Figure 29. Nitrous oxide from the caustic scoping SRAT runs

The impact of the ammonia scrubber flooding at -1.1 hours is apparent in the SB7B-4 data for N_2O also. The data are otherwise quite similar until about 2 hours after acid addition. Subsequently, SB7B-4 was producing slightly more N_2O per unit time compared to SB7B-5. The delta presumably reflects the larger concentration of available nitrite during the boiling period of the SRAT cycle in SB7B-4 that persisted into the SRAT product.

Mercury Results

SRAT slurry samples were taken for mercury at several different times once acid addition was complete. SRAT and SME product slurries were also sampled for mercury. The sampling was expanded in this group to support the on-going program to develop a better understanding of mercury chemistry during processing. SRAT samples had occasionally shown Hg concentrations that were not considered credible (too high based on samples prior and subsequent to the sample in question). This behavior was observed in the SB7b-Tank 40 data discussed in the main body as well as the SB7b-Tank 51 data in Appendix A.

It has been postulated that these off-trend samples contained one or more Hg beads that were not representative of the average bulk slurry in the vessel. In other words that the slurry is sufficiently heterogeneous, even while mixing, that composition varies with location. Two mechanisms could be at work. There could be a small population of Hg beads with only a 10-20% probability of being captured in a 1-2 g sample, or there could be a large population of beads of various sizes, but only a small probability of sampling a large bead. Samples taken during dewatering and reflux were taken in duplicate in order to develop some broad statistics on the likelihood of obtaining Hg enriched samples.

Data from SB7b-4 are given in Figure 30. Each Hg measurement is shown individually (as opposed to graphing averages of multiple results). SRAT product occurred after about 12 hours of boiling and SME product occurred after about 17 hours of boiling.

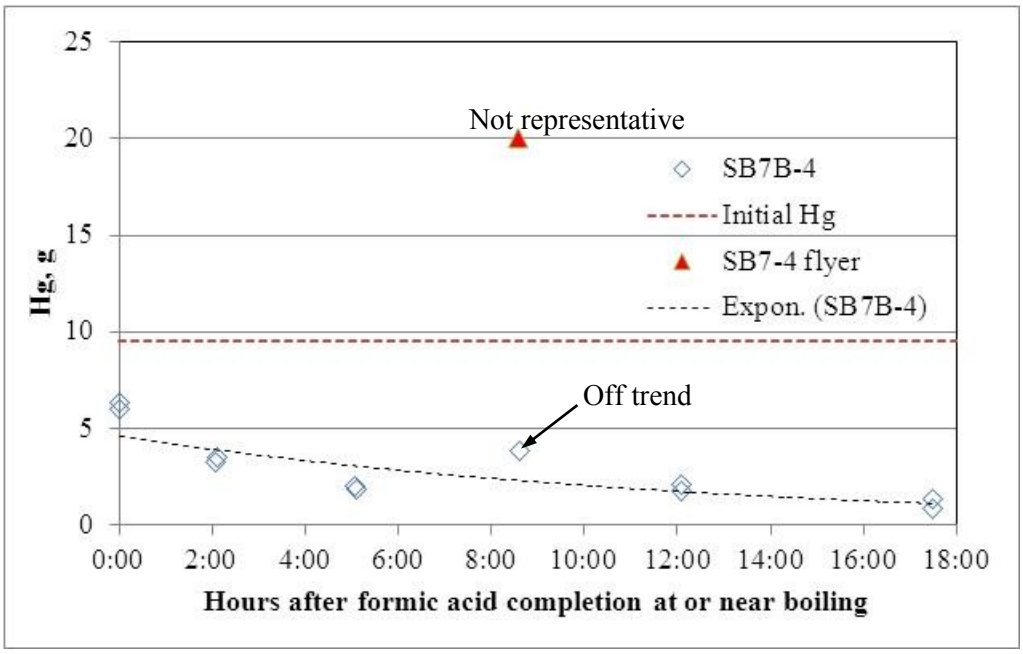

Figure 30. Quality of Hg Data Replication in SB7b-4

Five of the six pairs of samples had good agreement between the two results, but the sample just past eight hours had two suspect results. The result at 20 g Hg indicated more than twice the starting concentration of Hg and cannot possibly be representative. The second eight hour result at 4 g Hg is not physically impossible, but is higher than the two samples before and two samples after it in the sequence which is suspicious. Data for SB7b-5 are given in Figure 31.

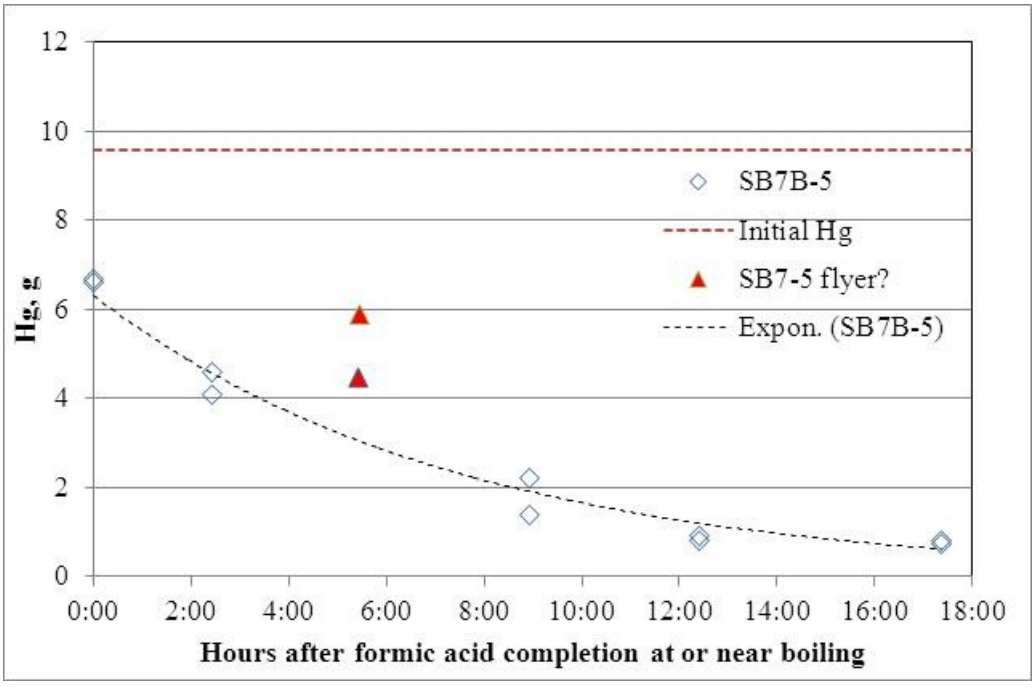

Figure 31. Quality of Hg Data Replication in SB7b-5

Good replication of sample pairs was obtained at four sample times. Fair replication was obtained at about 9 hours (average of 1.79 g with standard deviation of 0.57 g, or 32%). The results, however, seem to bracket the trend. Fair replication was obtained at about five hours as well (5.2 g with standard deviation of 1 g, or 19%). In this case the uncertainty in grams is larger than at nine hours even though the standard deviation in percent is smaller. Also, both results appear to be off the trend of the majority of the data.

So, out of 12 pairs of results (24 analyses), there were one major flyer, three results that were off the trend, and one pair that were near trend but not well reproduced. Consequently, based on this initial set of data there is roughly a 15-20% chance of getting a result that is off-trend. While the four off trend results occurred during reflux in these two runs, suspect data have been seen at all sampling times in prior testing from the end of SRAT acid addition through the process to the SME product.

SME Cycle Results

A selection of SME cycle and SME product results are given in Table 51.

Table 51. SME Cycle Results

	SB7B-4	SB7B-5
Acid stoichiometry, %	110	110
Formate loss, %	7	13
Nitrate loss, %	3	9
Wt. % total solids	47.1	46.3
Nitrite ion, mg/kg	570	<100
Slurry density, g/mL	1.37	1.39
Product pH at 25 °C	6.7	7.1

The formic acid in the frit slurry was not sufficient to complete nitrite destruction in SB7B-4. Formate and nitrate loss data indicate more reactivity in SB7B-5.

One surprise in the SME cycle was the hydrogen production in SB7B-5, Figure 32.

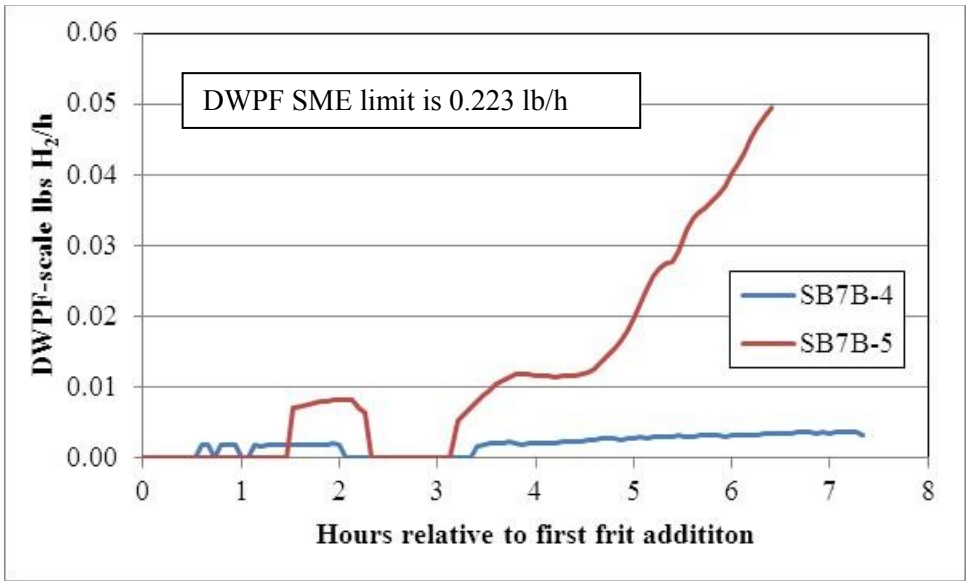

Figure 32. SME cycle hydrogen in caustic scoping runs

The formic acid in the first frit addition did not lead to much hydrogen generation in SB7B-5. It was likely consumed in completing nitrite destruction and perhaps in some residual Mn reduction. The formic acid in the second frit addition, however, led to a fairly rapid increase in hydrogen generation rate about an hour and a half after the slurry was brought back to boiling. The concern is that the noble metal concentrations are so high in SB7b that it takes very little excess acid to trigger a significant amount of hydrogen generation. SB7B-5 would normally be described as a near minimum acid stoichiometry run based on the presence of detectable nitrite ion in the SRAT product. In spite of this, hydrogen reached 23% of the DWPF SME cycle limit. The easiest way to avoid this would be to remove the formic acid from the frit slurry. Frit 418 does not gel when mixed with water, so formic acid is not needed to slurry the frit.

Both SME cycles produced hydrogen in spite of the presence of some nitrite ion. Evidence for continuing nitrite destruction was found in the N_2O data, Figure 33. SB7B-4 had more N_2O production, presumably because the SB7B-4 SRAT product had more nitrite ion. It is not possible to place a demarcation where N_2O produced from nitrite might have transitioned to N_2O produced from nitrate in SB7B-5 (and there may be no demarcation chemically). Past data indicate that nitrate does not convert to N_2O while nitrite is still available, so SB7B-4 N_2O is presumably all from nitrite destruction.

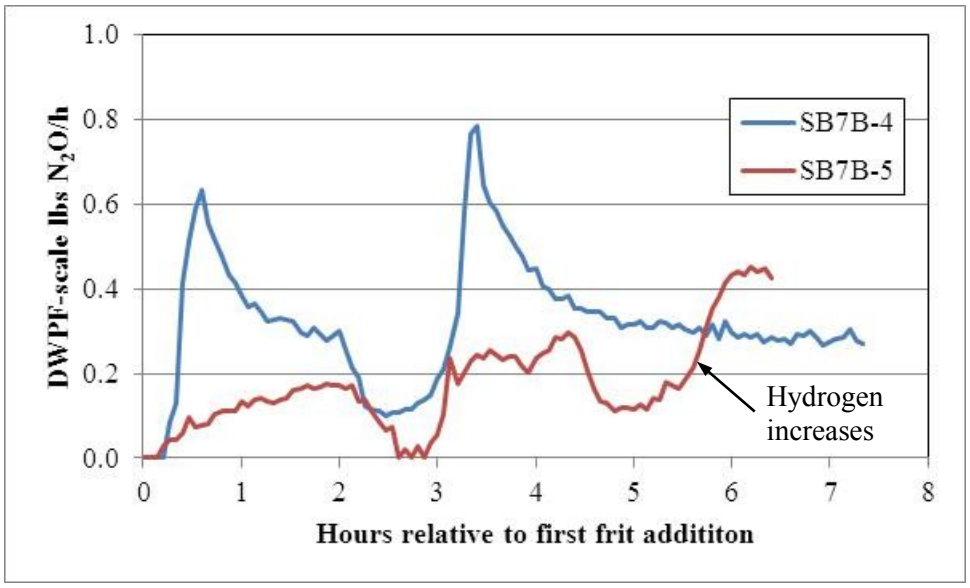

Figure 33. Scoping caustic run SME cycle N_2O

The period from 5-6 hours after first frit addition in SB7B-5 was the time when hydrogen generation accelerated. There was a matching increase in N_2O generation at this time. Why these two occurred together and did not occur sooner (N_2O fell between 4.5 and 5 hours) may relate to mixing or rheology issues or to some other aspect of the chemistry that is not well understood.

The SME carbon dioxide generation rate data are less dramatic than those above, Figure 34.

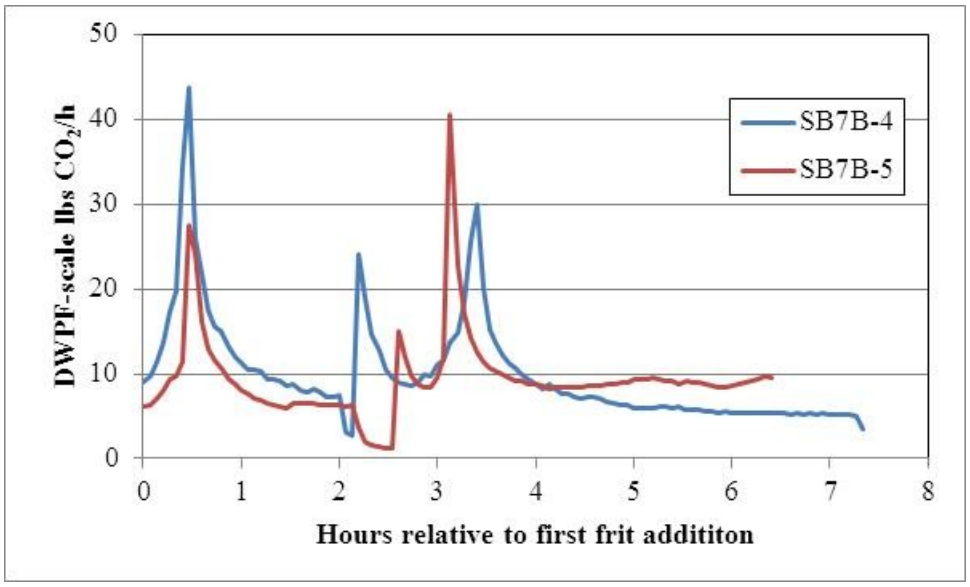

Figure 34. Scoping caustic run SME cycle CO_2

There is a peak in CO_2 generation rate following the onset of boiling after each of the two frit additions in both runs. These occur roughly at 0.5 hours and 3 hours after the first frit addition. They align with peaks in N_2O generation. They are traditionally associated with decomposition

of the fresh formic acid introduced with the frit slurry. There is no reflection of the hydrogen or N_2O generation rate increase of any consequence in the CO_2 data.

There is a lesser peak in CO_2 generation between 2 and 3 hours in both runs (more obvious in SB7B-4). In SB7B-4 the peak occurred about 20 minutes after the dewatering target was met for the first frit addition (heating rod power at 0%). It is not clear what triggered the surge in CO_2 production at this time. The technical analysts have reported some instances of off-gassing during frit addition, and the temperature data indicate that the frit for the second addition had probably been added. It may be that there was some retained CO_2 in the slurry, as bubbles perhaps, that was displaced when the frit was added (frit, formic acid, and water are added separately in the lab-scale simulations, one after the other, rather than as a slurry).

Summary

The main result from the two scoping runs with added caustic was to better define a target for the low acid flowsheet study run for SB7b blend simulant. Some additional data that can be used to enhance the Koopman minimum acid equation, particularly with respect to oxalate ion, was obtained. Another finding was the indication of high potential catalytic activity toward converting excess acid to hydrogen. Even in the presence of a small amount of nitrite ion, it was possible to produce a low level rate of hydrogen generation, and, once the nitrite was destroyed in SB7B-5, it was easy to transition to an intermediate hydrogen generation rate in a minimum acid stoichiometry run. This pairing is not desirable and has the potential to severely restrict acid additions in DWPF.

Investigations into mercury sampling show that there is a modest probability of getting flyer and off trend results of order 20%. These analytical results appear to be real (not analysis error), and they are likely due to capturing an above average sized bead of elemental mercury into the sample. For an average sample size of 1.5 g, and assuming these are single bead events, the beads would then be present at about one bead for every 7-8 grams of slurry or roughly about 400 beads in the lab-scale SRAT.

Distribution:

A. B. Barnes, 999-W
S. D. Fink, 773-A
B. J. Giddings, 786-5A
C. C. Herman, 999-W
S. L. Marra, 773-A
F. M. Pennebaker, 773-42A

J. M. Gillam, 766-H
J. F. Iaukea, 704-30S
J. E. Occhipinti, 704-S
D. K. Peeler, 999-W
J. W. Ray, 704-S
H. B. Shah, 766-H
D. W. McIlmoyle, 766-H
M. T. Keefer, 766-H
D. C. Sherburne, 704-S
M. E. Stone, 999-W
D. C. Koopman, 999-W
D. P. Lambert, 999-W
J. D. Newell, 999-W
J. R. Zamecnik, 999-W
S. H. Reboul, 773-A
J. M. Pareizs, 773-A
D. K. Peeler, 999-W
A. S. Choi, 773-42A

J. M. Bricker, 704-27S
T. L. Fellinger, 704-26S
E. W. Holtzscheiter, 704-15S
A. R. Shafer, 704-27S
H. P. Boyd, 704-27S